Atmospheric pollution in the Arctic: Sources, transport, and chemical processing

A dissertation presented

by

Jenny A. Fisher

to

The Department of Earth and Planetary Sciences

in partial fulfillment of the requirements
for the degree of
Doctor of Philosophy
in the subject of
Earth and Planetary Sciences

Harvard University
Cambridge, Massachusetts

August, 2011

Dissertation Advisor

Professor Daniel J. Jacob

Author

Jenny A. Fisher

Atmospheric pollution in the Arctic: Sources, transport, and chemical processing

Abstract

This dissertation applies a global chemical transport model (GEOS-Chem) together with ground-based, aircraft, and satellite observations to quantify the sources, transport pathways, and chemical processing of tropospheric pollution in the Arctic.

Asian anthropogenic emissions are shown to be the dominant source of carbon monoxide (CO) pollution throughout the Arctic troposphere, except near the surface where European anthropogenic emissions are similarly important. Despite anomalously large fires in spring 2008, biomass burning is found to contribute little to mean CO during that period. AIRS satellite data are used to demonstrate a link between El Niño and Asian pollution transport to the Arctic, with transport hindered in 2008 due to a weakened Aleutian Low associated with La Niña conditions.

Sulfate-ammonium aerosol in the Arctic is found to derive from a more complicated mix of sources. European and East Asian emissions are important but not dominant sources of sulfate. Anthropogenic emissions from West Asia (Russia and Kazakhstan) are shown to provide the largest source of sulfate to the Arctic lower troposphere in winter. Ammonium

is mostly from European and East Asian sources. In spring 2008, a large contribution from boreal fires resulted in a more neutralized aerosol in the free troposphere than at the surface. Aerosol transported to the Arctic from East Asia and Europe is found to be mostly neutralized, while West Asian and North American aerosol is highly acidic. Recent growth of sulfur emissions in West Asia may explain observations of increasing aerosol acidity in Alaska over the past decade.

Mercury in the Arctic shows a different seasonality from other pollutants, with a spring minimum driven by bromine chemistry over sea ice followed by a summer maximum. GEOS-Chem simulations of surface observations are used to argue that the summer peak cannot be explained by atmospheric transport, re-emission from snowpacks, or ocean kinetics. Instead, Russian rivers are proposed to provide a large flux of mercury to the Arctic Ocean in spring-summer, with subsequent evasion to the atmosphere driving the observed summer peak. The Arctic Ocean then provides a net source to the atmosphere, with rivers the dominant mercury source to the Arctic environment.

Contents

List of Figures

List of Tables

Citations to Previously Published Work

Chapters 2 and 3 have appeared previously in the following papers:

Fisher, J.A., D.J. Jacob, M.T. Purdy, M. Kopacz, P. Le Sager, C. Carouge, C.D. Holmes, R.M. Yantosca, R.L. Batchelor, K. Strong, G.S. Diskin, H.E. Fuelberg, J.S. Holloway, E.J. Hyer, W.W. McMillan, J. Warner, D.G. Streets, Q. Zhang, Y. Wang, S. Wu. (2010) Source attribution and interannual variability of Arctic pollution in spring constrained by aircraft (ARCTAS, ARCPAC) and satellite (AIRS) observations of carbon monoxide, *Atmospheric Chemistry and Physics* **10**: 977-996, doi: 10.5194/acp-10-977-2010.

Fisher, J.A., D.J. Jacob, Q. Wang, R. Bahreini, C.C. Carouge, M.J. Cubison, J.E. Dibb, T. Diehl, J.L. Jimenez, E.M. Leibensperger, Z. Lu, M.B.J. Meinders, H.O.T. Pye, P.K. Quinn, S. Sharma, D.G. Streets, A. van Donkelaar, and R.M. Yantosca. (2011) Sources, distribution, and acidity of sulfate-ammonium aerosol in the Arctic in winter-spring, *Atmospheric Environment*, in press, doi: 10.1016/j.atmosenv.2011.08.030.

Acknowledgments

I am extremely grateful to many people who have helped shape this dissertation. First and foremost, my advisor Daniel Jacob who has given me innumerable opportunities and helped me grow from a student to a scientist. I am honored to have been led through graduate school by such an outstanding scientist and even more outstanding mentor.

I am deeply appreciative of the students and post-docs of the Atmospheric Chemistry Modeling Group, who have created a fun, supportive, and intellectually stimulating environment. In particular, my officemates Monika Kopacz, Eric Leibensperger, and Eloïse Marais have provided me with countless hours of advice, much-needed tea breaks, and diverse and enriching perspectives. I have benefited tremendously from the selfless help of Bob Yantosca and from the scientific expertise of Elsie Sunderland, who over the past six months has been an unparalleled source of wisdom, enthusiasm, and support.

I would also like to thank the ARCTAS Science Team, who not only generously shared their data but also helped me truly understand the meaning of scientific community.

I am indebted to the mentors who inspired and fostered my passion for science – Earl Peters, Jobea Holt, and Mark Richardson – and to my parents, Bruce and Mindi Fisher, who first introduced me to science and have provided continuous support and encouragement. Finally, I cannot begin to express my gratitude for my husband, Richard Cook, who has been an unending source of help, ideas, motivation, and inspiration and who has ensured that, even while pursuing my PhD, my world has been bigger than graduate school.

dedicated to my grandmother, Peggy Evans

who always reminds me that life is what we make of it

Chapter 1

Overview

The Arctic is a harbinger of global environmental change. Unprecedented and rapid warming in the polar regions is evidenced by rising air temperatures (Trenberth et al., 2007), melting sea ice (Perovich and Richter-Menge, 2009; Serreze et al., 2007), permafrost degradation (Jorgenson et al., 2006; Osterkamp et al., 2009), decreasing snow cover (Brown et al., 2010), and retreating glaciers (Arendt et al., 2009; Barrand and Sharp, 2010). These changes in Arctic climate are strongly linked to atmospheric pollutants, which contribute to changes in radiative forcing, surface albedo, and cloud properties (Quinn et al., 2008).

Although the Arctic is largely devoid of local sources, it is a major receptor for anthropogenic pollution transported from mid-latitudes (Quinn et al., 2007), with important implications not only for Arctic climate but also for atmospheric chemistry and biogeochemical cycling. Atmospheric pollution was identified in the Arctic as early as the 1950s (Shaw, 1995). However, despite a long history of study, the sources and properties of pollutants in the Arctic troposphere remain highly uncertain (Shindell et al., 2008). This dissertation uses a suite of observational datasets combined with a chemical transport model to better

constrain the sources, transport pathways, and chemical properties of Arctic pollution.

1.1 Transport of pollution to the Arctic

Early studies of Arctic pollution sources took place in the 1970s and early 1980s and focused on attribution of particulate matter measured at surface sites. Using tracer correlations and meteorological analyses, these studies found dominant contributions to Arctic pollution from Europe and the former Soviet Union (Barrie, 1986; Carlson, 1981; Raatz and Shaw, 1984; Rahn, 1981). Since this early work took place, global emissions distributions have changed dramatically with the collapse of the Soviet Union, emission controls across North America and Europe, and rapid industrialization in East Asia. Furthermore, the source attribution obtained from surface data may not be representative of the sources to the overlying free troposphere, which in Arctic winter and spring is often decoupled from the boundary layer due to frequent thermal inversions (Bradley et al., 1993).

In recent years, global models have been increasingly used to pinpoint the sources of Arctic pollution. While diverse models agree that a variety of mid-latitude source regions contribute to pollutant distributions in the Arctic, they disagree quantitatively on the relative importance of Europe, North America, East Asia, and Russia (Koch and Hansen, 2005; Shindell et al., 2008; Stohl, 2006). In addition, models vary by more than 100% in simulation of Arctic pollutant distributions and are generally unable to reproduce either the concentrations or the seasonality of observed trace gases and aerosols (Shindell et al., 2008).

When I began this research in 2006, there had been little work linking models of Arctic pollution transport to observations, especially in the free troposphere. Using carbon monoxide (CO) as a tracer of anthropogenic pollution, I conducted an integrated analysis of pollution sources and transport using ground-based, aircraft, and satellite data combined with the GEOS-Chem chemical transport model (CTM). My work addressed the following questions:

- What are the relative contributions of different source regions (North America, Europe, East Asia) and types (fossil fuel, open burning) to CO pollution in the Arctic?
- How do these contributions vary as a function of altitude?
- Can we use satellite data to observe pollution transport to the Arctic?
- What drives the interannual variability of pollution transport to the Arctic?

1.2 Sources and properties of the Arctic aerosol

Sulfate is the dominant component of the aerosol pollution that accumulates in the Arctic in winter and spring in both the boundary layer (Quinn et al., 2002) and the free troposphere (Scheuer et al., 2003). Despite its prevalence and its importance as a climate forcer (Quinn et al., 2008), the sources of sulfate to the Arctic remain poorly understood, and simulations of Arctic sulfate vary by more than a factor of 1000 in the free troposphere (Shindell et al., 2008).

While pure sulfate is strongly acidic, the acidity of sulfate aerosol in the troposphere can range from very acidic to fully neutralized, with ammonium the dominant neutralizing agent. The extent of sulfate neutralization impacts the hygroscopicity of the aerosol, thereby influencing the magnitude of both direct and indirect climate effects (Abbatt et al., 2006; Baustian et al., 2010; Martin et al., 2004). Arctic ammonium has received limited study, and the sources have not been quantified.

Surface-based observations of aerosol concentrations at Barrow, Alaska show that ammonium aerosol has been decreasing more rapidly than sulfate over the past decade, despite concurrent increases in global ammonia emissions from agriculture (Galloway et al., 2008). This has led to an increasingly acidic aerosol at Barrow (Quinn et al., 2009). Meanwhile, this trend has not been observed in surface data from Alert, Canada (Hole et al., 2009). The differences between these sites and the drivers for these observed trends in aerosol acidity are not understood.

Using a combination of aircraft and surface data and the GEOS-Chem CTM, I sought to answer the following questions:

- What are the relative contributions of different sources to sulfate-ammonium aerosol in the Arctic boundary layer and free troposphere?
- How do the source influences evolve seasonally from winter to spring?
- How acidic is the Arctic aerosol, and how do different source regions impact this acidity?

- Can we understand the decadal-scale trends in aerosol acidity observed at Arctic surface sites?

1.3 Atmosphere-ocean cycling of Arctic mercury

Mercury is a neurotoxin that bioaccumulates and biomagnifies in aquatic ecosystems (Mergler et al., 2007). Human exposure to mercury is particularly problematic in the Arctic, where extremely high concentrations have been measured in a variety of marine fish and mammals that make up the traditional diets of some Northern communities (Van Oostdam et al., 1999). Measurements in fish and mammals indicate substantial increases in biotic mercury levels over the past few decades (Rigét et al., 2011); however, the drivers of this trend are not understood. Atmospheric deposition has been implicated as a source of mercury to the Arctic Ocean (Ariya et al., 2004; Lindberg et al., 2002; Lu et al., 2001; Skov et al., 2004), where biological uptake can occur, but cycling between the atmosphere and the ocean in the Arctic remains poorly quantified.

Mercury cycling in the Arctic differs from other environments. In Arctic spring, atmospheric mercury drops rapidly due to Atmospheric Mercury Depletion Events (AMDEs), which convert long-lived elemental mercury to its short-lived divalent form (Steffen et al., 2008). In summer, atmospheric concentrations rise to a level equivalent to or greater than their pre-AMDE values, a phenomenon known as the summer rebound (Holmes et al., 2010). While a substantial body of literature has been devoted to understanding the spring AMDEs (e.g., Ariya et al., 2004; Calvert and Lindberg, 2003; Steffen et al., 2008), less

work has focused on the drivers of the summer rebound. Understanding mercury cycling in summer is especially crucial given that sea ice is at a minimum during this time of year, allowing for enhanced atmosphere-ocean exchange.

Atmospheric mercury concentrations have been measured at sites across the Arctic since the mid-1990s (Berg et al., 2008; Cole and Steffen, 2010; Steffen et al., 2005). Using data from these long-term monitoring sites as constraints for the GEOS-Chem atmosphere-ocean mercury model, I addressed the following questions:

- Can the observed summer rebound in atmospheric mercury be explained using our current understanding of mercury cycling?
- What drives the observed summer rebound, and how does this impact atmosphere-ocean exchange?
- How important is the atmosphere as a source of mercury to the Arctic Ocean, and what other sources may be important?

1.4 Outline and major results

In Chapter 2, I use aircraft observations of CO from the NASA ARCTAS and NOAA ARCPAC campaigns in April 2008 together with multiyear (2003–2008) CO satellite data from the AIRS instrument and the GEOS-Chem CTM to better understand the sources, transport, and interannual variability of pollution in the Arctic in spring. From model simulation of the aircraft data, I find best estimates of CO emissions in April 2008 of

26 Tg month^{-1} for Asian anthropogenic, 9.4 for European anthropogenic, 4.1 for North American anthropogenic, 15 for Russian biomass burning (anomalously large that year), and 23 for Southeast Asian biomass burning. I find that Asian anthropogenic emissions are the dominant source of Arctic CO pollution everywhere except in surface air where European anthropogenic emissions are of similar importance. Russian biomass burning makes little contribution to mean CO (reflecting the long CO lifetime) but makes a large contribution to CO variability in the form of combustion plumes. I analyze two pollution events sampled by the aircraft to demonstrate that AIRS can successfully observe pollution transport to the Arctic in the mid-troposphere. I find that AIRS CO columns over Alaska are highly correlated with the Ocean Niño Index, suggesting a link between El Niño and Asian pollution transport to the Arctic. AIRS shows lower-than-average CO columns over Alaska during April 2008, despite the Russian fires, due to a weakened Aleutian Low hindering transport from Asia and associated with the moderate 2007–2008 La Niña.

In Chapter 3, I use GEOS-Chem simulations of sulfate-ammonium aerosol data from the NASA ARCTAS and NOAA ARCPAC aircraft campaigns in April 2008, together with longer-term data from surface sites, to better understand aerosol sources in the Arctic in winter-spring and the implications for aerosol acidity. Because Arctic pollution is dominated by transport from mid-latitudes, I first test the relevant ammonia and sulfur dioxide emission inventories in the model by comparison with wet deposition flux data over the source continents. I find that a complicated mix of natural and anthropogenic sources with different vertical signatures is responsible for sulfate concentrations in the Arctic. East

Asian pollution influence is weak in winter but becomes important in spring through transport in the free troposphere. European influence is important at all altitudes but never dominant. West Asia (non-Arctic Russia and Kazakhstan) is the largest contributor to Arctic sulfate in surface air in winter, reflecting a southward extension of the Arctic front over that region. Ammonium in Arctic spring mostly originates from anthropogenic sources in East Asia and Europe, with added contribution from boreal fires, resulting in a more neutralized aerosol in the free troposphere than at the surface. I find that East Asian and European aerosol transported to the Arctic is mostly neutralized, whereas West Asian and North American aerosol is highly acidic. I suggest that growth of sulfur emissions in West Asia may be responsible for the observed increase in aerosol acidity at Barrow over the past decade.

In Chapter 4, I use the GEOS-Chem coupled atmosphere-ocean model of mercury, constrained by multi-year observations of atmospheric mercury from surface sites across the Arctic, to better understand the drivers of the observed summer peak in atmospheric mercury concentrations. I show that the summer peak cannot be explained by atmospheric transport from mid-latitudes, re-emission from snowpacks, or ocean kinetics. Instead, I find that a previously unrecognized large source of mercury to the Arctic Ocean of 160 Mg a^{-1} is necessary to reproduce atmospheric observations, and for this I hypothesize discharge from large circumpolar rivers. I assess the importance of this source by constructing an annual budget for mercury in the atmosphere-ocean system and find that the Arctic Ocean acts as a net source to the atmosphere, with implications for biological mercury exposure.

Bibliography

Abbatt, J. P. D., Benz, S., Czizco, D. J., Kanji, Z., Lohmann, U., and Möhler, O.: Solid Ammonium Sulfate Aerosols as Ice Nuclei: A Pathway for Cirrus Cloud Formation, Science, 313, 1770–1773, 2006.

Arendt, A., Walsh, J., and Harrison, W.: Changes of Glaciers and Climate in Northwestern North America during the Late Twentieth Century, Journal of Climate, 22, 4117–4134, 2009.

Ariya, P. A., Dastoor, A. P., Amyot, M., Schroeder, W. H., Barrie, L., Anlauf, K., Raofie, F., Ryzhkov, A., Davignon, D., and Lalonde, J.: The Arctic: a sink for mercury, Tellus B, 56, 397–403, 2004.

Barrand, N. E. and Sharp, M. J.: Sustained rapid shrinkage of Yukon glaciers since the 1957–1958 International Geophysical Year, Geophysical Research Letters, 37, L07 501, 2010.

Barrie, L. A.: Arctic air pollution: An overview of current knowledge, Atmospheric Environment, 20, 643–663, 1986.

Baustian, K. J., Wise, M. E., and Tolbert, M. A.: Depositional ice nucleation on solid ammonium sulfate and glutaric acid particles, Atmospheric Chemistry and Physics, 10, 2307–2317, 2010.

Berg, T., Aspmo, K., and Steinnes, E.: Transport of Hg from Atmospheric mercury depletion events to the mainland of Norway and its possible influence on Hg deposition, Geophysical Research Letters, 35, L09 802, 2008.

Bradley, R. S., Keimig, F. T., and Diaz, H. F.: Recent changes in the North American Arctic boundary layer in winter, Journal of Geophysical Research, 98, 8851–8858, 1993.

Brown, R., Derksen, C., and Wang, L.: A multi-data set analysis of variability and change in Arctic spring snow cover extent, 1967–2008, Journal of Geophysical Research, 115, D16 111, 2010.

Calvert, J. and Lindberg, S.: A modeling study of the mechanism of the halogen-ozone-mercury homogeneous reactions in the troposphere during the polar spring, Atmospheric Environment, 37, 4467–4481, 2003.

Carlson, T. N.: Speculations on the movement of polluted air to the Arctic, Atmospheric Environment, 15, 1473–1477, 1981.

Cole, A. S. and Steffen, A.: Trends in long-term gaseous mercury observations in the Arctic and effects of temperature and other atmospheric conditions, Atmospheric Chemistry and Physics, 10, 4661–4672, 2010.

Galloway, J. N., Townsend, A. R., Erisman, J. W., Bekunda, M., Cai, Z., Freney, J. R., Martinelli, L. A., Seitzinger, S. P., and Sutton, M. A.: Transformation of the Nitrogen Cycle: Recent Trends, Questions, and Potential Solutions, Science, 320, 889–892, 2008.

Hole, L. R., Christensen, J. H., Ruoho-Airola, T., Tørseth, K., Ginzburg, V., and Glowacki, P.: Past and future trends in concentrations of sulphur and nitrogen compounds in the Arctic, Atmospheric Environment, 43, 928–939, 2009.

Holmes, C. D., Jacob, D. J., Corbitt, E. S., Mao, J., Yang, X., Talbot, R., and Slemr, F.: Global atmospheric model for mercury including oxidation by bromine atoms, Atmospheric Chemistry and Physics, 10, 12 037–12 057, 2010.

Jorgenson, M. T., Shur, Y. L., and Pullman, E. R.: Abrupt increase in permafrost degradation in Arctic Alaska, Geophysical Research Letters, 33, L02 503, 2006.

Koch, D. and Hansen, J.: Distant origins of Arctic black carbon: A Goddard Institute for Space Studies ModelE experiment, Journal of Geophysical Research, 110, D04 204, 2005.

Lindberg, S., Brooks, S., Lin, C., Scott, K., Landis, M., Stevens, R., Goodsite, M., and Richter, A.: Dynamic oxidation of gaseous mercury in the Arctic troposphere at polar sunrise, Environmental Science & Technology, 36, 1245–1256, 2002.

Lu, J., Schroeder, W., Barrie, L., Steffen, A., Welch, H., Martin, K., Lockhart, L., Hunt, R., Boila, G., and Richter, A.: Magnification of atmospheric mercury deposition to polar regions in springtime: the link to tropospheric ozone depletion chemistry, Geophysical Research Letters, 28, 3219–3222, 2001.

Martin, S. T., Hung, H. M., Park, R. J., Jacob, D. J., Spurr, R. J. D., Chance, K. V., and Chin, M.: Effects of the physical state of tropospheric ammonium-sulfate-nitrate particles on global aerosol direct radiative forcing, Atmospheric Chemistry and Physics, 4, 183–214, 2004.

Mergler, D., Anderson, H., Chan, L., Mahaffey, K., Murray, M., Sakamoto, M., and Stern, A.: Methylmercury exposure and health effects in humans: a worldwide concern, AMBIO: A Journal of the Human Environment, 36, 3–11, 2007.

Osterkamp, T. E., Jorgenson, M. T., Schuur, E. A. G., Shur, Y. L., Kanevskiy, M. Z., Vogel, J. G., and Tumskoy, V. E.: Physical and ecological changes associated with warming permafrost and thermokarst in Interior Alaska, Permafrost and Periglacial Processes, 20, 235–256, 2009.

Perovich, D. K. and Richter-Menge, J. A.: Loss of Sea Ice in the Arctic, Annual Reviews of Marine Science, 1, 417–441, 2009.

Quinn, P. K., Miller, T. L., Bates, T. S., Ogren, J. A., Andrews, E., and Shaw, G. E.: A 3-year record of simultaneously measured aerosol chemical and optical properties at Barrow, Alaska, Journal of Geophysical Research, 107, 4130, 2002.

Quinn, P. K., Shaw, G., Andrews, E., Dutton, E. G., Ruoho-Airola, T., and Gong, S. L.: Arctic haze: current trends and knowledge gaps, Tellus B, 59, 99–114, 2007.

Quinn, P. K., Bates, T. S., Baum, E., Doubleday, N., Fiore, A. M., Flanner, M., Fridlind, A., Garrett, T. J., Koch, D., and Menon, S.: Short-lived pollutants in the Arctic: their climate impact and possible mitigation strategies, Atmospheric Chemistry and Physics, 8, 1723–1735, 2008.

Quinn, P. K., Bates, T. S., Schulz, K., and Shaw, G. E.: Decadal trends in aerosol chemical composition at Barrow, Alaska: 1976-2008, Atmospheric Chemistry and Physics, 9, 8883–8888, 2009.

Raatz, W. E. and Shaw, G. E.: Long-Range Tropospheric Transport of Pollution Aerosols into the Alaskan Arctic, Journal of Applied Meteorology, 23, 1052–1064, 1984.

Rahn, K. A.: Relative importances of North America and Eurasia as sources of arctic aerosol, Atmospheric Environment, 15, 1447–1455, 1981.

Rigét, F., Braune, B., Bignert, A., Wilson, S., Aars, J., Born, E., Dam, M., Dietz, R., Evans, M., Evans, T., Gamberg, M., Gantner, N., Green, N., Gunnlaugsdóttir, H., Kannan, K., Letcher, R., Muir, D., Roach, P., Sonne, C., Stern, G., and Wiig, Ø.: Temporal trends of Hg in Arctic biota, an update, Science of The Total Environment, 409, 3520–3526, 2011.

Scheuer, E., Talbot, R. W., Dibb, J. E., Seid, G. K., DeBell, L., and Lefer, B.: Seasonal distributions of fine aerosol sulfate in the North American Arctic basin during TOPSE, Journal of Geophysical Research, 108, 8370, 2003.

Serreze, M. C., Holland, M. M., and Stroeve, J.: Perspectives of the Arctic's shrinking ice cover, Science, 315, 1533–1536, 2007.

Shaw, G.: The Arctic haze phenomenon, Bulletin of the American Meteorological Society, 76, 2403–2413, 1995.

Shindell, D. T., Chin, M., Dentener, F., Doherty, R. M., Faluvegi, G., Fiore, A. M., Hess, P., Koch, D. M., MacKenzie, I. A., Sanderson, M. G., Schultz, M. G., Schulz, M., Stevenson, D. S., Teich, H., Textor, C., Wild, O., Bergmann, D. J., Bey, I., Bian, H., Cuvelier, C., Duncan, B. N., Folberth, G., Horowitz, L. W., Jonson, J., Kaminski, J. W., Marmer, E., Park, R., Pringle, K. J., Schroeder, S., Szopa, S., Takemura, T., Zeng, G., Keating, T. J., and Zuber, A.: A multi-model assessment of pollution transport to the Arctic, Atmospheric Chemistry and Physics, 8, 5353–5372, 2008.

Skov, H., Christensen, J., Goodsite, M., Heidam, N., Jensen, B., Wåhlin, P., and Geernaert, G.: Fate of elemental mercury in the Arctic during atmospheric mercury depletion episodes and the load of atmospheric mercury to the Arctic, Environmental Science & Technology, 38, 2373–2382, 2004.

Steffen, A., Schroeder, W., Macdonald, R., Poissant, L., and Konoplev, A.: Mercury in the Arctic atmosphere: An analysis of eight years of measurements of GEM at Alert (Canada) and a comparison with observations at Amderma (Russia) and Kuujjuarapik (Canada), Science of the Total Environment, 342, 185–198, 2005.

Steffen, A., Douglas, T., Amyot, M., Ariya, P., Aspmo, K., Berg, T., Bottenheim, J., Brooks, S., Cobbett, F., Dastoor, A., Dommergue, A., Ebinghaus, R., Ferrari, C., Gårdfeldt, K., Goodsite, M. E., Lean, D., Poulain, A. J., Scherz, C., Skov, H., Sommar, J., and Temme, C.: A synthesis of atmospheric mercury depletion event chemistry in the atmosphere and snow, Atmospheric Chemistry and Physics, 8, 1445–1482, 2008.

Stohl, A.: Characteristics of atmospheric transport into the Arctic troposphere, Journal of Geophysical Research, 111, D11 306, 2006.

Trenberth, K. E., Jones, P., Ambenje, R., Bojariu, R., Easterling, D., Klein Tank, A., Parker, F., Rahimzadeh, J. A., Renwick, M., Soden, B., and Zhai, P.: Observations: Surface and Atmospheric Climate Change, in: Climate Change 2007: The Physical Science Basis. Contribution of Working Group I to the Fourth Assessment Report of the Intergovernmental Panel on Climate Change, edited by Solomon, S., Qin, D., Manning, M., Chen, Z., Marquis, M., Averyt, K. B., Tignor, M., and Miller, H. L., Cambridge University Press, Cambridge, United Kingdom and New York, NY, USA, 2007.

Van Oostdam, J., Gilman, A., Dewailly, E., Usher, P., Wheatley, B., Kuhnlein, H., Neve, S., Walker, J., Tracy, B., Feeley, M., et al.: Human health implications of environmental contaminants in Arctic Canada: a review, The Science of the Total Environment, 230, 1–82, 1999.

Chapter 2

Source attribution and interannual variability of Arctic pollution in spring constrained by aircraft (ARCTAS, ARCPAC) and satellite (AIRS) observations of carbon monoxide

Abstract

We use aircraft observations of carbon monoxide (CO) from the NASA ARCTAS and NOAA ARCPAC campaigns in April 2008 together with multiyear (2003–2008) CO satellite data from the AIRS instrument and a global chemical transport model (GEOS-Chem) to better understand the sources, transport, and interannual variability of pollution in the Arctic in spring. Model simulation of the aircraft data gives best estimates of CO emissions in April 2008 of 26 Tg month^{-1} for Asian anthropogenic, 9.4 for European anthropogenic, 4.1 for North American anthropogenic, 15 for Russian biomass burning (anomalously large that year), and 23 for Southeast Asian biomass burning. We find that Asian anthropogenic emissions are the dominant source of Arctic CO pollution everywhere except in surface air where European anthropogenic emissions are of similar importance. Russian biomass burning makes little contribution to mean CO (reflecting the long CO lifetime) but makes a large contribution to CO variability in the form of combustion plumes. Analysis of two pollution events sampled by the aircraft demonstrates that AIRS can successfully observe pollution transport to the Arctic in the mid-troposphere. The 2003–2008 record of CO from AIRS shows that interannual variability averaged over the Arctic cap is very small. AIRS CO columns over Alaska are highly correlated with the Ocean Niño Index, suggesting a link between El Niño and Asian pollution transport to the Arctic. AIRS shows lower-than-average CO columns over Alaska during April 2008, despite the Russian fires, due to a weakened Aleutian Low hindering transport from Asia and associated with the moderate 2007–2008 La Niña. This suggests that Asian pollution influence over the Arctic may be particularly large under strong El Niño conditions.

2.1 Introduction

The Arctic is a major receptor for mid-latitudes pollution (Quinn et al., 2007; Shaw, 1995). Radiative forcing by pollutants in the Arctic including ozone, aerosols, and black carbon deposited on snow could make a major contribution to regional and global warming (Koch and Hansen, 2005; Shindell et al., 2006a; McConnell et al., 2007; Quinn et al., 2008; Shindell and Faluvegi, 2009). Several studies have identified pollution transport pathways to the Arctic on the basis of model simulations and meteorological analyses (Eckhardt et al., 2003; Klonecki et al., 2003; Koch and Hansen, 2005; Shindell et al., 2008; Stohl, 2006), but our ability to verify these pathways through chemical observations has been limited. Polar-orbiting satellites offer unique platforms for this purpose. We present here an analysis of the sources and transport of Arctic pollution in spring using the GEOS-Chem chemical transport model (CTM) to interpret satellite observations of carbon monoxide (CO) from the Atmospheric InfraRed Sounder (AIRS) together with aircraft measurements from the NASA ARCTAS (Arctic Research of the Composition of the Troposphere from Aircraft and Satellites) and NOAA ARCPAC (Aerosol, Radiation, and Cloud Processes affecting Arctic Climate) campaigns.

Despite 50 years of observations of Arctic pollution, there remains considerable uncertainty concerning the sources. Surface-based studies conducted in the 1970s and 1980s focused on anthropogenic pollution transported from Eastern Europe and Siberia (Barrie, 1986; Carlson, 1981; Raatz and Shaw, 1984; Rahn, 1981). Wintertime influence from

these regions is facilitated by cold surface temperatures and stable conditions, enabling low-altitude isentropic transport to the Arctic (Barrie, 1986; Klonecki et al., 2003; Law and Stohl, 2007; Stohl, 2006). Pollutants from Asia and North America, emitted at lower latitudes and therefore warmer temperatures, were thought to be inhibited from entering the Arctic by the "polar dome", an isentropic transport barrier.

Recent research has called into question the predominance of Europe as the main source of Arctic pollution. Modeling studies have shown that while near-surface pollution may still be dominated by European sources, transport from Asia and North America is possible at higher altitudes, facilitated by lofting of pollutants by warm conveyor belts (WCBs) (Koch and Hansen, 2005; Shindell et al., 2008; Stohl, 2006). Furthermore, with the collapse of the Soviet Union, strict emission controls in the European Union, and the rapid industrialization of China and Southeast Asia, the global distribution of emissions has changed dramatically over the past 20 years. Several studies show increasing contributions from Asia but disagree quantitatively on the importance of this source for overall Arctic pollution (Koch and Hansen, 2005; Shindell et al., 2008; Stohl, 2006). As interest in Arctic pollution has broadened from air quality to climate impacts, there is a pressing need to understand pollution sources not only at the surface but throughout the troposphere.

Biomass burning has recently been suggested as an additional important source of Arctic pollution. Black carbon records in Greenland ice cores show large concentrations attributable to fire emissions dating back to the pre-industrial era (McConnell et al., 2007), and more recent measurements in snow suggest that biomass burning accounts for more

than 90% of the black carbon deposited in the Arctic in spring (Hegg et al., 2009). Fires in Eastern Europe and Russia have been shown to cause substantial increases in the atmospheric loading of pollutants including CO, ozone, and aerosols measured at surface sites in the European Arctic (Stohl et al., 2007). Early analysis of the ARCPAC aircraft data identified a substantial contribution from Russian forest fires and central Asian agricultural burning to atmospheric pollution over Alaska (Warneke et al., 2009).

CO is emitted by incomplete combustion, and we use it here as a tracer of pollution. Its atmospheric lifetime against oxidation by the hydroxyl radical (OH) is on average two months, long enough to track transport on intercontinental scales but short enough to show well-defined concentration gradients (Heald et al., 2003a; Liang et al., 2004; Liu et al., 2003; Staudt et al., 2001; Turquety et al., 2008; Yashiro et al., 2009). In a recent intercomparison of 11 CTMs, simulated CO concentrations disagreed by a factor of 2–3 at all altitudes in the Arctic due to model differences in emissions, transport, and OH concentrations (Shindell et al., 2008). There is a need to better understand CO sources and transport to the Arctic as an indicator of pollution influence.

Satellite observations present a unique perspective to address these issues. CO is readily detectable from space at infrared (IR) wavelengths, and data are available from a number of satellite instruments, including MOPITT, AIRS, TES, SCIAMACHY, and IASI. AIRS is particularly promising for studying pollution transport to the Arctic because of its high spatial density (up to 70% global coverage daily) (McMillan et al., 2005), sensitivity at high latitudes, cloud-clearing capabilities (Susskind et al., 2003), and multi-year record (con-

tinuous observations since mid-2002). It is a nadir-viewing thermal IR sounder onboard NASA's polar-orbiting Aqua satellite and retrieves CO at 4.7 μm (McMillan et al., 2011). As with all thermal IR sounders, the sensitivity to CO is strongest in the mid-troposphere and generally weak in the boundary layer, with little vertical resolution (McMillan et al., 2008; Warner et al., 2007); however, in some instances, AIRS can see CO enhancements down to the top of the boundary layer (McMillan et al., 2011, 2010). Validation of AIRS CO retrievals in the northern hemisphere indicates AIRS is biased approximately 10% high from 300–900 mb, with little quantitative sensitivity to the boundary layer (McMillan et al., 2011). AIRS CO observations have been shown to successfully track the transpacific transport of Asian pollution to North America (Zhang et al., 2008) and the transatlantic transport of North American wildfire emissions to Europe (McMillan et al., 2008). Total column AIRS CO retrievals have been validated at three high-latitude sites (Yurganov et al., 2010), but application to Arctic pollution transport had not previously been tested.

Aircraft data from the ARCTAS and ARCPAC campaigns based in Alaska in April 2008 can help evaluate the utility of the AIRS data for observing long-range transport to the Arctic. The in situ measurements provide highly accurate information on the structure of Arctic CO distributions, allowing an independent test of the AIRS CO data. The aircraft observations can further provide quantitative constraints on sources of CO in the Arctic.

We examine here the influence of different source types (fuel combustion, biomass burning) and mid-latitude source regions on Arctic pollution in spring, using the GEOS-Chem CTM as a platform for intercomparing the aircraft and satellite datasets. We first use

the aircraft observations to constrain the CO sources in the CTM and subsequently use the CTM to quantify the source contributions to Arctic CO pollution. The aircraft observations together with the CTM are used to test the ability of AIRS to observe high-latitude pollution transport. We then use AIRS observations to investigate the interannual variability of CO transport to the Arctic.

2.2 Model description

We use the GEOS-Chem CTM version 8-01-04 (http://acmg.seas.harvard.edu/geos/index.html) driven by GEOS-5 assimilated meteorology from the NASA Global Modeling and Assimilation Office (GMAO) Goddard Earth Observing System (GEOS). The native resolution of GEOS-5 is $0.5^\circ \times 0.667^\circ$ with 72 vertical levels; we regrid to $2^\circ \times 2.5^\circ$ for input to GEOS-Chem. The GEOS-Chem simulation of CO has previously been used to track intercontinental transport of pollution (Duncan and Bey, 2004; Heald et al., 2003a; Jaffe et al., 2004; Li et al., 2002; Liang et al., 2004; Liu et al., 2003; Zhang et al., 2008) and has been extensively compared to in situ and satellite observations (Duncan and Logan, 2008; Duncan et al., 2007; Heald et al., 2006; Hudman et al., 2008; Jaeglé et al., 2003; Kiley et al., 2003; Koike et al., 2006; Liu et al., 2003).

We simulate April 2008 preceded by a 10-month spin-up. Anthropogenic (fossil fuel and biofuel) sources of CO are simulated using state-of-the-science regional emission inventories as described in Table 2.1. Emissions from sources not accounted for in the regional inventories are taken from the EDGAR 3.2 FT2000 global emissions inventory for

2000 (Olivier et al., 1999; Olivier and Berdowski, 2001). Biomass burning emissions are from the Fire Locating and Monitoring of Burning Emissions (FLAMBE) inventory (Reid et al., 2009), which provides carbon emissions at $1^\circ \times 1^\circ$ spatial resolution and hourly temporal resolution based on both MODIS and GOES satellite fire counts (Naval Research Laboratory, http://www.nrlmry.navy.mil/flambe/). CO emissions are subsequently calculated using emission factors from Andreae and Merlet (2001). All emissions are injected into the local planetary boundary layer as defined from the GEOS-5 data. While this could cause an underestimate of vertical transport of CO from the most energetic fires, recent work has shown that direct free tropospheric injection of biomass burning plumes is infrequent (Kahn et al., 2008; Labonne et al., 2007; Val Martin et al., 2010).

Additional sources of CO in our simulation include oxidation of methane (CH_4) and non-methane volatile organic compounds (NMVOCs). Methane is specified using latitudinally-resolved observations from the NOAA/ESRL/GMD network (Dlugokencky et al., 2008). A yield of one CO molecule per oxidized CH_4 molecule is assumed. Oxidation of anthropogenic and biomass burning NMVOCs is simulated by increasing direct CO emissions from these sources by 19% and 11% respectively (Duncan et al., 2007). Biogenic NMVOC sources in the model include isoprene, monoterpenes, methanol, and acetone. All NMVOCs are assumed to oxidize immediately to CO with yields given by Duncan et al. (2007). These indirect emissions are not included in the regional CO emission totals given later in the paper.

We use a linear CO simulation (Duncan et al., 2007) with monthly mean archived OH

Table 2.1: Global CO sources for April 2008 used in GEOS-Chem simulations.

Source	CO Emission (Tg.month^{-1})	
	Prior Simulation[a]	Optimized Simulation[b]
Anthropogenic[c]	51	59
North America[d] (172.5–17.5° W, 24–88° N)	4.2	4.1
Europe[e] (17.5° W–60°E, 33–88° N)	6.2	9.4
Siberia[f] (60–172.5°E, 50–88° N)	0.4	0.4
Asia[g] (60–152.5°E, 0–50° N)	22	26
Rest of the world[f]	9.9	9.9
Secondary production from NMVOC oxidation[h]	8.1	9.4
Biomass Burning[i]	104	58
North America (172.5–17.5° W, 24–88° N)	0.3	0.3
Europe (17.5° W–60°E, 33–88° N)	2.0	2.0
Russia/Kazakhstan (60–152.5°E, 33–60° N)	29	15
Southeast Asia (60–152.5°E, 0–33° N)	51	23
Rest of the world	12	12
Secondary production from NMVOC oxidation[h]	10	5.8
Biogenic[j]	29	29
Methane	71	71
TOTAL	255	217

[a] Monthly source totals from the original GEOS-Chem emission inventories.

[b] Changes from the prior simulation reflect source corrections based on the ARCTAS and ARCPAC aircraft observations (Table 2.2).

[c] Anthropogenic sources include fossil fuel and biofuel emissions.

[d] North America includes Canada, the United States, and Mexico. Primary emissions over the US are derived by decreasing the US Environmental Protection Agency National Emission Inventory (EPA-NEI99, http://www.epa.gov/ttnchie1/net/1999inventory.html) CO emissions by 60%, following Hudman et al. (2008). Canadian emissions are from the Criteria Air Contaminants (CAC) inventory (Environment Canada, http://www.ec.gc.ca/pdb/cac/cac_home_e.cfm) and Mexican emissions are from the Big Bend Regional Aerosol and Visibility Observational Study Emissions Inventory (BRAVO) (Kuhns et al., 2005).

[e] European anthropogenic emissions are from the Cooperative Programme for Monitoring and Evaluation of the Long-range Transmission of Air Pollutants in Europe (EMEP) inventory (Vestreng and Klein, 2002).

[f] Siberian and "rest of the world" anthropogenic emissions are from the EDGAR 3.2 FT2000 inventory (Olivier et al., 1999; Olivier and Berdowski, 2001).

[g] Asian emissions are derived from the NASA INTEX-B inventory for 2006 (Zhang et al., 2009) with seasonality based on monthly activity levels of NO_x emissions (Zhang et al., 2007).

[h] Secondary CO sources are computed by increasing direct CO emissions by 11% for biomass burning emissions and by 19% for anthropogenic emissions (Duncan et al., 2007). Over the US, anthropogenic CO is increased by 39% rather than 19% to account for the improved CO source estimate from Hudman et al. (2008).

[i] Biomass burning CO emissions are from the FLAMBE inventory (Reid et al., 2009) and are computed as described in the text.

[j] The source from the oxidation of biogenic NMVOCs is computed following Duncan et al. (2007) and includes acetone and methanol as well as the Model of Emissions of Gases and Aerosols from Nature (MEGAN) inventory for isoprene and monoterpenes (Guenther et al., 2006).

concentrations from a previous GEOS-Chem full-chemistry simulation (Park et al., 2004). The annual global mean OH concentration in our simulation is 10.8×10^5 molecules cm^{-3}. This is close to the 25-model mean of $11.1\pm1.7\times10^5$ molecules cm^{-3} reported in the Shindell et al. (2006b) CTM intercomparison and higher than the 9.4×10^5 molecules cm^{-3} reported for GEOS-Chem in that comparison. For source attribution, the linearity of the model permits us to include tagged CO tracers from individual sources that are consistent with the overall CO simulation.

Model CO emissions for April 2008 are shown in Fig. 2.1 and summarized in Table 2.1. The highest emissions (red hotspots in Fig. 2.1) are due to biomass burning, with particularly intense fire activity over Southeast Asia (Vietnam and Myanmar) and over southern Russia near the Russia-China border. The FLAMBE inventory includes 51 Tg month^{-1} of CO emissions from Southeast Asian fires in April. This value is more than twice that reported in previous studies (e.g., 18 Tg month^{-1} for April in Duncan et al. (2003), and 23 Tg month^{-1} in Heald et al. (2003b)) and in other inventories (e.g., 6 Tg month^{-1} in GFED2). Satellite fire counts for the region show no significant increases in burning in 2008 relative to other years (Acker and Leptoukh, 2007). The FLAMBE emissions inventory is probably too high, as discussed further below. Russian fires during April 2008 were much more intense than usual at that time of year because of lower-than-normal snow cover during the previous winter (Warneke et al., 2009). Figure 2.2 shows a timeseries of 2001–2008 monthly fire counts from the MODIS instrument aboard the Terra satellite. Satellite fire counts over Russia in April 2008 were 2.5 times the April average and higher than for

any month of the record except May 2003.

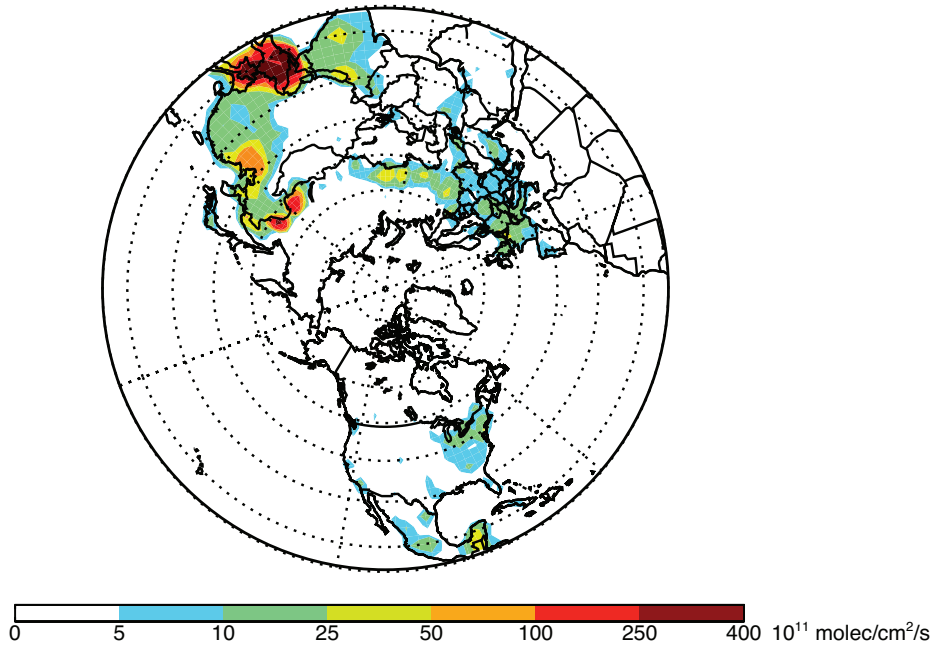

Figure 2.1: CO combustion sources for April 2008 (excluding secondary CO from oxidation of biogenic NMVOCs and methane). Values are shown for the optimized simulation but patterns are similar for the prior simulation.

To compare GEOS-Chem and in situ aircraft CO, the model is sampled along the flight track at the same time and location as the observations. The aircraft data are averaged over the GEOS-Chem grid and time-step. For comparison with AIRS, GEOS-Chem is sampled at the AIRS overpass locations and averaged over a 3-h window centered at the 13:30 local overpass time. AIRS retrieves CO profiles on nine trapezoidal pressure layers sampled from the 100 AIRS pressure levels. GEOS-Chem model profiles are convolved to AIRS retrieval space using the convolution equation (McMillan et al., 2011; Olsen et al., 2007)

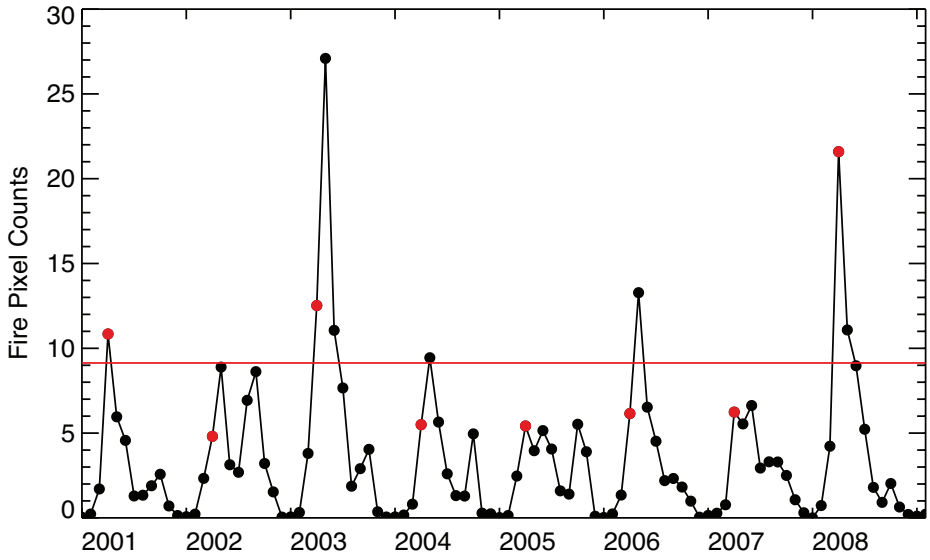

Figure 2.2: Monthly mean fire counts (cloud and overpass corrected) for southern Russia and Kazakhstan (33–60° N, 60–152.5° E) from the MODIS instrument aboard the Terra satellite. Fire counts for April of each year are in red. The red solid line shows the 2001–2008 April mean. Data courtesy of NASA Goddard Earth Sciences Data and Information Services Center.

and summed over the 100 pressure levels to compute the modeled total CO column:

$$\hat{y}_m = \sum_i z_{a,i} \exp\left(\mathbf{FAF}' \cdot \ln \frac{z_{m,i}}{z_{a,i}}\right), \tag{2.1}$$

where $\hat{y}_m$ is the convolved model column, $z_{m,i}$ is the original model profile of partial columns interpolated onto the 100 AIRS pressure levels i, $z_{a,i}$ is the AIRS retrieval a priori profile of partial columns, $\mathbf{F}$ is a 100×9 matrix that defines the nine vertical trapezoidal layers on which AIRS CO is retrieved, $\mathbf{F}'$ is its pseudo-inverse, and $\mathbf{A}$ is a 9×9 averaging kernel matrix in the trapezoidal space. The degrees of freedom (DOF) for signal, measuring the number of pieces of information in the vertical profile, are generally less than 1.5 (Kopacz et al., 2010), so we use total column CO rather than profiles. The column sensi-

tivity as indicated by the averaging kernels is low in the boundary layer and has a broad maximum at 300–600 hPa (McMillan et al., 2011, 2010; Warner et al., 2007).

In this study we use version 5 AIRS CO retrievals (available from http://disc.sci.gsfc.nasa.gov/AIRS/data-holdings/by-data-product/) and, following the recommendations in McMillan et al. (2011), include only daytime AIRS observations with DOF for signal greater than 0.5 retrieved over surfaces with temperature above 250 K. These thresholds eliminate on average 20% of the available daytime observations globally and 25% in the Arctic in April.

2.3 CO observations and constraints on sources

Jacob et al. (2010) give a general description of the NASA ARCTAS campaign. A major goal was to observe long-range transport of pollution to the Arctic using a DC-8 aircraft based in Fairbanks, Alaska from 1 to 19 April 2008. CO measurements were made using the Differential Absorption of CO Measurement (DACOM) instrument at a frequency of 1 Hz and accuracy of 2% (Sachse et al., 1987). The NOAA ARCPAC campaign (Warneke et al., 2009) took place concurrently using a WP-3D aircraft also based in Fairbanks with flights from 3 to 23 April 2008 (all but one after 11 April). CO measurements were made by vacuum ultraviolet resonance fluorescence at a frequency of 1 Hz and accuracy of 5% (Holloway et al., 2000).

Observed and modeled CO concentrations along the ARCTAS and ARCPAC flight tracks are shown in Fig. 2.3. Observed concentrations during ARCTAS ranged from 23 to

296 ppbv (excluding observations south of 55° N from transit flights). Less than 1% of the observations had concentrations greater than 250 ppbv. Low values signify stratospheric air and are removed for subsequent analysis as described below. Observed concentrations during ARCPAC ranged from 96 to 383 ppbv. The highest CO concentrations were observed over and around Alaska and were due to Asian pollution and Russian fires, as discussed below. High-CO layers were also sampled elsewhere, in particular near the North Pole by the DC-8. The GEOS-Chem simulation with prior emissions (Fig. 2.3, middle panels) shows qualitative agreement with the observations but quantitative discrepancies are evident. Modeled concentrations are generally too low, although they are sometimes too high in plumes over and around Alaska, suggesting different model errors for the different sources affecting the Arctic.

Figure 2.4 shows the median vertical distribution of the aircraft CO observations along with the corresponding model values. Stratospheric observations, diagnosed as $[O_3]/[CO] > 1.25\,\mathrm{mol\,mol^{-1}}$ (Hudman et al., 2007), were removed from the data set. The median observed CO concentration at the surface was 160 ppbv. The data show little or no decrease up to 5 km and a sharp decrease above. The ARCTAS data show the most variability in the mid-troposphere (3–6 km). The ARCPAC data show greater variability than the ARCTAS data at all altitudes.

The red lines in Fig. 2.4 show the median CO profiles from the GEOS-Chem simulation with prior emissions. Relative to both aircraft data sets, the model is 10 ppbv too low near the surface. This difference decreases with altitude and disappears in the up-

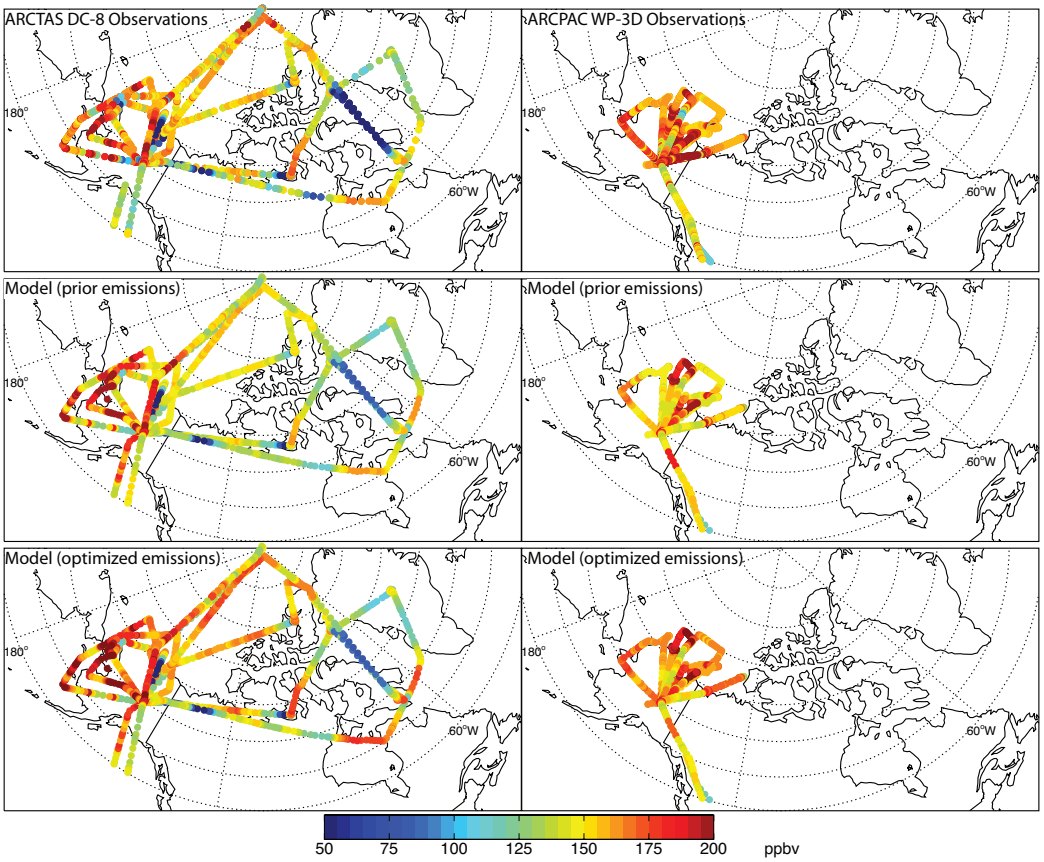

Figure 2.3: CO concentrations during ARCTAS (1 to 19 April 2008) and ARCPAC (3 to 23 April 2008). Aircraft observations (top) are compared to model values sampled along the flight tracks and using prior (middle) or optimized (bottom) emissions. The flight tracks extend from 0 to 12 km (ARCTAS) and 8 km (ARCPAC); low values correspond to the stratosphere. Observations south of 55° N taken during transit flights are excluded. For ARCTAS flights, observed CO concentrations range from 23 to 296 ppbv, while modeled concentrations range from 33 to 243 ppbv with prior emissions and 34 to 226 ppbv with optimized emissions. For ARCPAC flights, observed concentrations range from 96 to 383 ppbv, while modeled concentrations range from 112 to 255 ppbv with prior emissions and 115 to 221 ppbv with optimized emissions.

per troposphere. The underestimate of CO at northern extratropical latitudes in spring is a general problem in current CTMs (Shindell et al., 2006b). We correct the discrepancy here by adjusting emissions based on the assumption that emission errors in the model are systematic, model transport errors are random, and model OH errors are small. We thus estimate the correction to emissions by performing least squares multiple linear regression

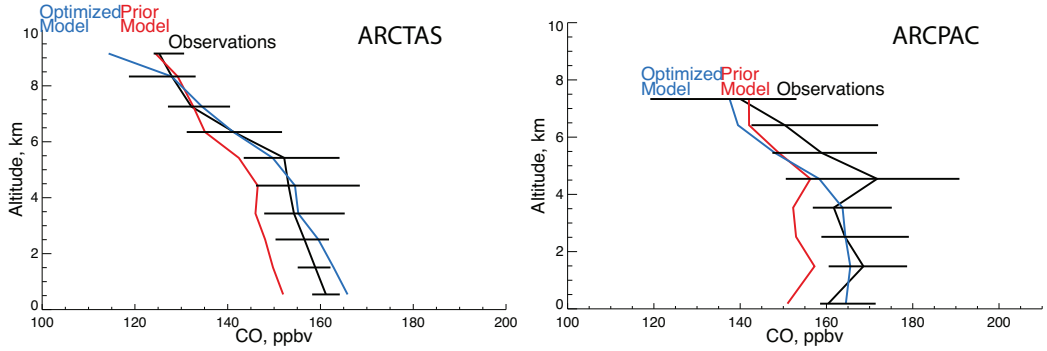

Figure 2.4: Median vertical distribution of CO concentrations in ARCTAS (1 to 19 April 2008) and ARCPAC (3 to 23 April 2008), averaged over 1-km altitude bins. Observations are compared to model values with prior and optimized emissions. Black horizontal bars show the interquartile range of the observations. Stratospheric observations identified by $[O_3]/[CO] > 1.25$ mol mol^{-1} have been removed.

to the aircraft observations of model results for five tagged tracers of CO sources: (1) North American anthropogenic (fossil fuel and biofuel), (2) European anthropogenic, (3) Asian anthropogenic, (4) Russian biomass burning, and (5) Southeast Asian biomass burning. Emissions from these five sources are assumed to represent the only sources of model error. The regression is performed after first subtracting the modeled contribution from all other sources from the total modeled and observed CO. The resulting fit coefficients represent the source corrections needed to minimize the discrepancy between observations and model. The fit is conducted using all tropospheric data from both ARCTAS (1454 points from 9 flight days) and ARCPAC (1251 points from 9 flight days), including data from transit flights to the Arctic.

Table 2.2 shows the emission scaling factors from the least squares fit with confidence intervals determined using the bootstrap method. The resulting emission estimates are given in Table 2.1 and Fig. 2.1. We find that we need to increase anthropogenic emissions

Table 2.2: Correction factors to prior CO combustion sources in GEOS-Chem[a].

Source	Correction factor
North American anthropogenic	0.96±0.16
European anthropogenic	1.52±0.18
Asian anthropogenic	1.18±0.11
Russian biomass burning	0.53±0.09
Southeast Asian biomass burning	0.45±0.11

[a] Source correction factors to the prior emission inventories of Table 2.1, derived using a multiple linear regression between GEOS-Chem tagged tracers and aircraft observations from ARCTAS (1 to 19 April 2008) and ARCPAC (3 to 23 April 2008) as described in the text. Anthropogenic sources include fossil fuel and biofuel. Errors show the 95% confidence interval calculated by the bootstrap method.

from East Asia and from Europe to correct the underestimate of the background (Fig. 2.4) and in the eastern part of the ARCTAS domain (Fig. 2.3). No correction is needed for our North American anthropogenic emissions (Table 2.2), where our prior emissions are consistent with other observational constraints (Hudman et al., 2008; Kopacz et al., 2010).

Our finding that current anthropogenic emission inventories for Europe and Asia are too low is consistent with the recent inverse model analysis of Kopacz et al. (2010), which was constrained by an ensemble of satellite data (MOPITT, AIRS, and SCIAMACHY) and verified against aircraft and ground-based measurements. They found that the inventories need to be increased in seasons other than summer. Their optimized April anthropogenic emissions of 8.0 Tg month^{-1} for Europe and 28 Tg month^{-1} for Asia are consistent with our estimates of 9.4 Tg month^{-1} for Europe and 26 Tg month^{-1} for Asia. Kopacz et al. (2010) suggested that the spring underestimate in the inventories may reflect emissions from residential fuel use and vehicle cold starts. These sources are included in the Zhang et al. (2009) inventory used as our prior for Asia but with the assumptions that residential fuel use peaks from November through March and that cold starts have no seasonal vari-

ation. It is unlikely that the discrepancy over Asia reflects growth in CO emissions since 2006 (the base year for the emissions inventory), as recent increased energy use has largely been offset by technology renewals (Zhang et al., 2009).

The ARCTAS and ARCPAC data suggest that we need to decrease biomass burning emissions in the FLAMBE inventory by a factor of 0.5 over southern Russia and by a factor of 0.4 over Southeast Asia. The downward correction results in an optimized estimate of 15 Tg CO from Russian fires and 23 Tg CO from Southeast Asian fires in April, the latter in agreement with previous estimates of 18–23 Tg month^{-1} (Duncan et al., 2003; Heald et al., 2003b).

Modeled CO concentrations from the optimized simulation are shown along the flight tracks in Fig. 2.3 (lower panels) and the profiles are shown as blue lines in Fig. 2.4. The source correction eliminates the model error below 4 km for both campaigns. Above 4 km, the optimization eliminates the error relative to ARCTAS but not ARCPAC. After source correction, the Pearson correlation coefficient between observations and simulation improves from $r = 0.50$ to $r = 0.60$ for ARCTAS and from $r = 0.49$ to $r = 0.53$ for ARCPAC. The low correlation coefficients are driven by the high CO values found in some fine-structure plumes, where large model error is expected due to both plume smearing and displacement (Rastigejev et al., 2010). We tried removing the plumes before performing the least squares fit but this did not significantly alter the resultant source correction factors.

To further test the optimization of sources, we conducted independent comparisons with observations using CO column data from a surface site at Eureka, Nunavut (80° N, 86° W)

and from the AIRS satellite instrument. The measurements at Eureka were made with a Bruker Fourier Transform Spectrometer (FTS) (Batchelor et al., 2009). Intercomparison with the DC-8 during a spiral over the site on 8 April 2008 showed agreement within 0.01×10^{18} molecules cm^{-2} (0.5%). Figure 2.5 shows that the source correction reduces the mean model bias relative to observations from -6% with prior sources to -1% with optimized sources.

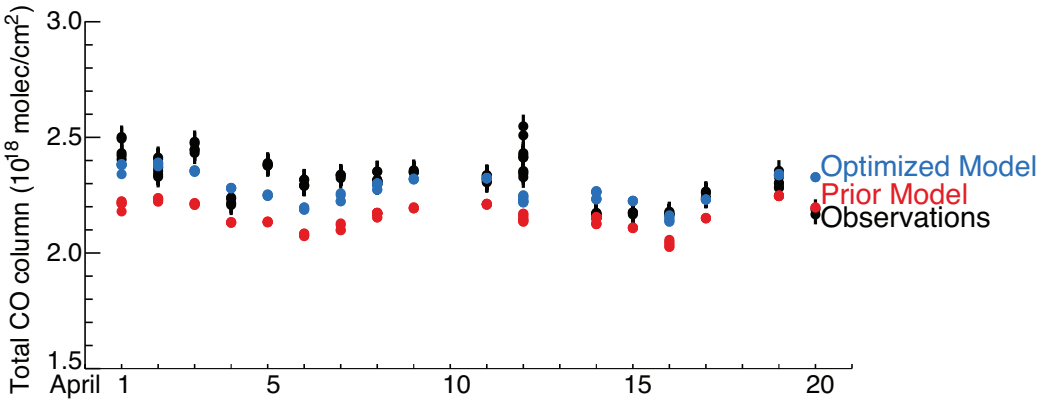

Figure 2.5: CO columns at Eureka, Nunavut, Canada (86.4° W, 80.0° N) from 1 to 20 April 2008. Measurements by a ground-based Fourier Transform Spectrometer are compared to model values with both prior and optimized sources. Black vertical bars show the uncertainties of the measurements.

Figure 2.6 shows the mean April 2008 AIRS CO columns compared to the GEOS-Chem model values from the optimized simulation. Both AIRS and GEOS-Chem show the highest pollution levels in the European sector of the Arctic, followed by the Asian sector. The North American Arctic is least polluted. Transport of European pollution takes place directly northward over Scandinavia, while transport from Asia is northeastward, entering the Arctic over Siberia and Alaska. Averaged over the Arctic, GEOS-Chem is 3% lower than AIRS. Comparison with the prior simulation (not shown) revealed positive errors over

the southern Russian fire source and outflow regions due to the significant overestimate of fire emissions. Meanwhile, the optimized GEOS-Chem simulation shows the largest underestimate over the region of the Russian fires, which may indicate that the factor of two downward correction to the FLAMBE inventory is too large.

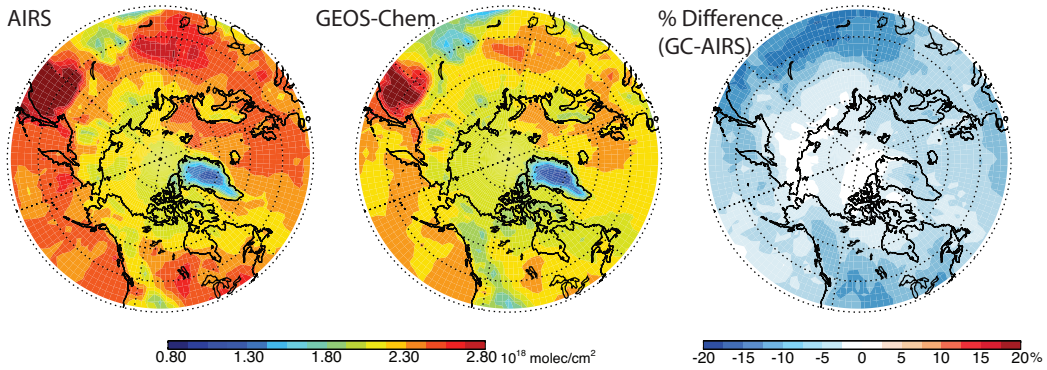

Figure 2.6: Mean CO columns during April 2008 observed by the AIRS satellite instrument (version 5) and simulated by GEOS-Chem with optimized sources (and AIRS averaging kernels applied). The right panel shows the percent difference between the two. GEOS-Chem was sampled along the AIRS orbit tracks at the time of successful retrievals (see text).

2.4 Sources of Arctic pollution in April 2008

We use the GEOS-Chem tagged tracers to decompose the optimized simulated CO vertical profiles from ARCTAS and ARCPAC (Fig. 2.4, blue lines) into the contributions from individual sources. Figure 2.7 shows the median profiles along the flight tracks of the five dominant sources, which on average account for 67% of total CO during the campaigns. For both campaigns, mean concentrations are dominated by Asian anthropogenic emissions along with a substantial contribution from European anthropogenic emissions, especially at low altitude. These mean contributions largely reflect the wintertime accumulation of

CO over the scale of the northern extratropical hemisphere. Emissions from Russian fires, which did not begin until April (Fig. 2.2), have much less impact on the mean pollution influence.

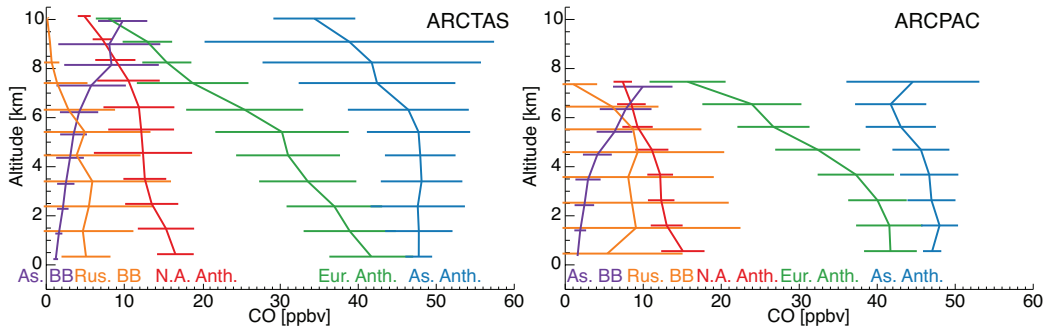

Figure 2.7: Median vertical distribution along the ARCTAS and ARCPAC flight tracks of GEOS-Chem CO concentrations tagged by source region and type: Asian anthropogenic (As. Anth., blue), European anthropogenic (Eur. Anth., green), North American anthropogenic (N.A. Anth., red), Russian biomass burning (Rus. BB, orange) and Southeast Asian biomass burning (As. BB, purple). Horizontal bars are standard deviations.

Conversely, Russian biomass burning makes a large contribution to CO variability (horizontal bars in Fig. 2.7). During ARCPAC, the variability at all altitudes is dominated by the Russian biomass burning source, consistent with the large biomass burning plume influence observed during the campaign (Warneke et al., 2009). The Russian biomass burning contribution is smaller during ARCTAS and is comparable to the contributions from the continental anthropogenic sources, reflecting differences in sampling strategy between the two campaigns. The Asian anthropogenic and Southeast Asian biomass burning sources dominate variability in the upper troposphere for the ARCTAS flights. This reflects the dominant pathway of Asian outflow in spring involving uplift in WCBs off the Pacific coast, as was previously observed in the TRACE-P aircraft campaign (Liu et al., 2003).

Stohl (2006) identified this as the only major transport pathway from Asia to the Arctic, with subsequent influence at the Arctic surface involving subsidence on a time scale of a month. The lifetime of CO is sufficiently long for this subsidence to operate, leading to a general Asian pollution influence in the Arctic background.

Figure 2.8 shows the April 2008 mean contributions of each tracer in different altitude bands over the scale of the Arctic. Asian anthropogenic emission is the dominant contributor throughout the Arctic above 2 km, reflecting the high-altitude WCB transport pathway. There is some lifting of European pollution affecting the middle troposphere in the European and Siberian sectors of the Arctic. In the boundary layer, Asian and European anthropogenic influences are of comparable magnitude but have distinct geographical signatures. European influence dominates in the European sector of the Arctic, reflecting near-surface northward transport over Scandinavia, and also over eastern Siberia, reflecting westerly transport. We see from Fig. 2.8 that this trans-Siberian transport is the dominant pathway by which European pollution affects Alaska. Our finding of European influence lifted to the middle troposphere and transported across Siberia in April differs from the prevailing winter situation (Klonecki et al., 2003; Stohl, 2006) when European pollution is strongly confined to the boundary layer and the circulation around the Siberian high carries it to the Arctic rather than eastward across Siberia.

Relative to other anthropogenic sources, pollution from North America makes little contribution to Arctic background concentrations. North American influence is limited to the lowest 5 km and to the Canadian Archipelago, Davis Strait, and Greenland. Like Asian

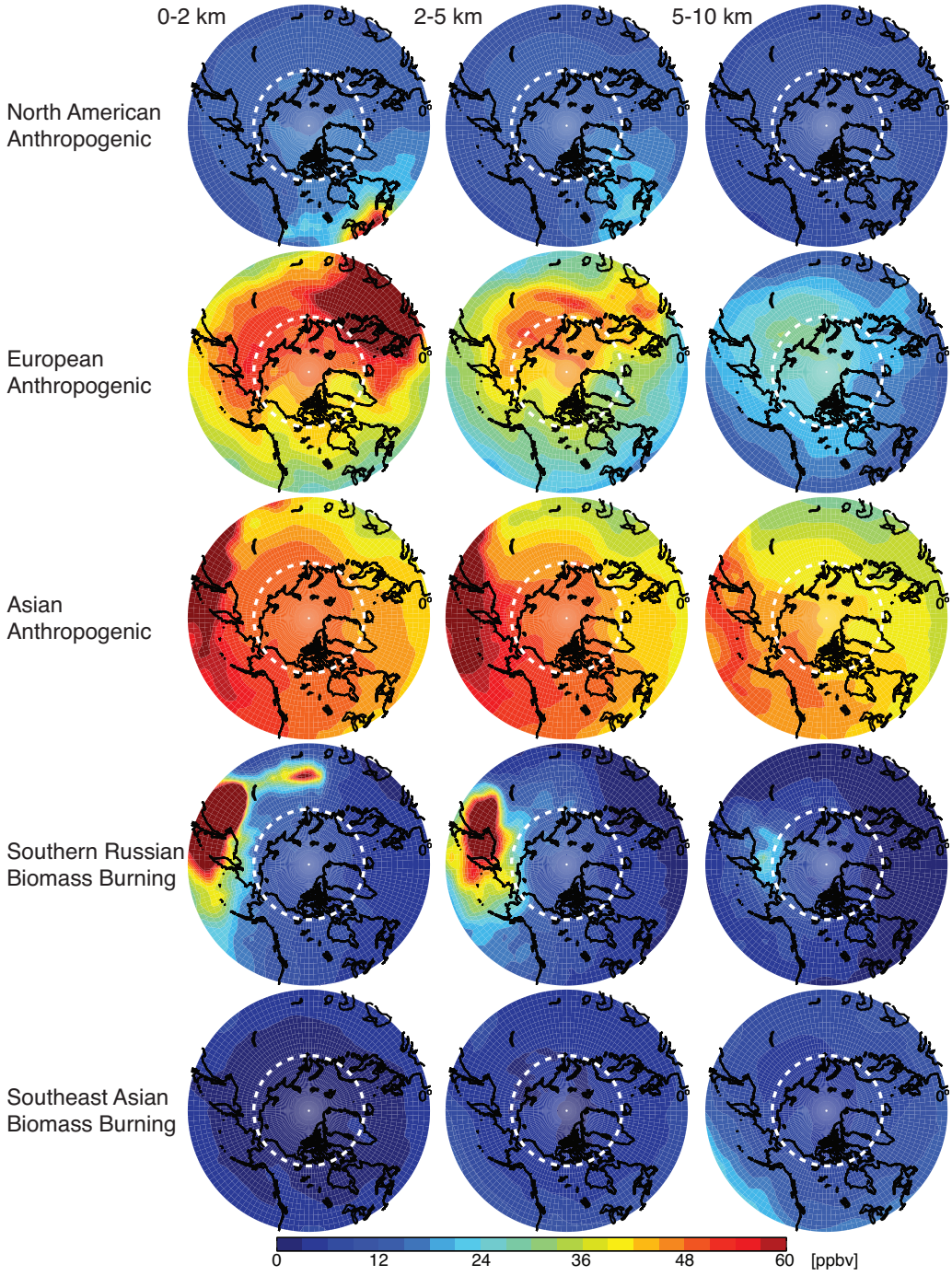

Figure 2.8: Contributions of different mid-latitude source regions to CO pollution in the Arctic in April 2008, as indicated by the GEOS-Chem simulation. Results are shown as mean CO mixing ratios in altitude bands of 0–2, 2–5, and 5–10 km. The Arctic Circle is indicated by a dashed white line.

sources, North American emissions reach the Arctic via uplift and transport associated with WCBs (Stohl, 2006); however, CO emissions in North America are much weaker than in Asia (Table 2.1).

Shindell et al. (2008) previously found in a multi-model CO intercomparison that the Arctic in spring was most sensitive to European sources, followed by North American then Asian sources. The difference with our results reflects the magnitude of emissions. The multi-model mean total emissions (anthropogenic and biomass burning) in Shindell et al. (2008) were 156, 90, and 129 $\mathrm{Tg\,a^{-1}}$ for East Asia, Europe, and North America, respectively; whereas our corresponding totals are 234, 135, and 77 $\mathrm{Tg\,a^{-1}}$ for anthropogenic sources alone. Our higher Asian emissions and lower North American emissions are consistent with recent inverse analyses (Fortems-Cheiney et al., 2009; Heald et al., 2004; Hudman et al., 2008; Kopacz et al., 2010, 2009; Streets et al., 2006; Tanimoto et al., 2008).

Although Southeast Asian fires were a large northern hemispheric source of CO during April 2008 (Fig. 2.1 and Table 2.1), their influence on the Arctic is minimal because of the low latitude of emissions and the dominance in spring of venting by deep convective events (Liu et al., 2003). The small fraction of these emissions that reaches the Arctic does so in the upper troposphere (Figs. 2.7 and 2.8), reflecting isentropic transport (Klonecki et al., 2003) along with transport by WCBs (Bey et al., 2001; Liang et al., 2004; Liu et al., 2003). Even in the upper troposphere, the Southeast Asian fire influence is smaller than the Asian anthropogenic influence.

2.5 Variability of Arctic pollution observed by AIRS

AIRS provides a unique perspective on variability of transport to the Arctic. In this section we first test the ability of AIRS to observe long-range pollution transport to the Arctic by investigating two pollution events of different origins observed by the aircraft during ARCTAS. We then assess the representativeness of the April 2008 observations using the AIRS multi-year record (2003–2008) and more generally interpret the interannual variability observed by AIRS.

AIRS version 5 total column retrievals for 2003–2007 have been validated against FTIR data at three high latitude sites and show excellent agreement (Yurganov et al., 2010). At Ny Alesund (80° N), the mean annual bias is near zero. Mean bias is also near zero at Kiruna (68° N) and Harestua (60° N) for DOF for signal greater than 0.7, but negative biases are observed at lower DOF. Overall, northern hemispheric AIRS total column observations in April show an 8% negative bias relative to FTIR data. Validation of AIRS CO retrievals in the northern hemisphere with aircraft in situ profiles indicates AIRS is biased approximately 10% high from 300–900 mb with little quantitative sensitivity to the boundary layer, like all thermal IR sounders (McMillan et al., 2011). In the Arctic, this lack of sensitivity may be compounded by the cold surface. We therefore expect AIRS to be capable of identifying transport to the Arctic in the mid-troposphere but not at low altitude, and test this below with two case studies of pollution plumes observed by ARCTAS.

Figure 2.9 shows CO concentrations on 16 April 2008 observed by the DC-8 aircraft

and total column CO observed by AIRS, together with the corresponding GEOS-Chem values. CO concentrations of up to 250 ppbv, among the highest during the ARCTAS campaign, were observed at altitudes of 3.5–5 km over western Alaska and the Norton Sound during this flight. The enhancement was well captured by GEOS-Chem, which shows the source to be a mix of Asian pollution and Eurasian fires. Further evidence for a biomass burning source comes from elevated observations of hydrogen cyanide (HCN) and acetonitrile (CH_3CN). More than half of the back trajectories shown in Fig. 2.10 passed directly over the agricultural fires in southeastern Russia and Kazakhstan at low altitude before being lifted, likely by WCBs, to the mid-troposphere. Turning to the satellite observations, we see qualitative agreement between measured and simulated total column CO throughout the Arctic, although AIRS is consistently higher than GEOS-Chem as previously discussed. Both AIRS and GEOS-Chem show an extensive plume stretching from Eastern Russia across the Pacific to Alaska. Forward trajectories from the sampled plume indicate that the plume did not travel poleward after being sampled; however, it eventually entered the Arctic over the Canadian Archipelago and the Davis Strait eight to ten days later. This example illustrates AIRS's ability to observe WCB lofting and outflow from Eurasia to the Arctic.

Figure 2.11 shows a different case on 9 April 2008, when a CO enhancement was observed by the aircraft at the North Pole at altitudes below 2 km. Concentrations in the plume were 165–170 ppbv. Backward trajectories (Fig. 2.12) indicate that the plume traveled slowly from northeastern Europe across Siberia, remaining at low altitude. Although

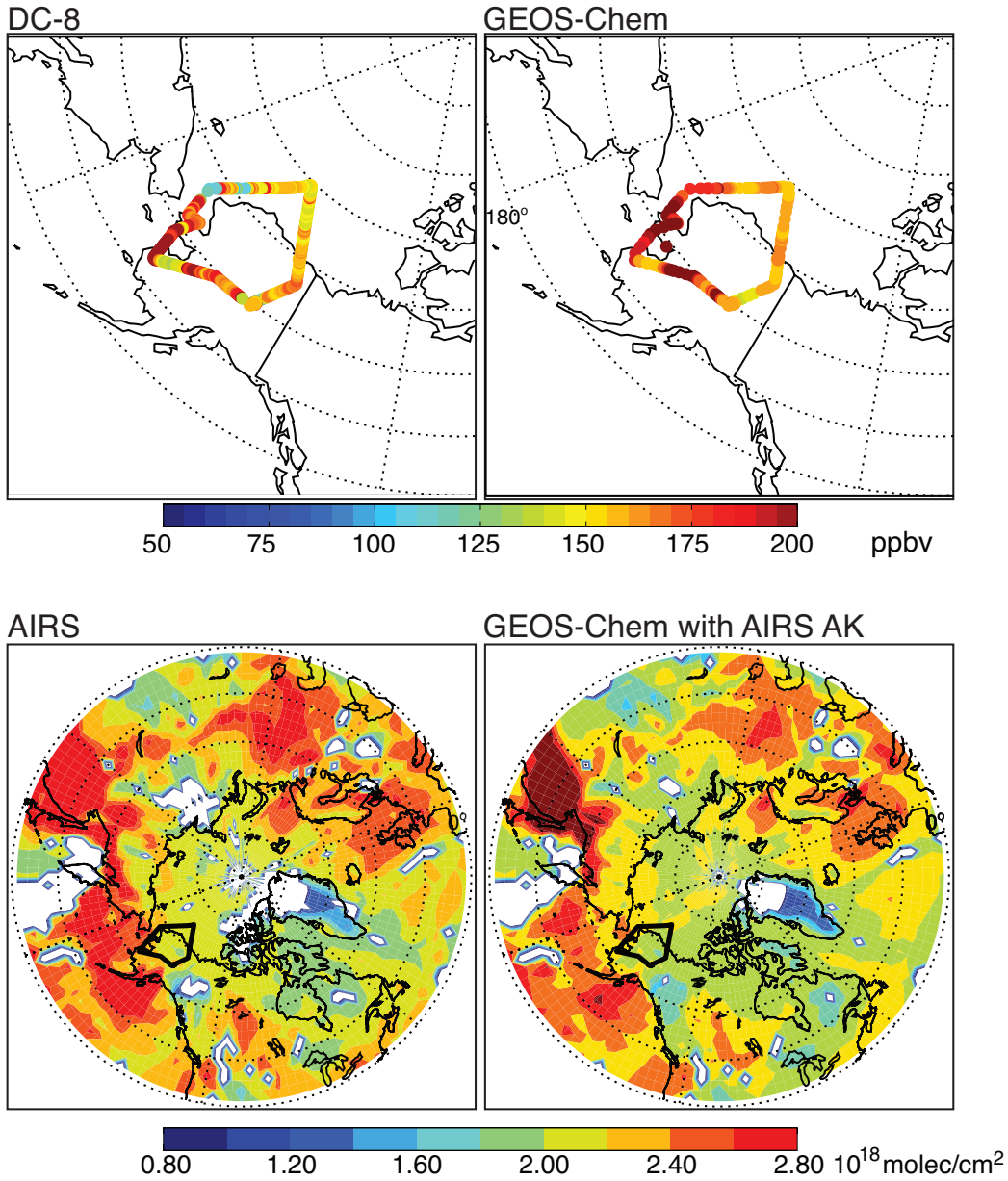

Figure 2.9: Russian biomass burning event over Alaska sampled by the DC-8 aircraft on 16 April 2008. The top panels show aircraft observations of CO concentrations compared to the GEOS-Chem model. The bottom panels show the AIRS CO column concentrations observed on that day compared to the GEOS-Chem model with AIRS averaging kernels applied.

trajectories pass over the Russian burning region, this was before the most intense fires began, and observed concentrations of HCN and CH_3CN were negligible. GEOS-Chem

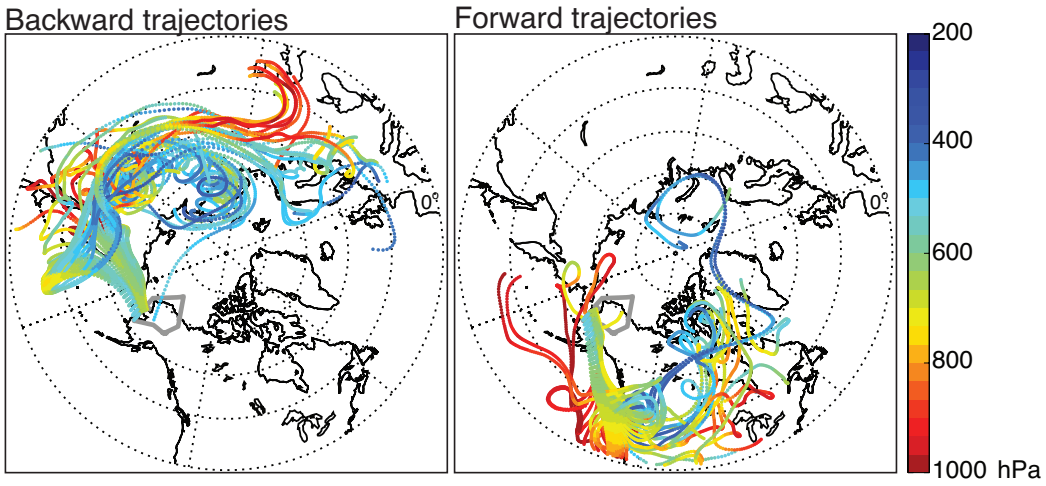

Figure 2.10: Ten-day backward and forward trajectories from the FLEXPART model using WRF meteorological fields and starting from the 16 April 2008 plume shown in Fig. 2.9. The color scale indicates altitude.

captures the plume and indicates that the primary source was European pollution mixed with some Asian pollution. Forward trajectories show that much of the polluted airmass remained at low altitude over the pole for at least the next ten days. We do not expect AIRS to be sensitive to such low-altitude transport, and indeed we see from Fig. 2.11 that neither AIRS nor the GEOS-Chem simulation weighted by AIRS averaging kernels could detect the plume.

The limited ability of AIRS to observe low-altitude CO enhancements prevents us from using AIRS to systematically identify near-surface transport events to the Arctic. As we have shown with the GEOS-Chem simulation, this mainly impacts our interpretation of pollution from European sources, which is primarily (though not exclusively) transported at low altitude. AIRS is most useful for identifying mid-tropospheric transport, which as we have seen privileges Asian influence.

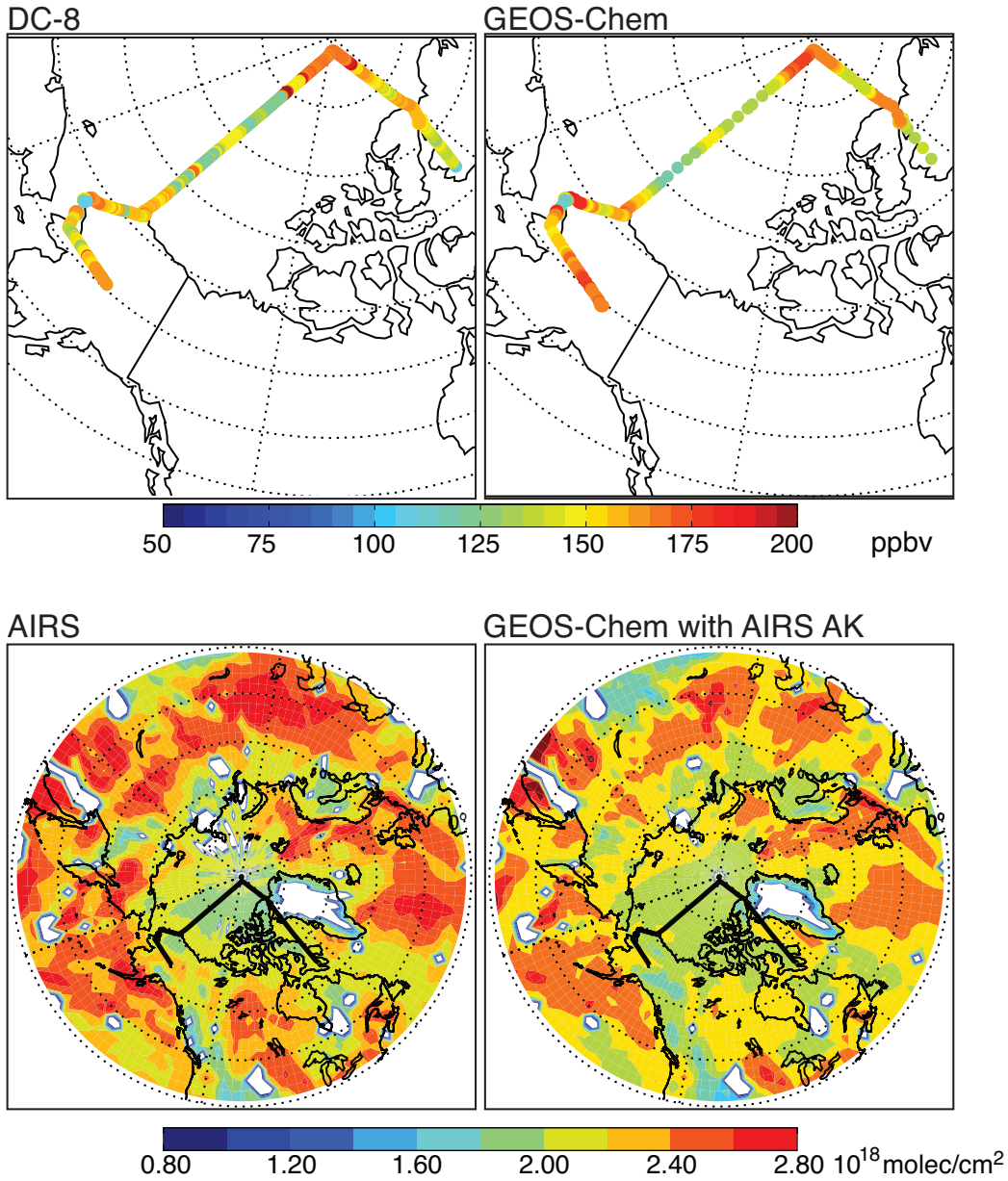

Figure 2.11: Same as Fig. 2.9, but for a European pollution event at the North Pole on 9 April 2008.

The 2003–2008 April mean CO columns from AIRS are shown in Fig. 2.13, along with the anomalies for each year. The major features described for 2008 (Fig. 2.6 and Sect. 2.3) are also seen in the multi-year mean, with the European sector of the Arctic being the most polluted and the North American sector the cleanest. The anomaly maps

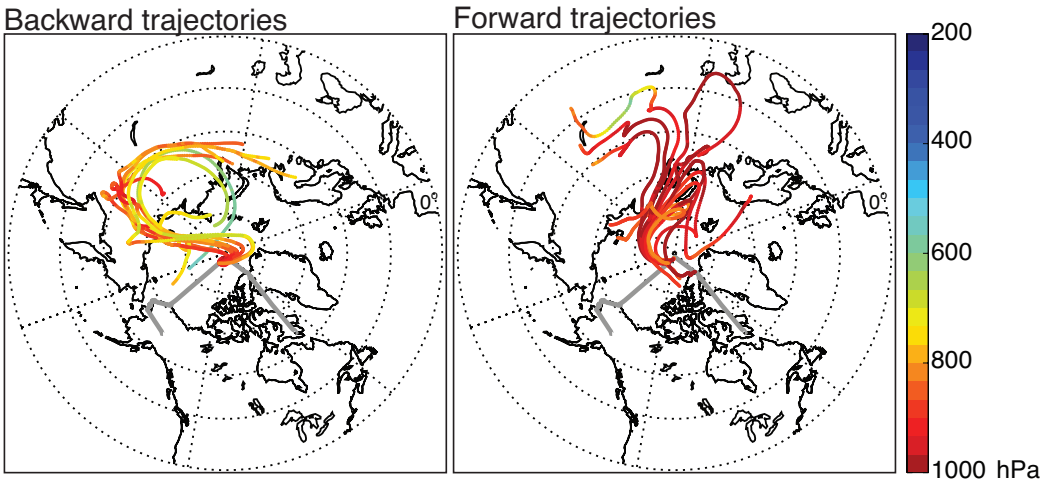

Figure 2.12: Same as Fig. 2.10, but for the European pollution event on 9 April 2008 shown in Fig. 2.11.

show little variability north of the Arctic Circle. Mean April CO column ranges from 2.06×10^{18} molecules cm^{-2} to 2.11×10^{18} molecules cm^{-2}, despite larger year-to-year differences at mid-latitudes, and is most strongly correlated with mean Arctic sea level pressure (SLP) in the GEOS-5 data ($r=-0.81$). We attribute this anti-correlation to the higher degree of Arctic isolation associated with high pressure conditions, preventing poleward transport of CO from mid-latitudes.

Pollution transport to the Arctic is thought to be enhanced under the positive phase of the North Atlantic Oscillation (NAO) (Duncan and Bey, 2004; Eckhardt et al., 2003) due to stronger surface westerlies and anomalous southerly flow (Hurrell et al., 2003). Previous studies found strong positive correlations, most pronounced at the surface, between NAO strength and Arctic pollution accumulation in winter and spring (Duncan and Bey, 2004; Eckhardt et al., 2003). However, we find no significant correlation of AIRS CO over the Arctic in April 2003–2008 with the February–April mean NAO index (taken from

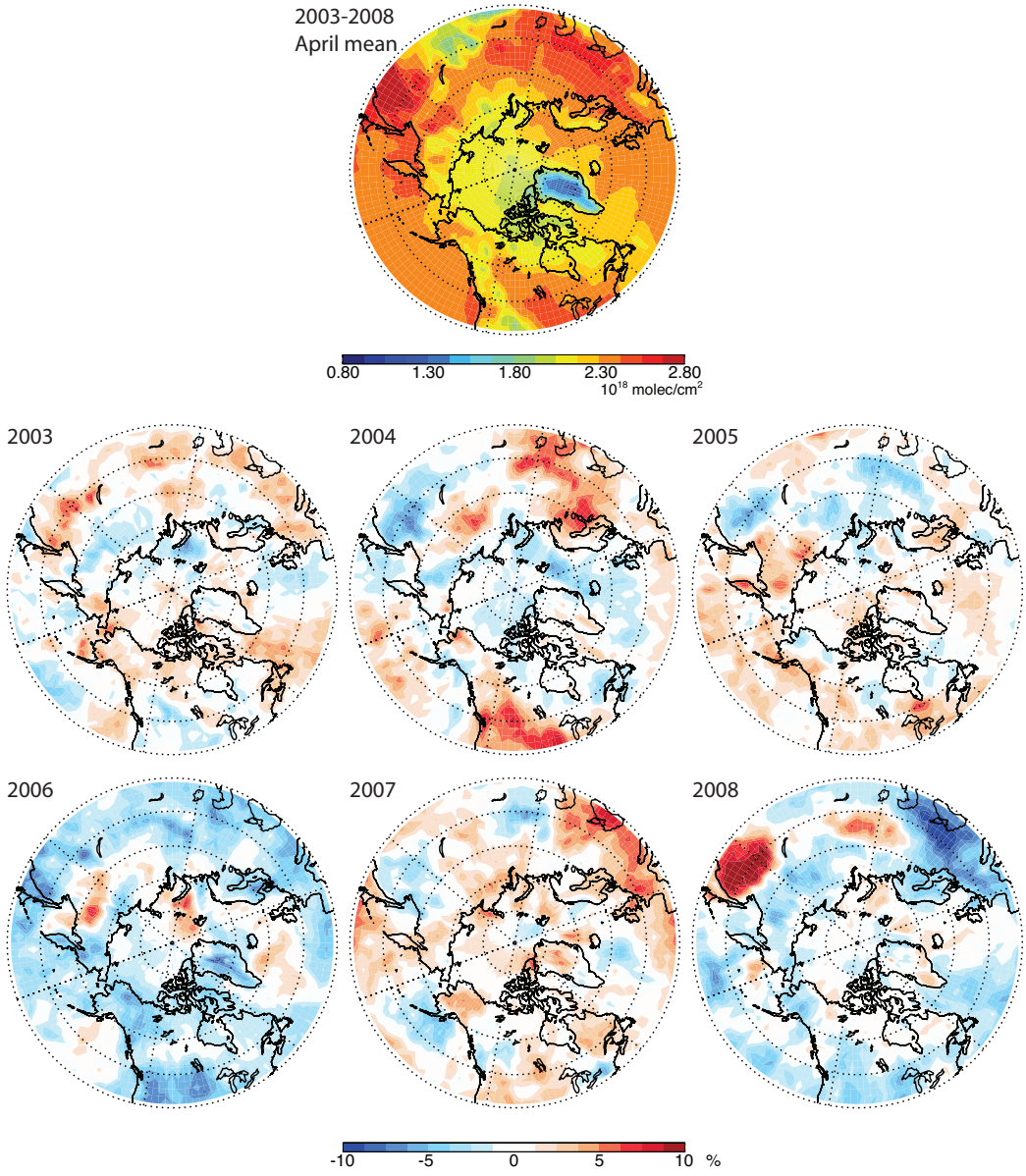

Figure 2.13: 2003–2008 mean April CO columns from AIRS (top) and CO column anomalies for each April in the AIRS record.

the NOAA Climate Prediction Center, available at http://www.cpc.noaa.gov). This could reflect limitations due to (1) our focus on spring, when the NAO index is typically weak (Hurrell et al., 2003), (2) the lack of sensitivity of AIRS to surface concentrations where the correlation is strongest, and (3) the limited range of NAO index variability (less than

±1) over the 2003–2008 period of the AIRS record.

AIRS observations for April 2008 show that despite the anomalously large Russian fire source, pollution influence over Alaska was much weaker than normal (Fig. 2.13). This can be explained by a strong SLP anomaly, as shown in Fig. 2.14. Positive pressure anomalies of more than 10 hPa were seen over the North Pacific with weaker negative anomalies further north, indicating that the climatological Aleutian low pressure system was less intense and shifted northward. Considering that the Aleutian low and associated storm tracks are a major driver for transport of Asian pollution to the Arctic (Fuelberg et al., 2010), this transport may have been weaker than normal in April 2008.

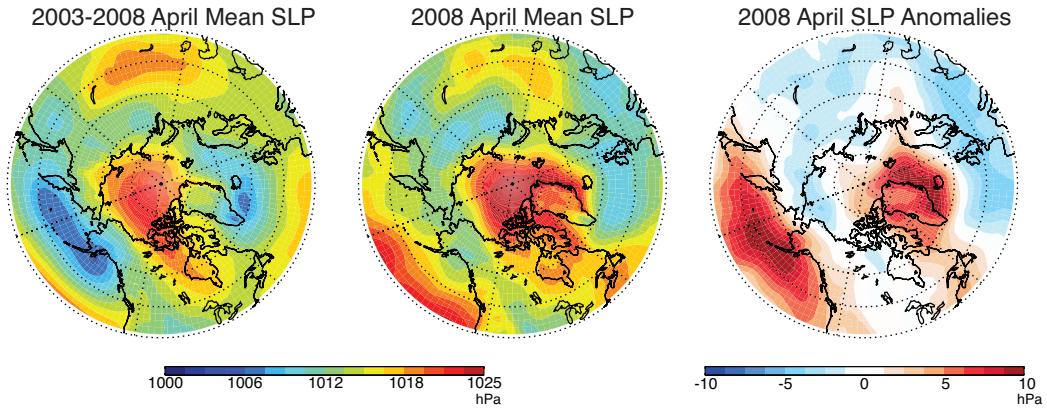

Figure 2.14: Mean sea level pressures from GEOS-5 for April 2003–2008 (left) and 2008 only (middle). The 2008 anomaly is shown at right.

We further examined the interannual variability of the AIRS April CO column over Alaska and find that it is highly correlated ($r = 0.80$) with the February-April mean Ocean Niño Index (ONI, a measure of the El Niño-Southern Oscillation, again taken from the NOAA Climate Prediction Center), as shown in Fig. 2.15. The correlation is significant at the $p = 0.10$ level. Atmospheric teleconnections from ENSO have long been known

to affect the strength and position of the Aleutian low pressure system (Bjerknes, 1966; Niebauer, 1988). During El Niño conditions, the Aleutian low intensifies and shifts to the southeast of its climatological mean position (52° N, 175° E; Rodionov et al., 2005), while during La Niña conditions it weakens and shifts to the west. Niebauer (1988) found that this change alters the low-level flow over the central Pacific, bringing Asian outflow north toward Alaska during El Niño years (see his Fig. 7) and decreasing the northward flow of Asian air during La Niña years. We suspect that this mechanism extends to higher altitudes and explains the correlation between the ONI and the AIRS CO column over Alaska. While there have been no strong El Niño years since the beginning of the AIRS record, a moderate La Niña with monthly ONI values up to -1.4 occurred from fall 2007 through spring 2008, resulting in a less intense Aleutian low and an associated decrease in Asian pollution influence during April 2008. The La Niña persisted through April (ONI $= -0.8$) and began to dissipate in May.

The specific meteorological conditions that characterized April 2008 have important implications for the interpretation of the ARCTAS and ARCPAC aircraft data. As discussed in Sect. 2.4, we find from these data that CO pollution throughout the Arctic is dominated by the Asian anthropogenic source, despite the anomalously weak poleward transport from this source in April 2008. El Niño conditions would be expected to lead to larger Asian influence and consequently more CO pollution in the Arctic. Such an effect may be further amplified by increased biomass burning, which has been shown to play a dominant role in increasing CO concentrations over Alaska during El Niño events (Szopa et al., 2007). In

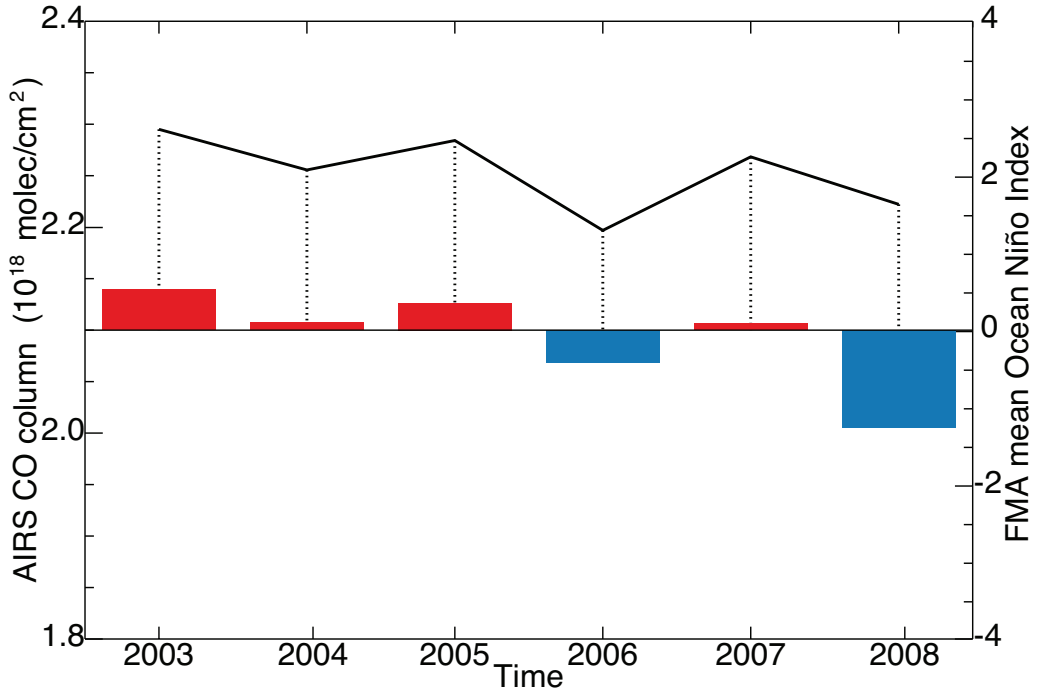

Figure 2.15: Year-to-year variability of the mean April AIRS-observed CO column over Alaska (168–140° W, 54–72° N) and mean Ocean Niño Index (ONI) averaged over February-April for each year. Positive values of the ONI (red) indicate El Niño conditions while negative values (blue) indicate La Niña conditions. The Pearson correlation coefficient of $r = 0.80$ is significant at the $p = 0.10$ level. The ONI data were obtained from the NOAA Climate Prediction Center, available at http://www.cpc.noaa.gov.

2003, the only El Niño year in our record, CO columns were indeed anomalously high over Alaska, the Chukchi Sea, and much of the North American Arctic (Fig. 2.13).

We further investigated the relationship between ENSO and CO concentrations in the Alaskan Arctic using GEOS-Chem. GEOS-5 meteorological fields are available only for 2005–2008, so we performed a sensitivity simulation using meteorology from 2005 (the highest ONI for those four years, see Fig. 2.15) while maintaining emissions at 2008 levels. Figure 2.16 compares simulated concentrations of the Asian fossil fuel tagged tracer in April using 2005 and 2008 meteorology. April 2005 shows stronger northward transport

of Asian pollution over the North Pacific and Alaska than April 2008. Whether this enhancement is indeed linked to the more positive phase of the ONI in 2005 is unclear, and additional data and simulations during a strong El Niño year would be needed to verify this link.

2.6 Conclusions

We used CO observations from the NASA ARCTAS and NOAA ARCPAC aircraft campaigns as top-down constraints in a global 3-D chemical transport model (GEOS-Chem) to quantify the sources of pollution to the Arctic in spring 2008. Through comparisons with aircraft and GEOS-Chem, we demonstrated that AIRS satellite measurements of CO captured the mean spatial structure of Arctic pollution in April 2008 as well as events in the free troposphere but did not detect events in the boundary layer because of low sensitivity in the thermal IR. We subsequently used the 2003–2008 record of AIRS CO observations in the Arctic in April to investigate the interannual variability of pollution transport from northern mid-latitudes.

Least squares regression of the GEOS-Chem CO simulation to the ARCTAS and ARCPAC aircraft observations suggests that anthropogenic CO emissions in Europe in April 2008 are underestimated by 50% in the EMEP inventory and anthropogenic emissions in Asia are underestimated by 20% in the Streets et al. (2006) inventory updated for 2008. The discrepancy likely represents an underestimate of seasonal CO emissions rather than a problem in global annual emissions. This result is consistent with the recent inverse anal-

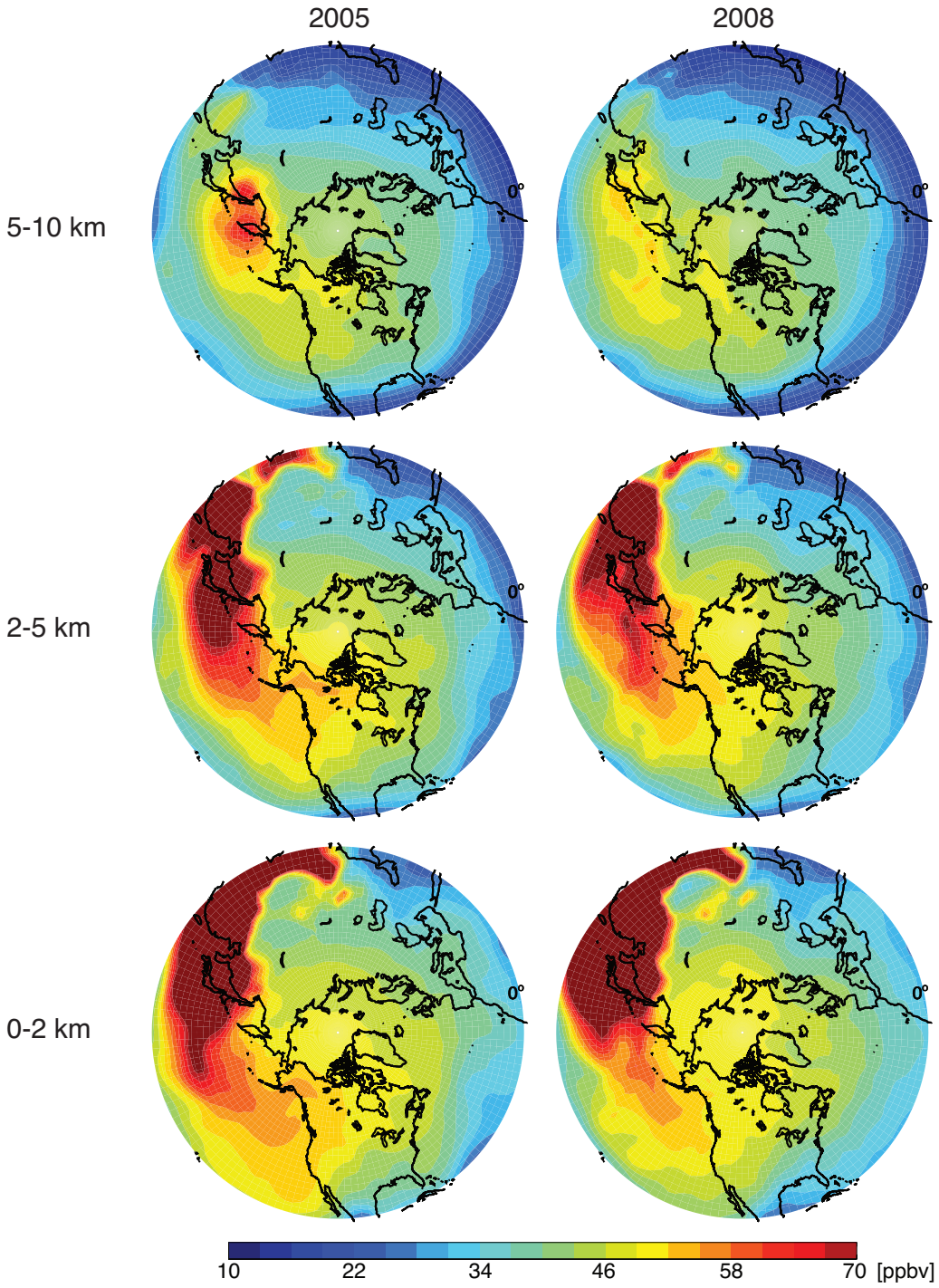

Figure 2.16: Concentrations of the Asian fossil fuel CO tagged tracer in the GEOS-Chem simulation for April 2005 versus April 2008 meteorology with identical April 2008 emissions for both years. Results are shown as April mean CO mixing ratios at 0–2, 2–5, and 5–10 km.

ysis of Kopacz et al. (2010) and may reflect a winter-spring underestimate of emissions from residential fuel use and vehicle cold starts. April 2008 saw anomalous fire activity in southern Russia in addition to seasonal biomass burning in Southeast Asia. We find that the FLAMBE inventory with hourly resolution based on MODIS and GOES fire data overestimates these emissions by a factor of two. Optimized April 2008 emissions obtained by fitting GEOS-Chem to the ARCTAS aircraft data are 26 Tg month^{-1} for Asian anthropogenic, 9.4 Tg month^{-1} for European anthropogenic, 4.1 Tg month^{-1} for North American anthropogenic, 15 Tg month^{-1} for Russian biomass burning, and 23 Tg month^{-1} for Southeast Asian biomass burning. The resulting simulation shows no significant bias (mean of -1%) relative to ground-based column data at Eureka (80° N, 86° W). It also shows a -3% underestimate relative to AIRS in the Arctic, although this may reflect in part a high bias in the AIRS data (McMillan et al., 2011).

We find in GEOS-Chem that CO concentrations over the Arctic in spring are dominated at all altitudes by Asian anthropogenic sources. The exception is at the surface where European anthropogenic sources are of comparable importance. This anthropogenic dominance, despite the large biomass burning emissions in April 2008, reflects the wintertime accumulation of anthropogenic CO on the scale of the northern extratropics. European pollution influence in April extends to the free troposphere and also across Siberia following westerly flow. This contrasts with the prevailing pattern in winter when stratification confines European pollution to the surface and the Siberian high pressure system suppresses westerly transport. Russian biomass burning makes little contribution to mean CO but

contributes substantially to CO variability. Asian and biomass burning synoptic transport events take place mainly in the free troposphere through warm conveyor belts (WCBs) and are followed by slow subsidence. Analysis of specific pollution events sampled by the aircraft shows that AIRS can successfully observe the long-range transport of pollution to the Arctic in the middle troposphere but not at the surface.

AIRS CO observations in April, both for 2008 and for the multiyear record (2003–2008), show the highest levels of pollution in the European Arctic sector, followed by the Asian sector and with the North American sector being cleanest. This is consistent with GEOS-Chem, where synoptic lifting of European pollution contributes to the European sector. The North American sector is relatively clean, despite WCB injections off the east coast of North America, because CO emissions there are relatively small. Mean April AIRS CO columns for 2003–2008 show little interannual variability when averaged over the Arctic polar cap. What little variability exists is most strongly correlated with Arctic sea level pressure ($r = -0.81$) and can be explained by decreased pollution inflow from mid-latitudes under high-pressure conditions. We find little correlation with the NAO index, which could reflect the limited range of this index in spring over the 2003–2008 period as well as AIRS's lack of sensitivity in the boundary layer.

AIRS CO columns over Alaska in April 2008 are anomalously low compared to other years, despite the anomalously high Russian biomass burning influence. We find that AIRS CO in this region is highly correlated with the Ocean Niño Index ($r = 0.80$). The low CO columns over Alaska in April 2008 were associated with La Niña conditions in fall 2007

through spring 2008 that weakened the Aleutian low pressure system. As a result, transport of Asian pollution to the Arctic was likely suppressed. We verified this result by comparing GEOS-Chem simulations for April 2005 (weak El Niño) and April 2008. This suggests that the impact of Asian pollution in the Arctic could be very large under strong El Niño conditions, so far missing from the AIRS record.

Bibliography

Acker, J. and Leptoukh, G.: Online analysis enhances use of NASA earth science data, Eos Trans. AGU, 88, 14, 17, 2007.

Andreae, M. O. and Merlet, P.: Emission of trace gases and aerosols from biomass burning, Global Biogeochemical Cycles, 15, 955–966, 2001.

Barrie, L. A.: Arctic air pollution: An overview of current knowledge, Atmospheric Environment, 20, 643–663, 1986.

Batchelor, R. L., Strong, K., Lindenmaier, R., Mittermeier, R. L., Fast, H., Drummond, J. R., and Fogal, P. F.: A new Bruker IFS 125HR FTIR spectrometer for the Polar Environment Atmospheric Research Laboratory at Eureka, Canada: measurements and comparison with the existing Bomem DA8 spectrometer, J. Atmos. Ocean. Tech., 26, 1328–1340, 2009.

Bey, I., Jacob, D. J., Logan, J. A., and Yantosca, R. M.: Asian chemical outflow to the Pacific in spring: Origins, pathways, and budgets, J. Geophys. Res., 106, 23 097–23 113, 2001.

Bjerknes, J.: A possible response of the atmospheric Hadley circulation to equatorial anomalies of the ocean temperature, Tellus, 18, 820–829, 1966.

Carlson, T. N.: Speculations on the movement of polluted air to the Arctic, Atmospheric Environment, 15, 1473–1477, 1981.

Dlugokencky, E., Lang, P. M., and Masarie, K. A.: Atmospheric Methane Dry Air Mole Fractions from the NOAA ESRL Carbon Cycle Cooperative Global Air Sampling Network, 1983-2007, Version: 2008-07-02, Path: ftp://ftp.cmdl.noaa.gov/ccg/ch4/flask/event/, 2008.

Duncan, B. N. and Bey, I.: A modeling study of the export pathways of pollution from Europe: Seasonal and interannual variations (1987–1997), J. Geophys. Res., 109, D08 301, 2004.

Duncan, B. N. and Logan, J. A.: Model analysis of the factors regulating the trends and variability of carbon monoxide between 1988 and 1997, Atmos. Chem. Phys., 8, 7389–7403, 2008.

Duncan, B. N., Martin, R. V., Staudt, A. C., Yevich, R., and Logan, J. A.: Interannual and seasonal variability of biomass burning emissions constrained by satellite observations, J. Geophys. Res., 108, 4100, 2003.

Duncan, B. N., Logan, J. A., Bey, I., Megretskaia, I. A., Yantosca, R. M., Novelli, P. C., Jones, N. B., and Rinsland, C. P.: Global budget of CO, 1988–1997: Source estimates and validation with a global model, J. Geophys. Res., 112, D22 301, 2007.

Eckhardt, S., Stohl, A., Beirle, S., Spichtinger, N., James, P., Forster, C., Junker, C., Wagner, T., Platt, U., and Jennings, S. G.: The North Atlantic Oscillation controls air pollution transport to the Arctic, Atmos. Chem. Phys., 3, 1769–1778, 2003.

Fortems-Cheiney, A., Chevallier, F., Pison, I., Bousquet, P., Carouge, C., Clerbaux, C., Coheur, P. F., George, M., Hurtmans, D., and Szopa, S.: On the capability of IASI measurements to inform about CO surface emissions, Atmos. Chem. Phys., 9, 8735–8743, 2009.

Fuelberg, H. E., Harrigan, D. L., and Sessions, W.: A meteorological overview of the ARCTAS 2008 mission, Atmos. Chem. Phys., 10, 817–842, 2010.

Guenther, A., Karl, T., Harley, P., Wiedinmyer, C., Palmer, P. I., and Geron, C.: Estimates of global terrestrial isoprene emissions using MEGAN (Model of Emissions of Gases and Aerosols from Nature), Atmos. Chem. Phys., 6, 3181–3210, 2006.

Heald, C. L., Jacob, D. J., Fiore, A. M., Emmons, L. K., Gille, J. C., Deeter, M. N., Warner, J., Edwards, D. P., Crawford, J. H., and Hamlin, A. J.: Asian outflow and trans-Pacific transport of carbon monoxide and ozone pollution: An integrated satellite, aircraft, and model perspective, J. Geophys. Res., 108, 4804, 2003a.

Heald, C. L., Jacob, D. J., Palmer, P. I., Evans, M. J., Sachse, G. W., Singh, H. B., and Blake, D. R.: Biomass burning emission inventory with daily resolution: Application to aircraft observations of Asian outflow, J. Geophys. Res.-Atmos., 108, 8811, 2003b.

Heald, C. L., Jacob, D. J., Jones, D. B. A., Palmer, P. I., Logan, J. A., Streets, D. G., Sachse, G. W., Gille, J. C., Hoffman, R. N., and Nehrkorn, T.: Comparative inverse analysis of satellite (MOPITT) and aircraft (TRACE-P) observations to estimate Asian sources of carbon monoxide, J. Geophys. Res., 109, D23 306, 2004.

Heald, C. L., Jacob, D. J., Park, R. J., Alexander, B., Fairlie, T. D., Yantosca, R. M., and Chu, D. A.: Transpacific transport of Asian anthropogenic aerosols and its impact on surface air quality in the United States, Journal of Geophysical Research, 111, D14 310, 2006.

Hegg, D. A., Warren, S. G., Grenfell, T. C., Doherty, S. J., Larson, T. V., and Clarke, A. D.: Source attribution of black carbon in arctic snow, Environ. Sci. Technol., 43, 4016–4021, 2009.

Holloway, J. S., Jakoubek, R. O., Parrish, D. D., Gerbig, C., Volz-Thomas, A., Schmitgen, S., Fried, A., Wert, B., Henry, B., and Drummond, J. R.: Airborne intercomparison of vacuum ultraviolet fluorescence and tunable diode laser absorption measurements of tropospheric carbon monoxide, J. Geophys. Res.-Atmos., 105, 24 251–24 261, 2000.

Hudman, R. C., Jacob, D. J., Turquety, S., Leibensperger, E. M., Murray, L. T., Wu, S., Gilliland, A. B., Avery, M., Bertram, T. H., and Brune, W.: Surface and lightning sources of nitrogen oxides over the United States: Magnitudes, chemical evolution, and outflow, Journal of Geophysical Research, 112, D12S05, 2007.

Hudman, R. C., Murray, L. T., Jacob, D. J., Millet, D. B., Turquety, S., Wu, S., Blake, D. R., Goldstein, A. H., Holloway, J., and Sachse, G. W.: Biogenic vs. anthropogenic sources of CO over the United States, Geophysical Research Letters, 35, L04 801, 2008.

Hurrell, J. W., Kushnir, Y., Ottersen, G., and Visbeck, M.: An overview of the North Atlantic oscillation, in: The North Atlantic Oscillation: Climatic Significance and Environmental Impact, edited by Hurrell, J. W., Kushnir, Y., Ottersen, G., and Visbeck, M., Geoph. Monog. Series, pp. 1–36, American Geophysical Union, 2003.

Jacob, D. J., Crawford, J. H., Maring, H., Clarke, A. D., Dibb, J. E., Emmons, L. K., Ferrare, R. A., Hostetler, C. A., Russell, P. B., Singh, H. B., Thompson, A. M., Shaw, G. E., McCauley, E., Pederson, J. R., and Fisher, J. A.: The Arctic Research of the Composition of the Troposphere from Aircraft and Satellites (ARCTAS) mission: design, execution, and first results, Atmospheric Chemistry and Physics, 10, 5191–5212, 2010.

Jaeglé, L., Jaffe, D. A., Price, H. U., Weiss-Penzias, P., Palmer, P. I., Evans, M. J., Jacob, D. J., and Bey, I.: Sources and budgets for CO and O3 in the northeastern Pacific during the spring of 2001: Results from the PHOBEA-II Experiment, J. Geophys. Res., 108, 8802, 2003.

Jaffe, D., Bertschi, I., Jaeglé, L., Novelli, P., Reid, J. S., Tanimoto, H., Vingarzan, R., and Westphal, D. L.: Long-range transport of Siberian biomass burning emissions and impact on surface ozone in western North America, Geophys. Res. Lett., 31, L16 106, 2004.

Kahn, R. A., Chen, Y., Nelson, D. L., Leung, F. Y., Li, Q., Diner, D. J., and Logan, J. A.: Wildfire smoke injection heights: Two perspectives from space, Geophysical Research Letters, 35, L04 809, 2008.

Kiley, C. M., Fuelberg, H. E., Palmer, P. I., Allen, D. J., Carmichael, G. R., Jacob, D. J., Mari, C., Pierce, R. B., Pickering, K. E., and Tang, Y.: An intercomparison and evaluation of aircraft-derived and simulated CO from seven chemical transport models during the TRACE-P experiment, J. Geophys. Res.-Atmos., 108, 8819, 2003.

Klonecki, A., Hess, P., Emmons, L., Smith, L., Orlando, J., and Blake, D.: Seasonal changes in the transport of pollutants into the Arctic troposphere-model study, Journal of Geophysical Research, 108, 8367, 2003.

Koch, D. and Hansen, J.: Distant origins of Arctic black carbon: A Goddard Institute for Space Studies ModelE experiment, Journal of Geophysical Research, 110, D04 204, 2005.

Koike, M., Jones, N. B., Palmer, P. I., Matsui, H., Zhao, Y., Kondo, Y., Matsumi, Y., and Tanimoto, H.: Seasonal variation of carbon monoxide in northern Japan: Fourier transform IR measurements and source-labeled model calculations, J. Geophys. Res.-Atmos., 111, D15 306, 2006.

Kopacz, M., Jacob, D. J., Henze, D. K., Heald, C. L., Streets, D. G., and Zhang, Q.: Comparison of adjoint and analytical Bayesian inversion methods for constraining Asian sources of carbon monoxide using satellite (MOPITT) measurements of CO columns, J. Geophys. Res.-Atmos., 114, D04 305, 2009.

Kopacz, M., Jacob, D. J., Fisher, J., Logan, J. A., Zhang, L., Megretskaia, I. A., Yantosca, R. M., Singh, K., Henze, D., Burrows, J., Buchwitz, M., Khlystova, I., McMillan, W. W., Gille, J. C., Edwards, D. P., Eldering, A., Thouret, V., and Nedelec, P.: Global estimates of CO sources with high resolution by adjoint inversion of multiple satellite datasets (MOPITT, AIRS, SCIAMACHY, TES), Atmos. Chem. Phys., 10, 855–876, 2010.

Kuhns, H., Knipping, E. M., and Vukovich, J. M.: Development of a United States-Mexico Emissions Inventory for the Big Bend Regional Aerosol and Visibility Observational (BRAVO) Study, J. Air Waste Manag., 55, 677–92, 2005.

Labonne, M., Bréon, F.-M., and Chevallier, F.: Injection height of biomass burning aerosols as seen from a spaceborne lidar, Geophys. Res. Lett., 34, L11 806, 2007.

Law, K. S. and Stohl, A.: Arctic Air Pollution: Origins and Impacts, Science, 315, 1537, 2007.

Li, Q., Jacob, D. J., Bey, I., Palmer, P. I., Duncan, B. N., Field, B. D., Martin, R. V., Fiore, A. M., Yantosca, R. M., and Parrish, D. D.: Transatlantic transport of pollution and its effects on surface ozone in Europe and North America, J. Geophys. Res.-Atmos., 107, 4166, 2002.

Liang, Q., Jaeglé, L., Jaffe, D. A., Weiss-Penzias, P., Heckman, A., and Snow, J. A.: Long-range transport of Asian pollution to the northeast Pacific: Seasonal variations and transport pathways of carbon monoxide, Journal of Geophysical Research, 109, D23S07, 2004.

Liu, H., Jacob, D. J., Bey, I., Yantosca, R. M., Duncan, B. N., and Sachse, G. W.: Transport pathways for Asian pollution outflow over the Pacific: Interannual and seasonal variations, Journal of Geophysical Research, 108, 8786, 2003.

McConnell, J. R., Edwards, R., Kok, G. L., Flanner, M. G., Zender, C. S., Saltzman, E. S., Banta, J. R., Pasteris, D. R., Carter, M. M., and Kahl, J. D. W.: 20th-century industrial black carbon emissions altered arctic climate forcing, Science, 317, 1381, 2007.

McMillan, W. W., Barnet, C., Strow, L., Chahine, M. T., McCourt, M. L., Warner, J. X., Novelli, P. C., Korontzi, S., Maddy, E. S., and Datta, S.: Daily global maps of carbon monoxide from NASA's Atmospheric Infrared Sounder, Geophys. Res. Lett., 32, L11 801, 2005.

McMillan, W. W., Warner, J. X., Comer, M. M., Maddy, E., Chu, A., Sparling, L., Eloranta, E., Hoff, R., Sachse, G., Barnet, C., Razenkov, I., and Wolf, W.: AIRS views transport from 12 to 22 July 2004 Alaskan/Canadian fires: Correlation of AIRS CO and MODIS AOD with forward trajectories and comparison of AIRS CO retrievals with DC-8 in situ measurements during INTEX-A/ICARTT, J. Geophys. Res., 113, D20 301, 2008.

McMillan, W. W., Pierce, R. B., Sparling, L. C., Osterman, G., McCann, K., Fischer, M., Rappenglück, B., Newsom, R., Turner, D., Kittaka, C., Evans, K., Biraud, S., Lefer, B., Andrews, A., and Oltmans, S.: An observational and modeling strategy to investigate the impact of remote sources on local air quality: A Houston, Texas case study from the Second Texas Air Quality Study (TexAQS II), J. Geophys. Res., 115, D01 301, 2010.

McMillan, W. W., Evans, K. D., Barnet, C. D., Maddy, E. S., Sachse, G. W., and Diskin, G. S.: Validating the AIRS Version 5 CO Retrieval With DACOM In Situ Measurements During INTEX-A and -B, IEEE Transactions on Geoscience and Remote Sensing, 49, 2802–2813, 2011.

Niebauer, H. J.: Effects of El Nino–Southern Oscillation and North Pacific weather patterns on interannual variability in the subarctic Bering Sea, J. Geophys. Res.-Oceans, 93, 5051–5068, 1988.

Olivier, J. G. J. and Berdowski, J. J. M.: Global emission sources and sinks, in: The Climate System, edited by Berdowski, J. J. M., Guicherit, R., and Heij, B., pp. 33–77, A.A. Balkema Publishers/Swets and Zeitlinger Publishers, Lisse, The Netherlands, 2001.

Olivier, J. G. J., Bloos, J. P. J., Berdowski, J. J. M., Visschedijk, A. J. H., and Bouwman, A. F.: A 1990 global emission inventory of anthropogenic sources of carbon monoxide

on 1 ° x 1 ° developed in the framework of EDGAR/GEIA, Chemosphere: Global Change Science, 1, 1–17, 1999.

Olsen, E., Fishbein, E., Lee, S.-Y., Manning, E., and McMillan, W. W.: AIRS/AMSU/HSB Version 5 Level 2 Product - Levels, Layers and Trapezoids, Tech. rep., Jet Propulsion Laboratory, 2007.

Park, R. J., Jacob, D. J., Field, B. D., Yantosca, R. M., and Chin, M.: Natural and transboundary pollution influences on sulfate-nitrate-ammonium aerosols in the United States: Implications for policy, Journal of Geophysical Research, 109, D15 204, 2004.

Quinn, P. K., Shaw, G., Andrews, E., Dutton, E. G., Ruoho-Airola, T., and Gong, S. L.: Arctic haze: current trends and knowledge gaps, Tellus B, 59, 99–114, 2007.

Quinn, P. K., Bates, T. S., Baum, E., Doubleday, N., Fiore, A. M., Flanner, M., Fridlind, A., Garrett, T. J., Koch, D., and Menon, S.: Short-lived pollutants in the Arctic: their climate impact and possible mitigation strategies, Atmospheric Chemistry and Physics, 8, 1723–1735, 2008.

Raatz, W. E. and Shaw, G. E.: Long-Range Tropospheric Transport of Pollution Aerosols into the Alaskan Arctic, Journal of Applied Meteorology, 23, 1052–1064, 1984.

Rahn, K. A.: Relative importances of North America and Eurasia as sources of arctic aerosol, Atmospheric Environment, 15, 1447–1455, 1981.

Rastigejev, Y., Park, R., Brenner, M. P., and Jacob, D. J.: Resolving intercontinental pollution plumes in global models of atmospheric transport, Journal of Geophysical Research, 115, D02 302, 2010.

Reid, J. S., Hyer, E. J., Prins, E. M., Westphal, D. L., Zhang, J., Wang, J., Christopher, S. A., Curtis, C. A., Schmidt, C. C., Eleuterio, D. P., Richardson, K. A., and Hoffman, J. P.: Global monitoring and forecasting of biomass-burning smoke: Description and lessons from the Fire Locating and Modeling of Burning Emissions (FLAMBE) program, IEEE Journal of Selected Topics in Applied Earth Observations and Remote Sensing, 2, 144–162, 2009.

Rodionov, S. N., Overland, J. E., and Bond, N. A.: The Aleutian Low and Winter Climatic Conditions in the Bering Sea. Part I: Classification, J. Climate, 18, 160–177, 2005.

Sachse, G. W., Hill, G. F., Wade, L. O., and Perry, M. G.: Fast-response, high-precision carbon monoxide sensor using a tunable diode laser absorption technique, J. Geophys. Res., 92, 2071–2081, 1987.

Shaw, G.: The Arctic haze phenomenon, Bulletin of the American Meteorological Society, 76, 2403–2413, 1995.

Shindell, D. T. and Faluvegi, G.: Climate response to regional radiative forcing during the twentieth century, Nature Geoscience, 2, 294–300, 2009.

Shindell, D. T., Faluvegi, G., Lacis, A., Hansen, J., Ruedy, R., and Aguilar, E.: Role of tropospheric ozone increases in 20th-century climate change, J. Geophys. Res., 111, D08 302, 2006a.

Shindell, D. T., Faluvegi, G., Stevenson, D. S., Krol, M. C., Emmons, L. K., Lamarque, J. F., Pétron, G., Dentener, F. J., Ellingsen, K., Schultz, M. G., Wild, O., Amann, M., Atherton, C. S., Bergmann, D. J., Bey, I., Butler, T., Cofala, J., Collins, W. J., Derwent, R. G., Doherty, R. M., Drevet, J., Eskes, H. J., Fiore, A. M., Gauss, M., Hauglustaine, D. A., Horowitz, L. W., Isaksen, I. S. A., Lawrence, M. G., Montanaro, V., Müller, J.-F., Pitari, G., Prather, M. J., Pyle, J. A., Rast, S., Rodriguez, J. M., Sanderson, M. G., Savage, N. H., Strahan, S. E., Sudo, K., Szopa, S., Unger, N., van Noije, T. P. C., and Zeng, G.: Multimodel simulations of carbon monoxide: Comparison with observations and projected near-future changes, J. Geophys. Res., 111, D19 306, 2006b.

Shindell, D. T., Chin, M., Dentener, F., Doherty, R. M., Faluvegi, G., Fiore, A. M., Hess, P., Koch, D. M., MacKenzie, I. A., Sanderson, M. G., Schultz, M. G., Schulz, M., Stevenson, D. S., Teich, H., Textor, C., Wild, O., Bergmann, D. J., Bey, I., Bian, H., Cuvelier, C., Duncan, B. N., Folberth, G., Horowitz, L. W., Jonson, J., Kaminski, J. W., Marmer, E., Park, R., Pringle, K. J., Schroeder, S., Szopa, S., Takemura, T., Zeng, G., Keating, T. J., and Zuber, A.: A multi-model assessment of pollution transport to the Arctic, Atmospheric Chemistry and Physics, 8, 5353–5372, 2008.

Staudt, A. C., Jacob, D. J., Logan, J. A., Bachiochi, D., Krishnamurti, T. N., and Sachse, G. W.: Continental sources, transoceanic transport, and interhemispheric exchange of carbon monoxide over the Pacific, J. Geophys. Res., 106, 32 571–32 590, 2001.

Stohl, A.: Characteristics of atmospheric transport into the Arctic troposphere, Journal of Geophysical Research, 111, D11 306, 2006.

Stohl, A., Berg, T., Burkhart, J. F., Fjæraa, A. M., Forster, C., Herber, A., Hov, Ø., Lunder, C., McMillan, W. W., and Oltmans, S.: Arctic smoke–record high air pollution levels in the European Arctic due to agricultural fires in Eastern Europe, Atmos. Chem. Phys., 7, 511–534, 2007.

Streets, D. G., Zhang, Q., Wang, L., He, K., Hao, J., Wu, Y., Tang, Y., and Carmichael, G. R.: Revisiting China's CO emissions after the Transport and Chemical Evolution over the Pacific (TRACE-P) mission: Synthesis of inventories, atmospheric modeling, and observations, J. Geophys. Res., 111, D14 306, 2006.

Susskind, J., Barnet, C. D., Blaisdell, J. M., Center, G. S. F., and Greenbelt, M. D.: Retrieval of atmospheric and surface parameters from AIRS/AMSU/HSB data in the presence of clouds, IEEE T. Geosci. Remote, 41, 390–409, 2003.

Szopa, S., Hauglustaine, D. A., and Ciais, P.: Relative contributions of biomass burning emissions and atmospheric transport to carbon monoxide interannual variability, Geophys. Res. Lett., 34, L18 810, 2007.

Tanimoto, H., Sawa, Y., Yonemura, S., Yumimoto, K., Matsueda, H., Uno, I., Hayasaka, T., Mukai, H., Tohjima, Y., and Tsuboi, K.: Diagnosing recent CO emissions and ozone evolution in East Asia using coordinated surface observations, adjoint inverse modeling, and MOPITT satellite data, Atmos. Chem. Phys, 8, 3867–3880, 2008.

Turquety, S., Clerbaux, C., Law, K., Coheur, P. F., Cozic, A., Szopa, S., Hauglustaine, D. A., Hadji-Lazaro, J., Gloudemans, A. M. S., Schrijver, H., Boone, C. D., Bernath, P. F., and Edwards, D. P.: CO emission and export from Asia: an analysis combining complementary satellite measurements (MOPITT, SCIAMACHY and ACE-FTS) with global modeling, Atmos. Chem. Phys., 8, 5187–5204, 2008.

Val Martin, M., Logan, J. A., Kahn, R., Leung, F.-Y., Nelson, D., and Diner, D.: Smoke injection heights from fires in North America: analysis of 5 years of satellite observations, Atmos. Chem. Phys., 10, 1491–1510, 2010.

Vestreng, V. and Klein, H.: Emission data reported to UNECE/EMEP: quality assurance and trend analysis and presentation of WebDab, MSC-W Status Report EMEP/MSC-W Note 1/02, Norwegian Meteorological Institute, 2002.

Warneke, C., Bahreini, R., Brioude, J., Brock, C. A., de Gouw, J. A., Fahey, D. W., Froyd, K. D., Holloway, J. S., Middlebrook, A., Miller, L., Montzka, S., Murphy, D. M., Peischl, J., Ryerson, T. B., Schwarz, J. P., Spackman, J. R., and Veres, P.: Biomass burning in Siberia and Kazakhstan as the main source for Arctic Haze over the Alaskan Arctic in April 2008, Geophysical Research Letters, 36, L02 813, 2009.

Warner, J., Comer, M. M., Barnet, C. D., McMillan, W. W., Wolf, W., Maddy, E., and Sachse, G.: A comparison of satellite tropospheric carbon monoxide measurements from AIRS and MOPITT during INTEX-A, J. Geophys. Res., 112, D12S17, 2007.

Yashiro, H., Sugawara, S., Sudo, K., Aoki, S., and Nakazawa, T.: Temporal and spatial variations of carbon monoxide over the western part of the Pacific Ocean, J. Geophys. Res., 114, D08 305, 2009.

Yurganov, L., McMillan, W. W., Grechko, E., and Dzhola, A.: Analysis of global and regional CO burdens measured from space between 2000 and 2009 and validated by ground-based solar tracking spectrometers, Atmos. Chem. Phys., 10, 3479–3494, 2010.

Zhang, L., Jacob, D. J., Boersma, K. F., Jaffe, D. A., Olson, J. R., Bowman, K. W., Worden, J. R., Thompson, A. M., Avery, M. A., and Cohen, R. C.: Transpacific transport of ozone

pollution and the effect of recent Asian emission increases on air quality in North America: an integrated analysis using satellite, aircraft, ozonesonde, and surface observations, Atmos. Chem. Phys, 8, 6117–6136, 2008.

Zhang, Q., Streets, D. G., He, K., Wang, Y., Richter, A., Burrows, J. P., Uno, I., Jang, C. J., Chen, D., and Yao, Z.: NOx emission trends for China, 1995-2004: The view from the ground and the view from space, Journal of Geophysical Research, 112, D22 306, 2007.

Zhang, Q., Streets, D. G., Carmichael, G. R., He, K. B., Huo, H., Kannari, A., Klimont, Z., Park, I. S., Reddy, S., Fu, J. S., Chen, D., Duan, L., Lei, Y., Wang, L. T., and Yao, Z. L.: Asian emissions in 2006 for the NASA INTEX-B mission, Atmospheric Chemistry and Physics, 9, 5131–5153, 2009.

Chapter 3

Sources, distribution, and acidity of sulfate–ammonium aerosol in the Arctic in winter–spring

Abstract

We use GEOS-Chem chemical transport model simulations of sulfate-ammonium aerosol data from the NASA ARCTAS and NOAA ARCPAC aircraft campaigns in the North American Arctic in April 2008, together with longer-term data from surface sites, to better understand aerosol sources in the Arctic in winter-spring and the implications for aerosol acidity. Arctic pollution is dominated by transport from mid-latitudes, and we test the relevant ammonia and sulfur dioxide emission inventories in the model by comparison with wet deposition flux data over the source continents. We find that a complicated mix of natural and anthropogenic sources with different vertical signatures is responsible for sulfate concentrations in the Arctic. East Asian pollution influence is weak in winter but becomes important in spring through transport in the free troposphere. European influence is important at all altitudes but never dominant. West Asia (non-Arctic Russia and Kazakhstan) is the largest contributor to Arctic sulfate in surface air in winter, reflecting a southward extension of the Arctic front over that region. Ammonium in Arctic spring mostly originates from anthropogenic sources in East Asia and Europe, with added contribution from boreal fires, resulting in a more neutralized aerosol in the free troposphere than at the surface. The ARCTAS and ARCPAC data indicate a median aerosol neutralization fraction $NH_4^+/(2SO_4^{2-}+NO_3^-)$ of 0.5 mol mol^{-1} below 2 km and 0.7 mol mol^{-1} above. We find that East Asian and European aerosol transported to the Arctic is mostly neutralized, whereas West Asian and North American aerosol is highly acidic. Growth of sulfur emissions in West Asia may be responsible for the observed increase in aerosol acidity at Barrow over the past decade. As global sulfur emissions decline over the next decades, increasing aerosol neutralization in the Arctic is expected, potentially accelerating Arctic warming through indirect radiative forcing and feedbacks.

3.1 Introduction

Long-range transport of pollution from mid-latitudes is a major source of aerosols to the Arctic, with a winter-spring maximum known as Arctic haze (Rahn, 1981a; Quinn et al., 2009). Sulfate is the dominant component of this aerosol (Quinn et al., 2007), and it may range from highly acidic to fully neutralized depending on the availability of ammonia. The extent to which sulfate aerosol is neutralized has implications for aerosol radiative forcing (Martin et al., 2004), ice cloud nucleation (Abbatt et al., 2006; Eastwood et al., 2009; Baustian et al., 2010), and heterogeneous chemistry (Fan and Jacob, 1992; Fickert et al., 1999). Here we use the GEOS-Chem 3-D global chemical transport model (CTM) to interpret observations of sulfate-ammonium aerosol composition and acidity from the NASA ARCTAS (Arctic Research of the Composition of the Troposphere from Aircraft and Satellites) and NOAA ARCPAC (Aerosol, Radiation, and Cloud Processes affecting Arctic Climate) aircraft campaigns conducted in the North American Arctic in April 2008, using also ground-based measurements to place the aircraft data in a broader seasonal context. Our objective is to better understand the sources contributing to sulfate, ammonium, and aerosol acidity through the depth of the Arctic troposphere over the winter-spring season.

High aerosol concentrations in the Arctic in winter-spring reflect a combination of fast transport from mid-latitudes, reduced vertical mixing, and lack of precipitation (Barrie et al., 1981; Raatz and Shaw, 1984; Iversen and Joranger, 1985; Barrie, 1986; Shaw, 1995;

Quinn et al., 2007; Garrett et al., 2010). The resulting aerosol radiative forcing may play a major role in driving climate change in the Arctic (Shindell and Faluvegi, 2009), where recent warming has been especially rapid (Trenberth et al., 2007). Scattering sulfate aerosols reflect incoming solar radiation, generally resulting in atmospheric cooling (Quinn et al., 2008). However, warming may result where the surface albedo is very high (Pueschel and Kinne, 1995) or if the sulfate is internally mixed with absorbing aerosol (Jacobson, 2001b). Hygroscopic growth of particles leads to absorption of terrestrial radiation, inducing a direct warming effect that can be particularly efficient during polar night (Ritter et al., 2005). Indirect effects of aerosols on cloud properties typically cause surface cooling (Quinn et al., 2008) but can also warm the surface through interactions with terrestrial radiation (Garrett and Zhao, 2006; Lubin and Vogelmann, 2006). The warming is expected to dominate during Arctic winter (Lubin and Vogelmann, 2007).

The chemical composition of the Arctic aerosol, in particular the extent to which sulfate aerosol is neutralized, has major implications for aerosol radiative forcing. Observations show that ammonia (NH_3) is the main neutralizing agent. It is quantitatively absorbed by the acidic sulfate aerosol, titrating its acidity, reducing its hygroscopicity, and producing solid ammonium sulfate at low relative humidity. The resulting decrease in aerosol water content both reduces the direct radiative forcing of sulfate (Boucher and Anderson, 1995; Adams et al., 2001; Jacobson, 2001a; Martin et al., 2004; J. Wang et al., 2008b) and inhibits homogenous ice nucleation by liquid sulfate-containing particles (Koop et al., 2000). Solid ammonium sulfate particles can also play a role in cold cloud formation by serving as

heterogeneous ice nuclei (Abbatt et al., 2006; Wise et al., 2009; Baustian et al., 2010). Hydrophobic dust particles coated with ammonium sulfate are efficient ice nuclei, whereas particles coated with pure sulfuric acid are not (Eastwood et al., 2009). Sulfate aerosol neutralization also suppresses acid-catalyzed heterogeneous bromine reactions thought to be critical in driving ozone and mercury depletion events in Arctic spring (Fan and Jacob, 1992; Ayers et al., 1999; Fickert et al., 1999; Piot and von Glasow, 2008).

Most of the information on sulfate aerosol in the Arctic has come from surface sites. Early studies attributed sulfate in the North American Arctic to sulfur dioxide (SO_2) sources in Europe and the Soviet Union based on metal tracers (Rahn, 1981b; Raatz and Shaw, 1984; Lowenthal and Rahn, 1985). More recently, Quinn et al. (2009) used the same methodology with data from Barrow, Alaska to show that despite large decreases in emissions and a decreasing trend in sulfate concentrations, the attribution of sulfate sources has not changed over the past 30 years. In contrast, data from Alert, Canada suggest a growing relative contribution from North America as the influence from Eurasian sources has decreased (Gong et al., 2010; Hirdman et al., 2010a). Eurasian emissions are still thought to dominate sulfate concentrations at both Barrow and Alert (Hirdman et al., 2010a; Hirdman et al., 2010b).

Because the highly stable Arctic boundary layer is decoupled from the free troposphere in winter-spring, measurements at the surface are not representative of the tropospheric column. The sources of sulfate in the Arctic free troposphere are not as well understood as the sources at the surface, and source contributions may vary greatly with altitude (Shindell

et al., 2008). Back-trajectory analyses of 1983-1992 aircraft data from the Arctic Gas and Aerosol Sampling Program (AGASP) implied dominant sulfate sources in both the boundary layer and the free troposphere from Europe and the former Soviet Union (Sheridan and Musselman, 1985; Herbert et al., 1989; Parungo et al., 1993). More recent aircraft measurements and model analyses from the Tropospheric Ozone Production about the Spring Equinox (TOPSE) campaign in February-May 2000 suggested dominant sulfate sources from Europe in the boundary layer and from North America in the mid-troposphere (Klonecki et al., 2003; Scheuer et al., 2003).

A number of CTM studies have investigated the sources of sulfate in the Arctic, with varying results. Simulations for the late 1980s and early 1990s showed a major contribution to Arctic sulfate from the Norilsk industrial site in Siberia. Christensen (1997) found Norilsk to be responsible for 30% of low-altitude sulfate in the Arctic in all seasons, with the remainder from western Europe and Russia. At higher altitudes, Russian and European sources were found to dominate (Christensen, 1997; Tarrasn and Iversen, 1998). More recent work has recognized the growing importance of East Asian emissions, especially in the free troposphere (Koch and Hansen, 2005; Shindell et al., 2008; Huang et al., 2010). While most models agree that Arctic sulfate can be attributed to a mix of anthropogenic sources from Europe, Russia, North America, and East Asia, they disagree considerably both on the relative importance of these sources and on the absolute concentrations of sulfate in the Arctic atmosphere. A recent multi-model sulfate intercomparison by Shindell et al. (2008) showed concentrations varying between models by a factor of 1000 in the Arctic

free troposphere, with none of the models able to successfully reproduce observed surface sulfate concentrations or seasonality.

Little attention has been paid so far to the factors determining the neutralization of acidic sulfate aerosol by ammonia in the Arctic. Combined observations of aerosol sulfate and ammonium, providing a diagnostic of sulfate neutralization, are available from a few Arctic surface sites. Ammonium concentrations also peak in winter-spring but the seasonal amplitude is less than for sulfate, resulting in peak aerosol acidity in winter (Toom-Sauntry and Barrie, 2002). While northern hemispheric NH_3 emissions are estimated to have increased by 20% over the last decade due to agricultural activity (Galloway et al., 2008; Clarisse et al., 2009), data from Barrow show decreasing Arctic ammonium concentrations over the last decade (Quinn et al., 2009). Concurrent decreases in sulfate are proceeding more slowly, resulting in increasing aerosol acidity at Barrow (Quinn et al., 2009). Data at Alert also show a long-term decline in ammonium, but proceeding less rapidly than for sulfate, leading to more neutralized aerosol (Hole et al., 2009). The differences between Barrow and Alert point to different source influences affecting different regions of the Arctic in a time-dependent way.

Data from the April 2008 ARCTAS and ARCPAC aircraft campaigns based in Fairbanks, Alaska (Brock et al., 2010; Jacob et al., 2010) provide unprecedented information on the vertical distribution of sulfate-ammonium aerosols through the depth of the troposphere in the North American Arctic. Both aircraft included extensive chemical payloads. We use here the GEOS-Chem CTM in combination with the aircraft data and seasonal

observations from surface sites to probe the sources of sulfate-ammonium aerosols in the Arctic in winter-spring and the implications for aerosol acidity. Other studies have applied GEOS-Chem to interpretation of ARCTAS/ARCPAC observations of CO (Fisher et al., 2010), carbonaceous aerosols (Q. Wang et al., 2011), HO_x radicals (Mao et al., 2010), and mercury (Holmes et al., 2010).

3.2 GEOS-Chem Simulation

We use the GEOS-Chem CTM version 8-02-03 (http://geos-chem.org) to simulate coupled aerosol-oxidant chemistry on the global scale. The model is driven by GEOS-5 assimilated meteorological data from the NASA Goddard Earth Observing System (GEOS) with 6-hour temporal resolution, 47 vertical levels, and $0.5^\circ \times 0.667^\circ$ horizontal resolution, regridded to $2^\circ \times 2.5^\circ$ for input to GEOS-Chem. We initialize the model with a one-year spin-up followed by simulation of January-May 2008.

The GEOS-Chem coupled aerosol-oxidant simulation was originally described by Park et al. (2004), but the present version includes a number of updates. NH_3 and SO_2 emissions for the simulation period are compiled in Table 3.1 and shown in Fig. 3.1. Direct emission of anthropogenic sulfate is included as a small fraction of anthropogenic SO_2 (Chin et al., 2000) and is not included in Table 3.1. Open biomass burning emissions are from the Fire Location and Monitoring of Burning Emissions (FLAMBE) inventory (Reid et al., 2009), injected into the local planetary boundary layer, with SO_2 and NH_3 emissions scaled to carbon emissions using emission factors from Andreae and Merlet (2001). Unusually large

Russian wildfires affected the North American Arctic during ARCTAS/ARCPAC (Warneke et al., 2009). Fisher et al. (2010) found that the FLAMBE emissions for CO needed to be reduced by 47% for Russia and 55% for Southeast Asia to match the aircraft observations and we apply the same corrections here for SO_2 and NH_3. We also include SO_2 emission from both eruptive and non-eruptive (continuous degassing) volcanism. In winter-spring 2008, sustained eruptive activity was recorded at Karymsky and Shiveluch in Kamchatka and Cleveland in the Aleutian Islands. Non-eruptive activity was common throughout our simulation period at a number of volcanoes in Iceland, Kamchatka, and the Aleutian Islands.

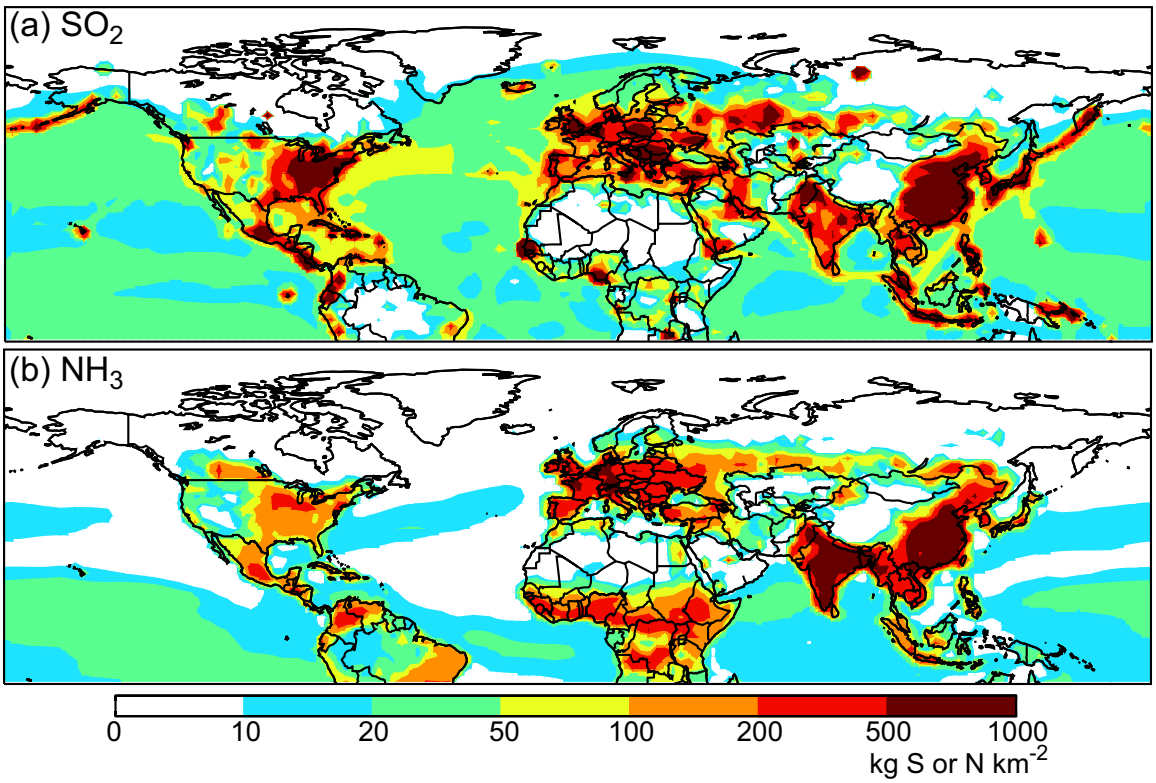

Figure 3.1: January-May 2008 GEOS-Chem emissions of (a) SO_2 (kg S km^{-2}) and (b) NH_3 (kg N km^{-2}), averaged over the 2°x2.5° model grid. Regional totals are given in Table 3.1.

Table 3.1: Global SO_2 and NH_3 emissions for 2008.[a]

Source	SO_2, Tg S	NH_3, Tg N
Anthropogenic[b]	64 (27)	39 (15)
Continguous U.S. and Canada (south of 60°N)	8.0 (3.3)[c,d]	2.6 (0.82)[d]
Europe (south of 60°N)	6.9 (3.2)[e]	5.2 (2.3)[e]
West Asia and Siberia (south of 60°N)	3.3 (1.4)	1.2 (0.30)
East Asia	23 (9.7)[f]	21 (7.4)[g]
North American Arctic (60-90°N, 180-37.5°W)	0.016 (0.0067)[d]	0.0015 (0.0006)[d]
Eurasian Arctic (60-90°N, 37.5°W-180°E)	0.58 (0.25)[e]	0.14 (0.049)[e]
Rest of world	13 (5.3)	8.5 (3.8)
Ships	8.5 (3.5)[h]	–
Aircraft	0.070 (0.028)[i]	–
Open biomass burning[j]	2.0 (0.56)[k]	9.5 (2.3)[k]
Natural sources	31 (13)	14.3 (5.9)
Oxidation of biogenic dimethyl sulfide (DMS)	18 (8.1)[l]	–
Volcanism	13 (5.1)[m]	–
Ocean, soil, crop decomposition, wild animals	–	14.3 (5.9)[n]
TOTAL	97 (41)	62 (23)

[a] Annual totals for 2008 used in GEOS-Chem. Totals for January-May are given in parentheses.

[b] Including fuel and industrial emissions of SO_2 and agricultural and fuel emissions of NH_3. Fuel emissions are mostly from coal for SO_2 and from biomass (biofuel) for NH_3. Default anthropogenic emission inventories are EDGAR 3.2 for SO_2 in 2000 (Olivier et al., 1999) and the Bouwman et al. (1997) implementation of the Global Emissions Inventory Activity (GEIA) for NH_3 in 1990 with seasonality from Park et al. (2004). These inventories are overwritten for specific regions as indicated in footnotes. See Fig. 3.3a for region definitions.

[c] U.S. anthropogenic SO_2 emissions are from the US Environmental Protection Agency National Emission Inventory for 1999 (EPA-NEI99, http://www.epa.gov/ttnchie1/net/1999inventory.html).

[d] Canadian anthropogenic emissions are from the Criteria Air Contaminants (CAC) inventory for 2005 (Environment Canada, http://www.ec.gc.ca/pdb/cac/cac_home_e.cfm).

[e] European anthropogenic emissions are from the Cooperative Programme for Monitoring and Evaluation of the Long-range Transmission of Air Pollutants in Europe (EMEP) inventory for 2005 (Vestreng and Klein, 2002). These are also used for the European Arctic, while EDGAR 3.2 is used for the Asian Arctic in the absence of better information.

[f] Asian SO_2 emissions are from the NASA INTEX-B inventory for 2006 (Zhang et al., 2009) with seasonality based on monthly NOx emissions (Zhang et al., 2007b).

[g] East Asian annual NH_3 emissions are from Streets et al. (2003) with superimposed relative seasonal variation based on the length of the growing season for fertilizer use and on temperature and wind speed for everything else (L. Bouwman, personal communication).

[h] Ship emissions of SO_2 are based on EDGAR 2000 (Eyring et al., 2005a; Eyring et al., 2005b), overwritten over Europe by the EMEP inventory.

[i] Aircraft emissions of SO_2 are based on mean fuel consumption from the NASA Atmospheric Effects of Aviation Project (Baughcum et al., 1996) as described by Chin et al. (2000).

[j] Excluding biofuel, which is included in the anthropogenic source.

[k] Biomass burning emissions are from the FLAMBE inventory (Reid et al., 2009) corrected by Fisher et al. (2010), and are computed as described in the text.

[l] The source from DMS oxidation is as described by Park et al. (2004).

[m] Volcanic SO_2 emissions are from the AEROCOM inventory (Diehl, 2009). Emissions from continuous (non-eruptive) volcanic degassing are injected at the altitude of the volcanic crater. Eruptive emissions are emitted evenly over the top third of the volcanic plume, as described by Chin et al. (2000).

[n] Natural NH_3 emissions (ocean, soil, crop decomposition, and wild animals) are from Bouwman et al. (1997).

Emitted SO_2 is oxidized to sulfate by the hydroxyl radical (OH) in the gas phase and by ozone (O_3) and hydrogen peroxide (H_2O_2) in the aqueous phase at temperatures above 258 K. Unlike in previous versions of the model (Park et al., 2004; Alexander et al., 2009), cloud volume fraction (used to determine where aqueous SO_2 chemistry occurs) and cloud liquid water content (used to compute the aqueous SO_2 chemistry reaction rates) are now taken directly from the GEOS-5 assimilated meteorological fields for each gridbox. Ammonia and nitric acid are partitioned between the gas and the sulfate-nitrate-ammonium aerosol phases using the ISORROPIA II thermodynamic equilibrium model (Fountoukis and Nenes, 2007). Nitrate was usually negligible compared to sulfate in ARCTAS/ARCPAC, both in the observations and the model, owing to the general acidic nature of the aerosol. We discuss the nitrate data briefly in Section 3.6.

Aerosol is removed by dry and wet deposition. Dry deposition in GEOS-Chem follows a resistance-in-series scheme (Wesely, 1989) originally described by Y. Wang et al. (1998). Over snow and ice surfaces, we impose an aerosol dry deposition velocity of 0.03 cm s^{-1} based on eddy-covariance flux measurements by Nilsson and Rannik (2001) and consistent with earlier estimates (Ibrahim et al., 1983; Duan et al., 1988). Wet deposition in the model is based on the scheme described by Liu et al. (2001) with improved representation of scavenging by ice clouds and snow as described by Q. Wang et al. (2011). We assume 100% sulfate and ammonium incorporation into liquid cloud droplets and rime ice for warm and mixed-phase clouds ($T>258$ K) and no incorporation into ice crystals for cold clouds ($T<258$ K). We also use a higher below-cloud scavenging efficiency for

snow than for rain (Murakami et al., 1983). Gaseous NH_3 in the model is efficiently scavenged by liquid precipitation but has a retention efficiency of only 0.05 upon riming (which drives precipitation in mixed-phase clouds) and is not scavenged at all in cold clouds (J. Wang et al., 2008a). A sensitivity study assuming complete scavenging of gaseous NH_3 in cold and mixed-phase clouds showed no significant difference in the Arctic relative to the standard simulation because most of the total NH_X ($\equiv NH_3 + NH_4^+$) in the Arctic is present as ammonium.

3.3 Testing emission inventories with wet deposition flux data

SO_2 and NH_3 emissions in North America, Europe, and East Asia are potential major sources of sulfate and ammonium aerosol to the Arctic. The corresponding emission inventories used in the model can be tested by comparison with wet deposition flux data over these source continents. Because most of what is emitted is deposited near the source, wet deposition data provide a better constraint on emission than concentration data. While there are large uncertainties associated with modeled precipitation (Dentener et al., 2006; Stephens et al., 2010), we expect the effect of precipitation errors to be small since we consider monthly mean flux data and continental-scale statistics. We used for this analysis data from the ensemble of sites of the U.S. National Atmospheric Deposition Program (NADP; National Atmospheric Deposition Program, 2010), the Cooperative Programme for Monitoring and Evaluation of the Long-range Transmission of Air Pollutants in Eu-

rope (EMEP; EMEP/CCC, 2010), and the Acid Deposition Monitoring Network in East Asia (EANET; http://www.eanet.cc/product/index.html). The EANET network includes a large number of sites labeled as urban, and these were excluded from the comparison as potentially non-representative.

Figure 3.2 compares distributions of observed and modeled sulfate and ammonium wet deposition fluxes in April 2008, along with correlation coefficients (r) and normalized mean biases (NMB = $100\% \times [\sum_i (M_i - O_i / \sum_i O_i]$, where M_i and O_i are the modeled and observed values, respectively, and the summation is over all sites). The GEOS-Chem sulfate simulation shows good agreement with deposition observations over the U.S. (r = 0.72, NMB = +4.7%), consistent with prior model evaluations for this region (Park et al., 2004; Liao et al., 2007; Pye et al., 2009; Drury et al., 2010). Ammonium deposition over the U.S. shows good agreement with NADP observations at low values but a low bias for deposition greater than 0.5 kg NH_4^+ ha^{-1} (r = 0.73, NMB = -40%). As seen in Fig. 3.2b, this bias is driven by the agricultural upper Midwest where spring emissions are apparently underestimated. Because transport from North America to the Arctic in spring is mostly from warm conveyor belts over the U.S. east coast (Stohl, 2006; Fisher et al., 2010), we expects errors over the upper Midwest to have limited impact on our Arctic simulation. Over Europe, the model-observation agreement is best at low sulfate values, with model underestimates of high sulfate concentrations observed at a few sites (r = 0.69, NMB = -14%). Simulated ammonium deposition over Europe agrees well with observations (r = 0.61, NMB = +1.0%). Wet deposition over East Asia is on average too low in GEOS-Chem for both

sulfate (r = 0.85, NMB = -40%) and ammonium (r = 0.60, NMB = -20%). This bias is driven by a few sites with extremely high deposition values (2-3 kg NH_4^+ ha^{-1}, 4-17 kg SO_4^{2-} ha^{-1}), highlighted in white trim in Fig. 3.2. When these sites are removed from the comparisons the NMB improves to -0.98% (r = 0.71) for sulfate and -6.3% (r = 0.42) for ammonium. Overall, our SO_2 and NH_3 emission inventories appear unbiased except for the NH_3 underestimate in the upper Midwest U.S.

In Table 3.2 we diagnose the acidity of emissions originating from each region as the NH_3/SO_2 emission ratio and the NH_4^+/SO_4^{2-} wet deposition flux ratio. Some difference between these two measures of acidity is expected because of differences in dry deposition, wet scavenging efficiencies, and source locations for SO_2 and NH_3. We do not include NO_x emissions and nitrate wet deposition in this analysis nitric acid (unlike sulfuric acid or bisulfate) generally does not partition into the aerosol unless neutralized by a basic counterion and therefore does not contribute significantly to aerosol acidity. The model emission ratios in Table 3.2 indicate that emissions in the U.S. lead to highly acidic aerosol, whereas they promote fully neutralized aerosol in Europe and East Asia, at least on the continental scale. While SO_2 emissions in our inventory are similar in Europe and the U.S., NH_3 emissions are much lower in the U.S. (Table 3.1), consistent with recent estimates (Reis et al., 2009). This difference reflects higher emissions associated with livestock housing, storage, and grazing in Europe (Beusen et al., 2008).

The differences in emission ratios are reflected in the simulated and observed molar NH_4^+/SO_4^{2-} wet deposition ratios for Europe and the U.S. (Table 3.2). Over East Asia, wet

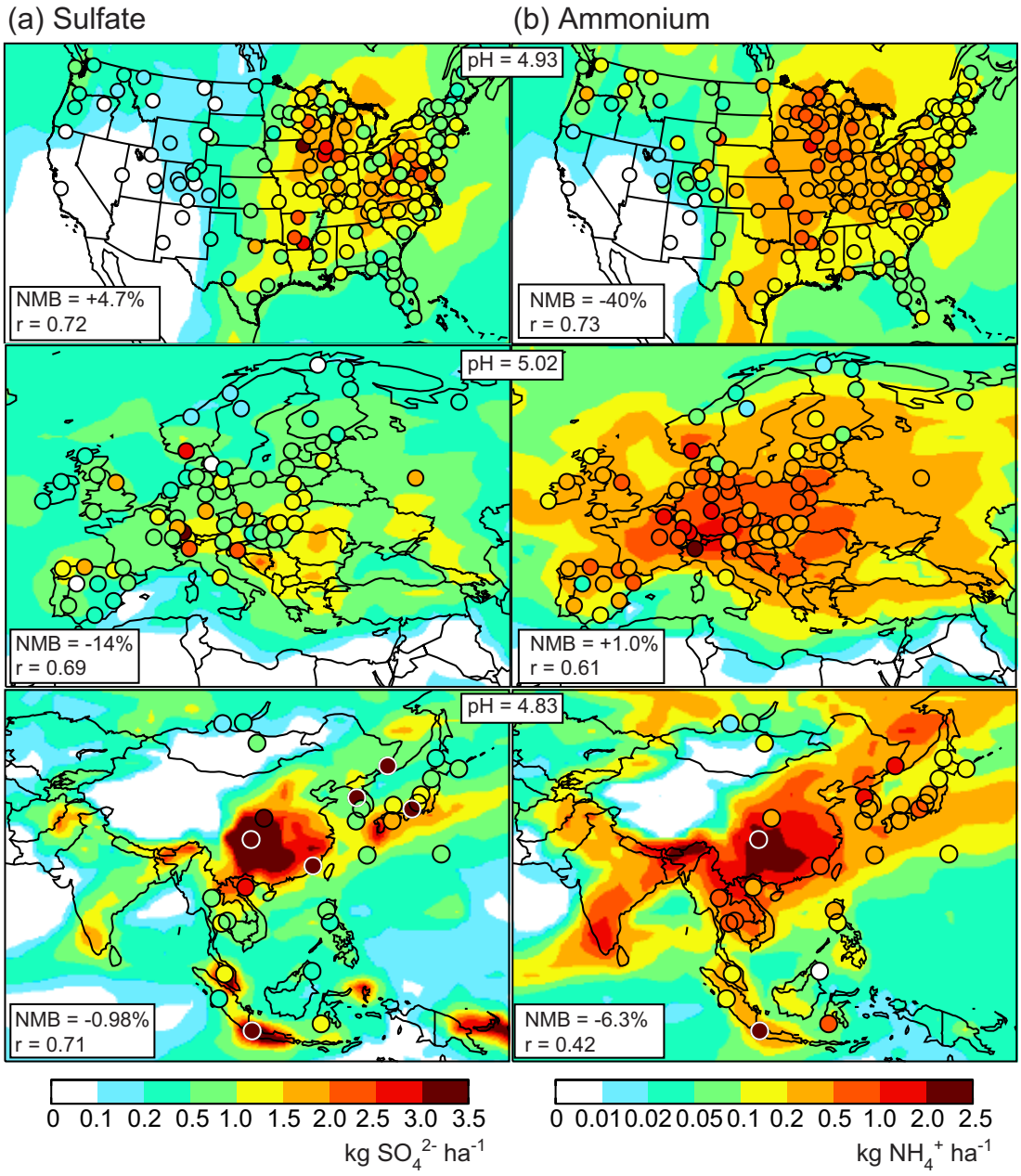

Figure 3.2: (a) Sulfate and (b) ammonium wet deposition fluxes over North America, Europe, and East Asia in April 2008. Model results (background) are compared to observations (circles) from the NADP, EMEP, and EANET networks. Major outliers in the observations (sulfate deposition > 4 kg ha^{-1}, ammonium deposition > 1.5 kg ha^{-1}) are highlighted in white trim. Correlation coefficients (r) and normalized mean biases (NMB), computed after removing major outliers, are given inset. Mean observed pH for each network (computed by averaging the mean precipitation-weighted [H$^+$] at each site) is also given inset.

Table 3.2: Sulfate neutralization ratios by source region.[a]

Region[b]	Emissions[c] $E_{NH3}/2E_{SO2}$ (mol mol^{-1})	Wet deposition (source region)[d] $[NH_4^+]/(2[SO_4^{2-}])$ (mol mol^{-1})	
		Observations	Model
East Asia	1.2	0.76	0.87
Europe	1.3	1.4	1.7
North America	0.29	0.76	0.45
West Asia	0.23	–	–

[a] Values are for April 2008.
[b] Region definitions are given in Fig. 3.3a.
[c] Ratio of regional emissions as given in Table 3.1, for April only.
[d] Ratios of mean precipitation-weighted concentrations at the NADP, EMEP, and non-urban EANET sites.

deposition at EANET sites appears moderately acidic in both the observations ($[NH_4^+]/2[SO_4^{2-}] = 0.76$) and the model ($[NH_4^+]/2[SO_4^{2-}] = 0.87$), whereas the continental emissions suggest full neutralization. The EANET sites are not, however, representative of the East Asian region as a whole, in large part because there are no observational sites over agricultural regions in India where the NH_3/SO_2 emission ratio is particularly high (Figure 3.1). GEOS-Chem deposition fluxes averaged over the whole region show aerosol deposition to be as neutralized as expected from the emissions. The NH_4^+/SO_4^{2-}ratios indicate more acidic deposition over North America ($[NH_4^+]/2[SO_4^{2-}] = 0.76$) than over Europe ($[NH_4^+]/2[SO_4^{2-}] = 1.4$). Observed pH shows less regional variation, with average deposition only marginally more acidic over the U.S. (pH = 4.93) than over Europe (pH = 5.02). This is due to higher wet deposition fluxes of nitrate (from both aerosol nitrate and gas-phase nitric acid) over Europe. The wet deposition data also indicate partial neutralization by alkaline dust over all three continents. Aircraft observations from ARCPAC indicate that dust particles in the Arctic are generally externally mixed with sulfate, with

sulfate mostly in the fine mode (<0.7 μm) and dust mostly in the coarse mode (Brock et al., 2010). Further, observations of Asian outflow from the INTEX-B aircraft campaign show the dominant sulfate counterion to be ammonium, not dust (McNaughton et al., 2009; Fairlie et al., 2010). We thus expect that mid-latitude dust would not neutralize the acidity of the submicron sulfate aerosol in the Arctic.

3.4 Simulation and source attribution of Arctic sulfate

3.4.1 Aircraft data

The NASA ARCTAS campaign (1-19 April 2008) is described in detail by Jacob et al. (2010). We use here data collected onboard the DC-8 aircraft that was based in Fairbanks, Alaska and covered a large swath of the North American Arctic over 74 flight hours. All concentrations are used for STP conditions (1 atm, 273 K). Speciated aerosol composition data were obtained with an Aerosol Mass Spectrometer (AMS) (Dunlea et al., 2009) measuring submicron aerosol mass and with the SAGA instrumentation package (Dibb et al., 2003) measuring fine aerosol sulfate (<1 μm) using a mist chamber/ion chromatograph (MC/IC) and bulk sulfate, ammonium, nitrate, calcium, and sodium using filters analyzed by ion chromatography. Speciated aerosol data were also collected during the NOAA ARCPAC campaign (3-23 April 2008) using an AMS onboard the WP-3D aircraft also based in Fairbanks, Alaska (Brock et al., 2010). Flight tracks for ARCTAS and ARCPAC are shown in Fig. 3.3b. The ARCPAC flights covered much less area than ARCTAS, spent more time in the boundary layer, and frequently sampled biomass burning and pollution

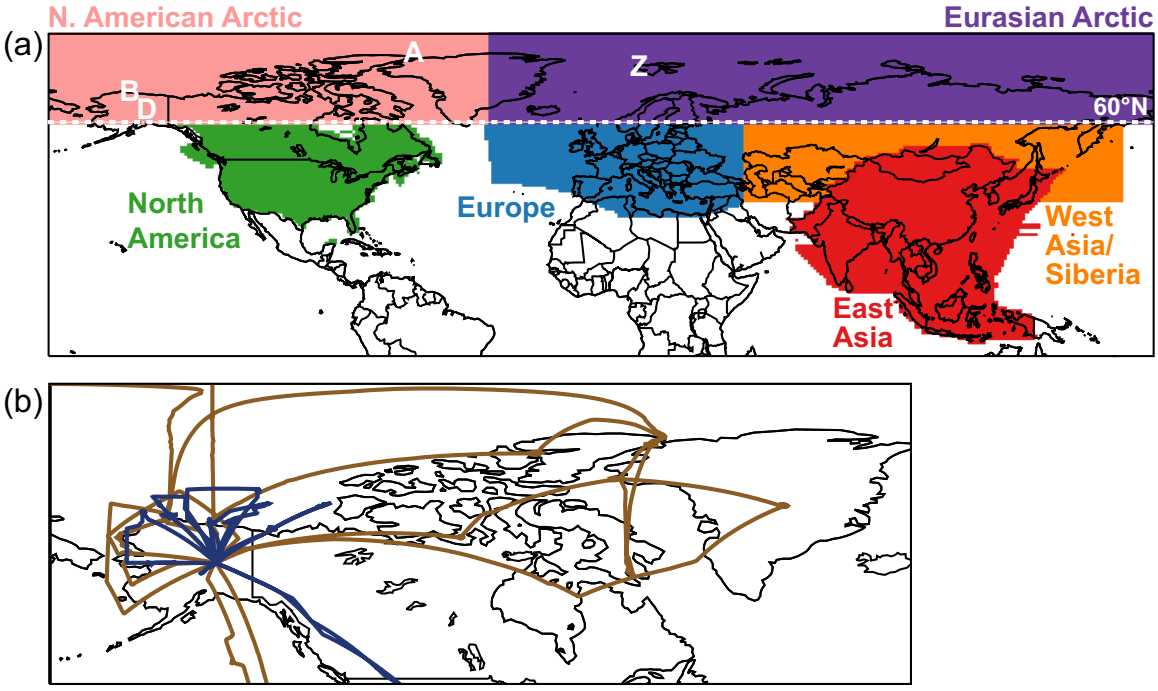

Figure 3.3: (a) Regions used for source attribution of sulfate-ammonium aerosol in the Arctic. Model sensitivity simulations were conducted with anthropogenic emissions from each of these regions shut off individually. Additional sensitivity simulations were conducted shutting off global ship, biomass burning and natural emissions. Also shown are the locations of surface stations used for model evaluation: Alert (A), Barrow (B), Denali (D), and Zeppelin (Z). (b) Flight tracks for ARCTAS (brown) and ARCPAC (dark blue).

plumes.

For comparison to the aircraft data, the GEOS-Chem simulation is sampled along the flight track at the times and locations of the aircraft observations, averaging over either the instrument sampling time or the three-dimensional model grid and time step (Section 3.2), whichever is coarser. Observations outside the Arctic region (south of 60°N) and those from the stratosphere (diagnosed as $[O_3]/[CO] > 1.25$ mol mol^{-1}; Hudman et al., 2008) are excluded. Data from the first two ARCTAS flights (1 and 4 April 2008) are also excluded due to apparent problems with the AMS instrument. Fine-structure plumes are not

well simulated by Eulerian CTMs due to numerical diffusion and displacement (Rastigejev et al., 2010). We thus exclude strong biomass burning plumes as diagnosed by observed acetonitrile (CH_3CN) in excess of 225 pptv (Heald et al., 2006; Hudman et al., 2007; Hudman et al., 2008), amounting to 3% of the ARCTAS data and 10% of the ARCPAC data. We use a high CH_3CN threshold for this purpose in order to avoid removing biomass burning contributions to background aerosol concentrations, which should be captured by the CTM. We also exclude observations likely to be contaminated by local pollution in Alaska, diagnosed as points below 4 km altitude and within 0.5° of Fairbanks or the Prudhoe Bay oil field. This filter excludes 20% of the ARCPAC data and less than 2% of the ARCTAS data. Finally, we remove one major outlier from each campaign with sulfate in excess of 60 nmol m^{-3} STP. These two outliers represent singularly large concentrations for which we have no explanation.

Sulfate in the observations includes a contribution from primary sea salt sulfate ($ssSO_4^{2-}$) that is not included in GEOS-Chem. We subtract this contribution from the SAGA filter observations by using a $[ssSO_4^{2-}]/[Na^+]$ mass ratio of 0.252 (Calhoun et al., 1991). Primary sea salt sulfate estimated in this way accounts for only a small fraction of total bulk sulfate (1.5±2.9% on average) and peaks in the boundary layer (2.6±3.7% on average below 2 km). No sodium data are available from the AMS measurements, but we assume the sea salt contribution to be negligible. This assumption is reasonable because sodium sulfate does not volatilize rapidly at the temperatures used by the AMS instrument and because these data are only for submicron aerosol while sea salt aerosol is mostly supermicron.

We compared the three ARCTAS sulfate datasets using reduced major axis regression (Hirsch and Gilroy, 1984). Submicron sulfate measured by the SAGA MC/IC and by the AMS show good agreement (r = 0.88, slope = 1.0). SAGA bulk sulfate from the filters generally agrees well with the submicron measurements (AMS: r = 0.80, slope = 1.1; SAGA MC/IC: r = 0.77, slope = 1.1), except during flights on 5 and 8 April 2008 when bulk sulfate concentrations from the SAGA filters were two to three times higher than measured by the other instruments (AMS: slope = 2.1; SAGA MC/IC: slope = 2.8). A large contribution from supermicron sulfate aerosol may arise from sulfate uptake on dust particles (Dibb et al., 2003); however, the data from those two flights were not correlated with dust tracers. We therefore exclude sulfate observations from these two flights from comparisons with GEOS-Chem. For all subsequent ARCTAS analysis, we use the SAGA filter observations due to the similar information content of the SAGA and AMS data.

Figure 3.4a shows scatterplots of modeled versus observed sulfate for ARCTAS and ARCPAC. The model has some success in reproducing the variability in the ARCTAS data (r = 0.60), with a mean model overestimate of +5.6% and model underestimates at high sulfate concentrations. Model representation of variability is much poorer for ARCPAC (r = 0.28), although the mean bias is again small (-5.4%). The small cluster of model points with values in excess of 30 nmol m^{-3} STP reflects a misplaced volcanic plume; without these points the correlation coefficient increases to r = 0.47. We conducted model sensitivity simulations to try to understand the poor simulation of variability in ARCPAC but could not relate it to a specific source or conditions, and could not find corrections that

would not compromise the simulation of ARCTAS or surface data. The observations do not appear biased as there was internal consistency between the physical, optical and chemical measurements made during ARCPAC (Brock et al., 2010). Our best explanation is that the small sampling domain and time spent in plumes during ARCPAC makes model simulation of the observed variability difficult, especially at the 2°x2.5° resolution used here. The ARCTAS data cover a much larger domain and we view them as more representative.

Figure 3.5a shows the mean vertical distributions of observed and modeled sulfate concentrations along the aircraft flight tracks. Model values are decomposed into the contributions from individual sources and regions, as diagnosed by a series of sensitivity simulations with individual sources shut off either globally (ships, biomass burning, natural sources) or for each region shown in Fig. 3.3a (anthropogenic sources). There is some nonlinearity associated with titration of H_2O_2 in clouds (Chin and Jacob, 1996), the effects of which are included in the relatively small "other" term.

We find that there is little mean vertical gradient of sulfate concentrations in either the observations or the model, and that a diversity of sources contributes to sulfate burdens in the North American Arctic at all altitudes. Individual source contributions in the model show much more vertical structure than total sulfate. Below 2 km we find that East Asian, European, and North American anthropogenic sources have comparable influences, each contributing 10-20% of modeled sulfate. The North American influence is limited to the lower troposphere, while European and East Asian contributions are substantial throughout the column. Above 2 km, East Asian emissions are dominant, although still accounting for

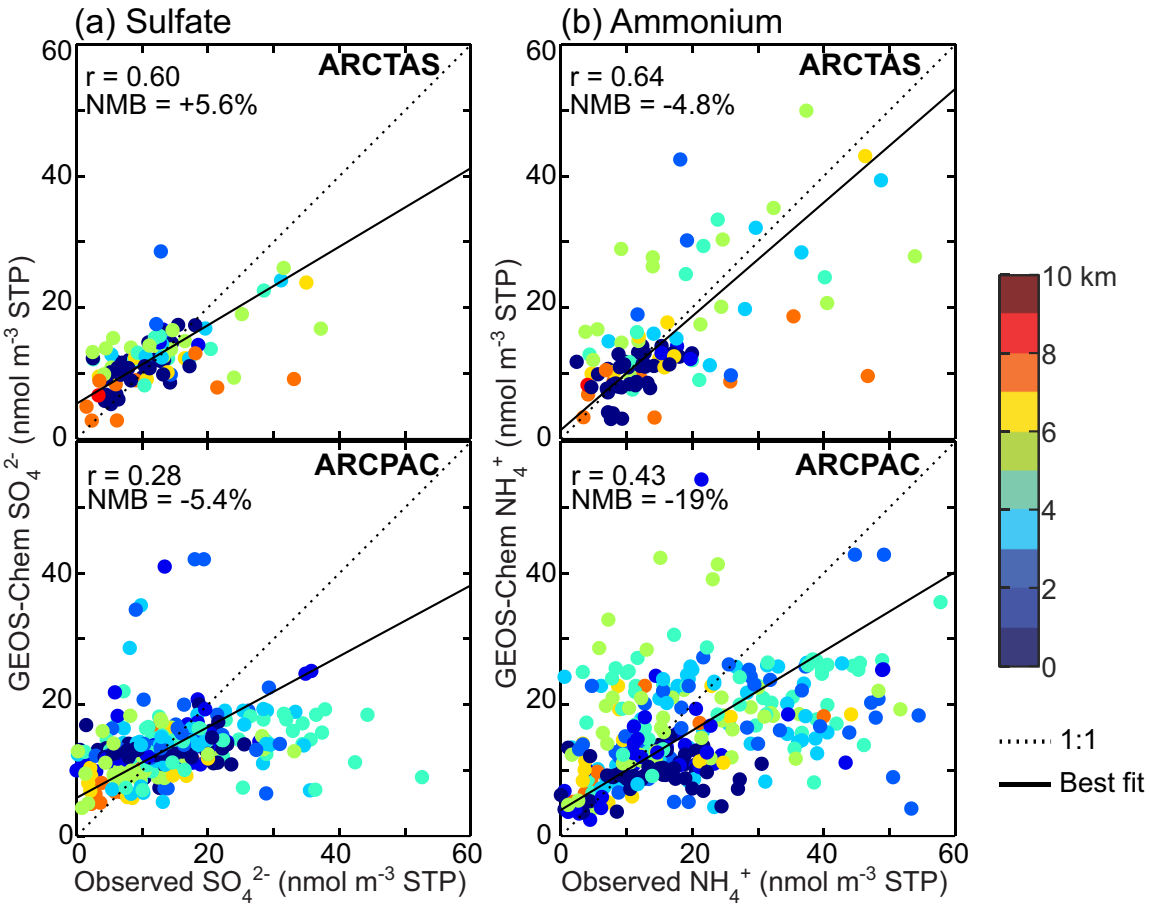

Figure 3.4: Comparison of modeled and observed (a) sulfate and (b) ammonium during ARCTAS (top) and ARCPAC (bottom), colored by altitude. Biomass burning plumes, stratospheric air, local pollution, observations south of 60°N, and major outliers have been removed from the comparisons as described in the text. All concentrations are reported in nmol m^{-3} at standard temperature and pressure (STP). Also shown are the 1:1 lines (dashed) and reduced-major-axis regression lines (solid). Correlation coefficients (r) and normalized mean biases (NMB) are given inset. There are many more comparison points for ARCPAC than ARCTAS, despite fewer flight hours and smaller sampling domain, because of the long integration time (4-24 minutes) of the SAGA filters on the ARCTAS aircraft.

less than half of the mean total sulfate burden.

Natural sources also make substantial contributions to total sulfate. Volcanic sources account for 12-24% of the modeled sulfate at all altitudes, with peak contribution in the mid-troposphere. The volcanic influence arises primarily from the Aleutian Islands and

Kamchatka, where non-eruptive volcanism is active throughout our simulation period. The volcanic source is discharged directly in the free troposphere and is thus less affected by deposition than surface sources (Chin and Jacob, 1996). Dimethyl sulfide (DMS) oxidation is a major source in the lower troposphere, responsible for up to 25% of sulfate below 2 km in the aircraft flight domain during ARCTAS and ARCPAC. We find little contribution ($\leq$2%) from open burning to sulfate along the aircraft flight tracks. Recent analyses show sulfate enhancements of up to 30% in biomass burning plumes encountered during both ARCPAC (Warneke et al., 2010) and ARCTAS (Kondo et al., 2011), suggesting that SO_2 emissions from fires in Russia may be larger than assumed in current inventories. Even with increased fire emissions, however, the global SO_2 source would still be dominated by anthropogenic emissions, and the impact of burning on Arctic sulfate would be small. Furthermore, because Asian anthropogenic emissions and Russian fire emissions follow similar pathways of uplift and transport (Fisher et al., 2010), mixing of anthropogenic sulfate with biomass burning plumes en route to the Arctic is likely and may explain the high observed sulfate concentrations in these plumes.

Roughly 10% of the model sulfate along the flight tracks originates from emissions in West Asia and Southern Siberia (hereafter abbreviated as "West Asia" as most of the emissions are in that part of the region, see Fig. 3.1). The region includes major industrial areas and oil fields in southwestern Russia and Kazakhstan and represents a sizable source of SO_2 that has likely been growing in recent years based on energy and economic indicators (Grammelis et al., 2006; IEA Statistics, 2009). Emissions from this source are subject to

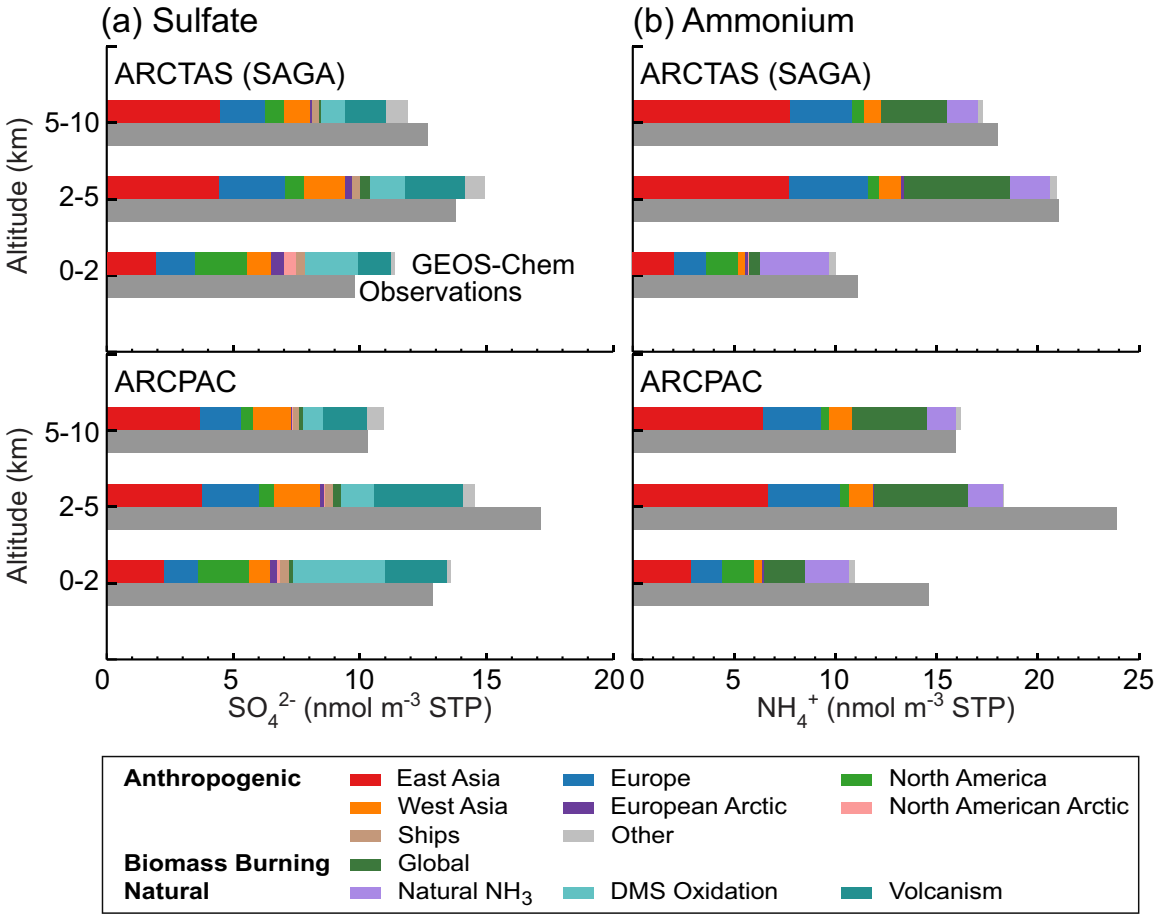

Figure 3.5: Mean vertical distributions of (a) sulfate and (b) ammonium during ARCTAS (top) and ARCPAC (bottom). Dark gray bars show mean observed concentrations, and colored bars show mean model results. Modeled concentrations are decomposed into contributions from various sources as indicated in the legend. Biomass burning refers to open biomass burning; biofuel is included in the anthropogenic source. The "other" anthropogenic term also includes minor non-linear effects in source attribution (see text). Biomass burning plumes, stratospheric air, local pollution, observations south of 60°N, and major outliers have been removed from the data as described in the text.

rapid and direct transport to the Arctic around the Siberian high pressure system (Raatz and Shaw, 1984), still active in April during the ARCTAS/ARCPAC period (Fuelberg et al., 2010).

Recent studies have suggested a large influence on Arctic sulfate from smelters at No-

rilsk and the Kola Peninsula (Yamagata et al., 2009; Hirdman et al., 2010a; Hirdman et al., 2010b) on the basis of backward trajectories and Lagrangian particle dispersion simulations. In our simulation, these sources (included in our European Arctic region) provide negligible contributions at all altitudes to observed sulfate over the North American Arctic. Indeed, they contribute less than 10% to mean concentrations over the High Arctic ($>75°$N), even in surface air in winter. This result is not inherently inconsistent with the back trajectory calculations – the sampled air masses may have encountered emissions from West Asia prior to the 5-day period covered by the back trajectories. Nor does it reflect a major discrepancy with the Lagrangian simulations – examination of the statistical source maps developed by Hirdman et al. (2010a) reveals a hot-spot of sensitivity in West Asia that is larger than the sensitivity at Norilsk in winter and spring. Further, our finding of limited influence from Norilsk agrees with analyses from the 1980s showing on the basis of trace element signatures that the Norilsk source had no discernible impact on sulfate at Barrow (Rahn et al., 1983). Since that time, emissions from Norilsk have shown only modest growth, and those from the Kola peninsula have decreased (Boyd et al., 2009; Prank et al., 2010). More recent evidence of limited impact from northern Russian sources comes from a statistical analysis of Arctic snow samples by Hegg et al. (2010) showing that a pollution source associated with high metal loadings characteristic of smelters was

responsible for less than 20% of observed sulfur.

3.4.2 Surface data

Surface aerosol data provide a seasonal context for the ARCTAS and ARCPAC results. Figure 3.6a shows monthly mean January-May sulfate concentrations at four surface sites: Alert, Zeppelin, Barrow, and Denali (locations shown in Fig. 3.3a). Observations for both 2008 (thin line) and the 2004-2008 five-year mean (thick line) are shown; the 2008 data are generally representative of the five-year record. Other Alaskan sites from the IMPROVE network (Malm et al., 1994) are not shown as they are located near Denali and have similar concentrations. Sampling frequency varies by site. At Alert and Zeppelin, sampling is continuous with filters changed daily (Zeppelin) or weekly (Alert). At Denali, 24-hr filter samples are collected every three days. Sampling times at Barrow vary by time of year, with 24-hr samples in winter when aerosol concentrations are highest. The Barrow data are subject to large data gaps due to both occasional equipment malfunction and sector-controlled sampling that prevents collection of aerosol contaminated by sources in the town of Barrow. These data gaps, often of a week or more, may introduce biases in the monthly means. In 2008, 24-hr filter samples were collected for 6 days in January, 7 in February, 15 in March, 5 in April, and 18 in May. Also shown in Fig. 3.6a are modeled sulfate concentrations at each site, decomposed into contributions from various sources. For comparison to the surface data, GEOS-Chem is sampled in the lowest model level of the grid box containing the site. Modeled monthly means are calculated based on averages over all days in each month (not just days with valid samples).

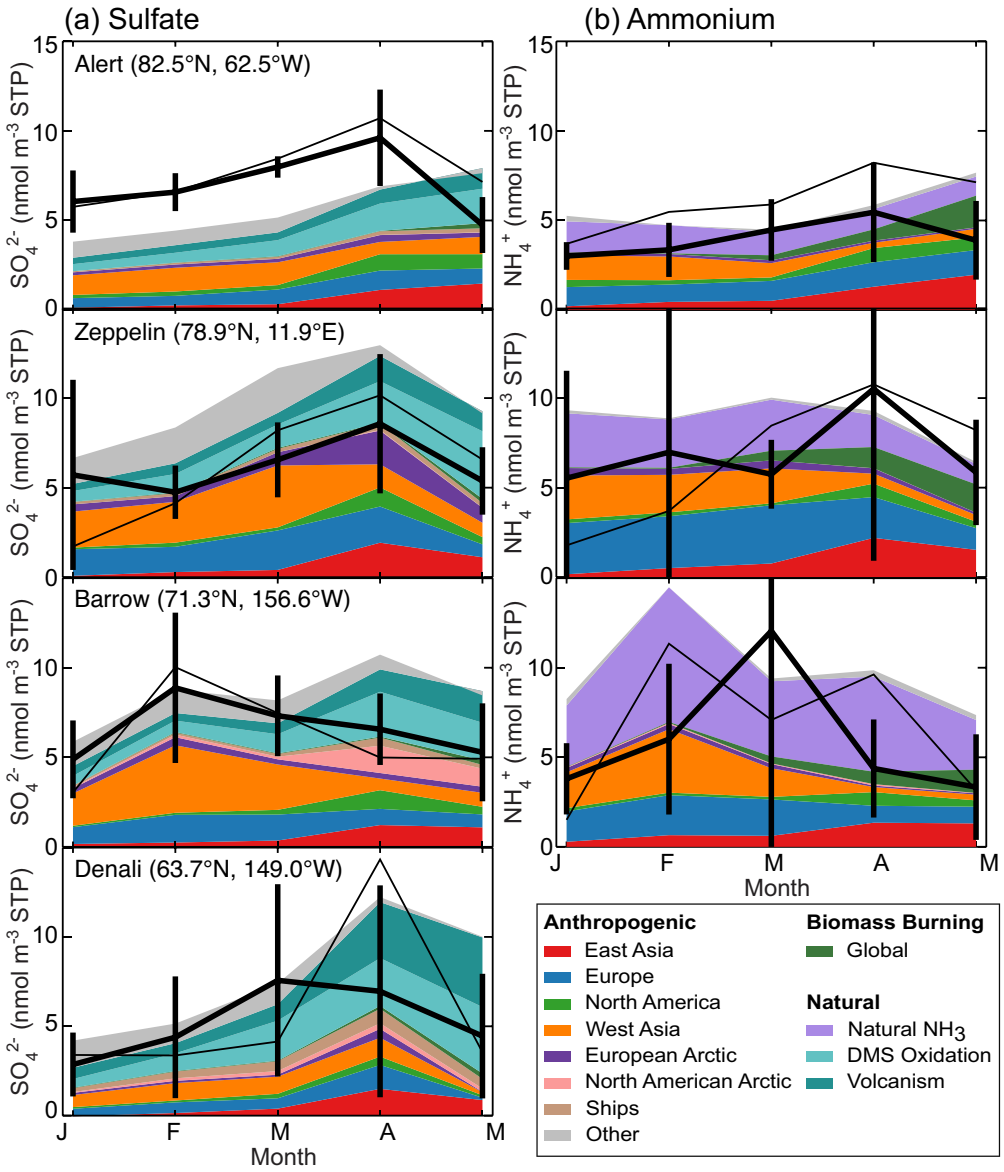

Figure 3.6: January-May monthly mean (a) sulfate and (b) ammonium concentrations observed and modeled at Arctic surface sites. No ammonium data are available at Denali or other IMPROVE sites. The thick black lines show the observed 2004-2008 monthly means and interannual standard deviations; 2008 monthly means are shown as thin lines. Modeled concentrations are subdivided into contributions from individual sources as indicated in the legend. Biomass burning refers to open biomass burning; biofuel is included in the anthropogenic source. The "other" anthropogenic term also includes minor non-linear effects in source attribution (see text). Data sources are as follows: Alert Environment Canada (Gong et al., 2010); Zeppelin EMEP (http://ebas.nilu.no); Barrow the NOAA Pacific Marine Environmental Laboratory (http://saga.pmel.noaa.gov/data/); Denali - the IMPROVE network (Malm et al., 1994).

We find that the surface data in April 2008 are consistent across sites (except for Barrow) and with the aircraft data, with mean concentrations of 10-14 nmol m^{-3} STP. Relative to the 2004-2008 mean, Barrow was lower than average in April 2008 (in contrast to the other sites), which could reflect either a sampling bias or the influence of sector-controlled sample collection. GEOS-Chem has moderate but non-systematic biases relative to April 2008 observations at all sites and is close to or within the interannual variability of the April means. Model source attribution in April is similar to that in the low-altitude aircraft data, with large contributions from East Asia, DMS oxidation, and volcanism. Local Arctic sources such as Prudhoe Bay, Norilsk, and the Kola Peninsula are important at Barrow and Zeppelin, but their influence does not extend to other sites or to the aircraft flight domain.

Observations at the High Arctic sites (Alert, Zeppelin, Barrow) show only weak seasonal variation from winter to spring, whereas Denali is distinctly lower in winter. We find in the model that the West Asian source is a major contributor to winter sulfate burdens at the High Arctic sites (30-45%), in agreement with back trajectories for black carbon at Alert and Barrow (Sharma et al., 2006). This source is much less important at Denali, which is generally south of the Arctic front (Barrie and Hoff, 1984). Over Eurasia, the Arctic front in winter often extends as far south as 40N (Barrie and Hoff, 1984; Stohl, 2006), thus encompassing the sources in the West Asian region. Isentropic transport from these sources to other regions within the Arctic front is enhanced by blocking anticyclones associated with the climatological Siberian high pressure system (Raatz and Shaw, 1984; Iversen and Joranger, 1985) and by limited precipitation (Barrie, 1986), while mixing across the Arc-

tic front to areas further south is limited. Southward transport toward Denali is further inhibited by the Brooks Range (Quinn et al., 2002).

We find that West Asian sources are far more important than Arctic sources in contributing to sulfate concentrations at the Arctic sites in winter. This is because the lower latitudes of the West Asian emissions enables the SO_2 emitted there to be oxidized to sulfate even in winter. By contrast, oxidation of SO_2 emitted from Arctic sources (such as Norilsk and Prudhoe Bay) is restricted by darkness and cold clouds, and we find that most of that SO_2 is deposited rather than oxidized within the Arctic. Heterogeneous SO_2 oxidation mechanisms not included in our model could possibly cause a greater influence from Arctic sources (Alexander et al., 2009), although wintertime sulfate would then be overestimated at Zeppelin and Barrow (not at Alert). The other component of our source attribution reflects in part the nonlinearity of the SO_2-sulfate system under oxidant-limited conditions, as discussed above, and is largest in winter when oxidant limitation is most severe. This could also cause some underestimate of our Arctic source contribution.

All four sites in the model indicate a sharp seasonal transition in source influence from winter to spring, even though changes in total sulfate concentrations are relatively small. In April, the impact of West Asian emissions decreases dramatically at the High Arctic sites while the contributions from East Asia, North America, local Arctic sources, volcanism, and DMS oxidation grow. This transition reflects several processes associated with the end of polar night, including the dissipation of the Siberian High (Raatz and Shaw, 1984), the increase in local oxidant levels, the increase in biogenic DMS emissions (Quinn et al.,

2007), and the increasing frequency of warm conveyor belt transport of pollution from East Asia to the Arctic (Liu et al., 2003). Without the West Asian source of SO_2, we find in the model that sulfate concentrations in the High Arctic would be much lower in winter than in spring.

3.4.3 Budget for the High Arctic

We used GEOS-Chem to construct a circumpolar budget of sulfate in the High Arctic (75-90°N), as shown in Fig. 3.7. Mean concentrations in April are up to 40% lower than along the aircraft flight tracks, reflecting both the greater remoteness and the targeting of plumes by the aircraft. Relative contributions from different sources are similar, although the European contribution is somewhat larger in the High Arctic while the North American contribution is smaller. The contribution from sources in the European Arctic (mainly Norilsk and the Kola Peninsula) is also somewhat larger although still very small, especially in the free troposphere.

In winter, sulfate sources in the High Arctic are more stratified than in spring (Fig. 3.7), reflecting the lack of vertical mixing. Consistent with our simulation of the surface sites, the low-altitude winter sulfate budget is dominated by West Asian emissions (32%) followed by European emissions (17%). No other source contributes more than 10%. Concentrations in the free troposphere are much lower than in the boundary layer due to limited poleward transport from sources south of the Arctic front in winter. In particular, prevailing transport from East Asia in winter is to the south (winter monsoon) rather than to the north (Liu et

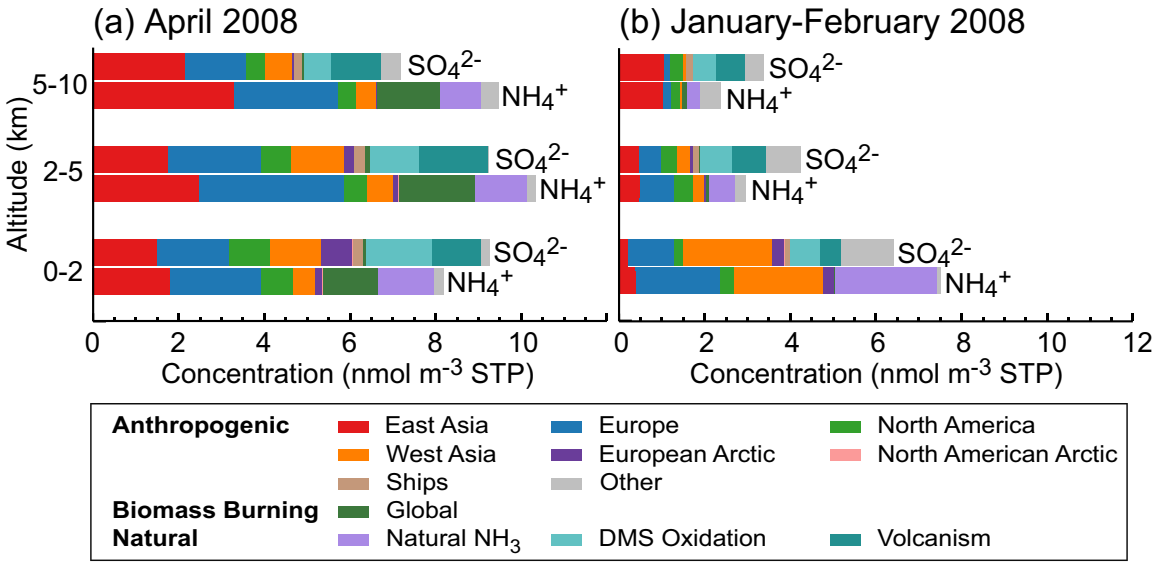

Figure 3.7: GEOS-Chem budgets of sulfate and ammonium aerosols in the High Arctic (75-90°N) in (a) April 2008 and (b) January-February 2008. Aerosol concentrations from 10 different sources are shown for three altitude bands. Biomass burning refers to open biomass burning; biofuel is included in the anthropogenic source. The "other" anthropogenic term also includes minor non-linear effects in source attribution (see text).

al., 2003). Above 5 km, the only substantive contributions to Arctic sulfate are from East Asia (31%), volcanism (20%), and DMS oxidation (15%).

Our sulfate source attribution in spring disagrees with the multi-model ensemble analysis of Shindell et al. (2008), which examined the relative sensitivity of Arctic sulfate to sources from North America, Europe, East Asia, and Southeast Asia (but did not consider West Asia). Rather than quantify the absolute burdens associated with each source as we have done here, the authors calculated the decrease in Arctic sulfate associated with a 20% decrease in emissions from each source region. While both approaches are valid, the difference in methodology means that our results can be compared qualitatively but not quantitatively. In contrast to our finding of similar contributions to Arctic surface sulfate

from Europe and East Asia, their mean contribution from Europe was more than three times that from East Asia (although with a large spread between models; Shindell et al., 2008). This is because our European SO_2 emissions (7 Tg S a^{-1} for 2005) are much lower than those used in the Shindell et al. (2008) models (8-25 Tg S a^{-1} for 2001, with a multi-model mean of 18 Tg S a^{-1}). Smith et al. (2010) show a reduction of only 15-20% in European SO_2 emissions from 2000 to 2005, so that cannot explain the difference. Substantially higher European SO_2 emissions in our simulation would cause an overestimate of sulfate wet deposition in Europe (Section 3.3) larger than the $\sim$30% attributable to differences in wet removal mechanisms between models (Dentener et al., 2006).

3.5 Simulation and source attribution of Arctic ammonium

3.5.1 Aircraft data

Ammonium was measured during ARCTAS by both the AMS and the SAGA filters. Comparison of these two datasets shows a persistent bias. The two are well correlated (r = 0.91), but the AMS ammonium is consistently lower than the SAGA ammonium, with a normalized mean difference of -31%. Conversion of gas-phase NH_3 by acidic aerosols on the filters (especially between sampling and analysis) may explain some of the AMS/SAGA discrepancy. We use the SAGA observations in what follows as they agree better with the concentrations observed during ARCPAC, although some difference might be expected due to location differences between the two aircraft. Using the AMS observations instead of SAGA would decrease observed ARCTAS ammonium concentrations by 30% relative to

the values reported here but would not otherwise affect our conclusions. As for sulfate (Section 3.4.1), the data have been filtered to exclude stratospheric observations, biomass burning plumes, local pollution, and major outliers. For ammonium, outliers (defined by $[NH_4^+] > 60$ nmol m^{-3} STP) include three data points during ARCTAS and six during ARCPAC. We attribute model ammonium to individual sources by conducting sensitivity simulations where we shut off NH_3 emissions from each source while leaving SO_2 emissions unchanged to prevent nonlinearities associated with sulfate availability.

Figures 3.4b and 3.5b show that GEOS-Chem reproduces both the mean vertical structure and much of the variability of ammonium in the ARCTAS observations (r = 0.64, NMB = -4.8%). Simulation of ammonium during ARCPAC indicates substantial model underestimates, especially below 5 km, as previously found for sulfate (Section 3.4.1), with r = 0.43 and NMB = -19%. As for sulfate, we cannot resolve the discrepancy between GEOS-Chem and ARCPAC in a manner consistent with the other data sets, and we view the ARCTAS data as more representative of the North American Arctic.

Vertical distributions shown in Fig. 3.5b indicate peak ammonium concentrations in the mid-troposphere and depletion in the boundary layer, with a larger vertical gradient than for sulfate. Because the aerosol was in general acidic (Section 3.6), ammonium can be regarded as representing total ammonia; gaseous ammonia was not measured on the aircraft but should be negligible based on thermodynamics (Seinfeld and Pandis, 2006). The source influences for ammonium are less complex than for sulfate, with more than 80% of Arctic ammonium originating from three sources: East Asian anthropogenic, European an-

thropogenic, and open biomass burning. The anthropogenic source is mainly from agriculture. East Asia is the largest source, accounting for 35-45% of modeled ammonium. Open biomass burning is responsible for 20-25%, which reflects the unusually intense Russian fire activity in April 2008 (Warneke et al., 2009; Fisher et al., 2010; Warneke et al., 2010). Below 2 km, the North American anthropogenic and the natural contribution become comparable to the East Asian and European influences, similarly to sulfate. The larger gradient between the boundary layer and the free troposphere for ammonium reflects the greater relative contributions of East Asian and biomass burning sources, which are mainly transported to the Arctic in the free troposphere following lifting by warm conveyor belts (Stohl, 2006; Fisher et al., 2010).

3.5.2 Surface data

Ammonium data from surface sites (Fig. 3.6b) provide seasonal context for the aircraft data. There is a tendency for higher values in spring than winter but interannual variability is large. The model tends to overestimate observations in winter and this appears driven by the natural source. The GEIA natural NH_3 source used in GEOS-Chem, originally described by Bouwman et al. (1997), includes both oceanic and continental (soil and crop decomposition) emissions. The continental source is dominant at mid-latitudes but there is a non-negligible ocean source in the Arctic including in particular wintertime emission from some areas normally covered by sea ice. It appears likely that the GEIA inventory overestimates oceanic NH_3 emissions in the Arctic in winter and that this is the cause for the model ammonium overestimates at Barrow and Zeppelin.

We find in the model that anthropogenic sources in Europe and West Asia each contribute 20-30% of winter ammonium at Arctic surface sites, even though Europe is a much larger source of NH_3 than West Asia (Fig. 3.1b, Table 3.1). This is because West Asian air masses are more readily transported to the Arctic around the Siberian High, as discussed previously for sulfate. In addition, a greater fraction of NH_3 emitted from Europe remains as gaseous NH_3 because of the high NH_3/SO_2 emission ratio (Table 3.2) and is therefore effectively dry deposited (unlike the aerosol ammonium component) during transport to the Arctic.

The winter-spring transition in ammonium source contributions in the model is similar to that for sulfate. Dissipation of the polar front increases the influence from East Asia and suppresses the influence from West Asia. For ammonium, the transition is amplified by increased springtime agricultural emissions and biomass burning, whereas in the case of sulfate it was amplified by increased oxidant availability and oceanic biological activity.

3.5.3 Budget for the High Arctic

Our model budget for ammonium in the High Arctic in April 2008 (Fig. 3.7b) shows source contributions consistent with those derived from the aircraft campaigns. East Asian and European anthropogenic emissions contribute similarly at all altitudes, with additional contributions from biomass burning and natural sources. The European influence peaks in the Eurasian sector of the Arctic beyond the flight domain of the ARCTAS and ARCPAC aircraft, explaining the larger contribution from European emissions to ammonium in the High

Arctic (25-35%) than during the aircraft campaigns (15-20%). The spatial heterogeneity of the European influence in spring was also seen in simulation of the surface sites (Fig. 3.6), which showed more European ammonium at Zeppelin (25%) than Barrow (10%). There is less variation in the East Asian influence, which peaks in the free troposphere for both the aircraft campaigns and the High Arctic domain.

As for sulfate, ammonium is more stratified in winter than spring, with concentrations more than two times higher below 2 km than above. Consistent with simulation of the surface sites, the low-altitude winter ammonium budget reflects dominant contributions from European, West Asian, and natural sources, although the ocean component of the natural source is probably too high as previously discussed. At 2-5 km the ammonium concentrations represent a diverse mix of sources, while above 5 km East Asia is the single most important source.

3.6 Acidity of the Arctic aerosol

3.6.1 Aircraft data

The aerosol observed during the April 2008 aircraft campaigns ranged from highly acidic to fully neutralized. Figure 3.8a shows the observed aerosol acidity as defined by the relationship of $2[SO_4^{2-}]+[NO_3^-]$ versus $[NH_4^+]$ (Zhang et al., 2007a). We define the mean neutralized fraction as $f = [NH_4^+]/(2[SO_4^{2-}]+[NO_3^-])$ with all concentrations in molar units. We include nitrate for anion closure, but observed nitrate concentrations were generally very small relative to sulfate, with median (interquartile) values of 2.0 (1.2-3.3)

nmol m^{-3} STP during ARCTAS and 0.9 (0.2-2.7) nmol m^{-3} STP during ARCPAC. Even when sulfate was neutralized ($f > 0.9$), nitrate contributed on average only 15% of the total anion concentration. Thus $f = 1$ implies a $(NH_4)_2SO_4$ sulfate aerosol (solid or aqueous), while $f = 0.5$ implies a NH_4HSO_4 sulfate aerosol in the bulk. Observations with $f > 1$ (excess aerosol ammonium) cannot be reconciled with sulfate-nitrate-ammonium aerosol thermodynamics, but are possible due to the neutralization of organic acids with ammonia (e.g., Dinar et al., 2008; Mensah et al., 2011). These data are also within the precision of the ARCPAC AMS measurement ($\pm$35%). These values were mainly associated with biomass burning plumes (identified on the basis of acetonitrile concentrations), where sulfate should be fully neutralized because of the large NH_3 source and where large organic aerosol concentrations and organic acid aerosol markers could result in some additional uptake of ammonium.

We see from Figure 3.8a that the aerosol was most acidic below 2 km, with median neutralized fraction in the observations of $f = 0.53$ for ARCTAS and $f = 0.50$ for ARCPAC. We find no mean vertical gradient in aerosol acidity above 2 km and thus lump those points together in Figure 3.8. The aerosol above 2 km was still predominantly acidic, with median observed neutralized fractions of $f = 0.69$ for ARCTAS and $f = 0.65$ for ARCPAC. The vertical gradient in acidity is due to large free tropospheric sources of NH_3 from East Asia and biomass burning, as discussed in Section 3.5. Figure 3.8b shows that GEOS-Chem provides a good simulation of the aerosol acidity along the flight tracks, although it slightly underestimates the median neutralized fractions both below 2 km (ARCTAS: $f = 0.45$, AR-

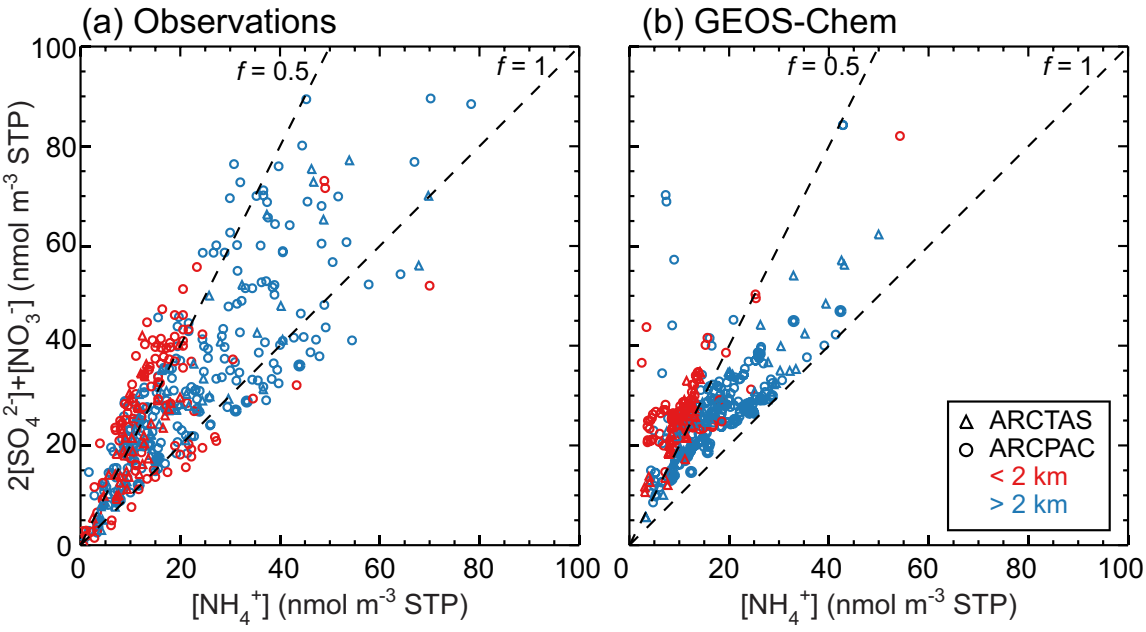

Figure 3.8: Scatterplots of (a) observed and (b) modeled acid aerosol neutralization during ARCTAS and ARCPAC, as given by the $2[SO_4^{2-}]+[NO_3^-]$ vs. $[NH_4^+]$ relationship. Dashed lines indicate the degree of aerosol neutralization, with fully neutralized aerosols falling along the $f = 1$ line.

CPAC: $f = 0.40$) and above (ARCTAS: $f = 0.60$, ARCPAC: $f = 0.66$). The underestimates are largest near the surface, where GEOS-Chem does not simulate the neutralized population observed during ARCPAC, consistent with the low-altitude sulfate overestimates and ammonium underestimates seen in April in the aircraft and surface data (Figs. 3.5, 3.6). Observations with f > 1 cannot be predicted by the model.

We used the GEOS-Chem sensitivity simulations with suppressed SO_2 and NH_3 emissions from individual source regions to interpret the aerosol acidity observed during ARCTAS and ARCPAC. The simulated aerosol neutralization signatures from the four major anthropogenic source regions (East Asia, Europe, West Asia, and North America) are shown in Fig. 3.9 as scatter plots of the reductions in sulfate and ammonium along the aircraft

trajectories that arise from suppressing each source in the model. Aerosol from North America and West Asia is more acidic than aerosol from East Asia and Europe due to lower NH_3/SO_2 emission ratios (Table 3.2). Averaged over both campaigns, neutralized fractions in the model are f = 0.99, 0.75, 0.51, and 0.41 for the aerosol originating from East Asia, Europe, West Asia, and North America, respectively. The aerosol acidity source attribution in the model helps to explain the observed vertical gradient in aerosol acidity in Fig. 3.8. The East Asian influence peaks above 2 km, supplying neutralized aerosol to the free troposphere, while the highly acidic North American aerosol is largely confined below 2 km (Fig. 3.5).

3.6.2 Surface data

The high acidity of the low-altitude aerosol during the aircraft campaigns is consistent with observations at surface sites. In April 2008, the observed surface-level aerosol neutralized fractions were f = 0.36 at Alert, f = 0.39 at Zeppelin, and f = 0.40 at Barrow. Modeled neutralized fractions were f = 0.41 at Alert, f = 0.36 at Zeppelin, and f = 0.43 at Barrow. Figure 3.10 indicates little seasonal variation over winter-spring in aerosol neutralization at any of the sites in the five-year mean. Averaged over January-May for 2004-2008, observed aerosol is most acidic at Alert (mean f = 0.26) and most neutralized at Barrow (mean f = 0.49); however, this spatial gradient was not evident in 2008 when both model and observations indicate similar neutralization at both sites.

Long-term observations at Barrow and Alert show conflicting trends in aerosol acidity. At Barrow, January-April ammonium decreased more rapidly than sulfate between 1998

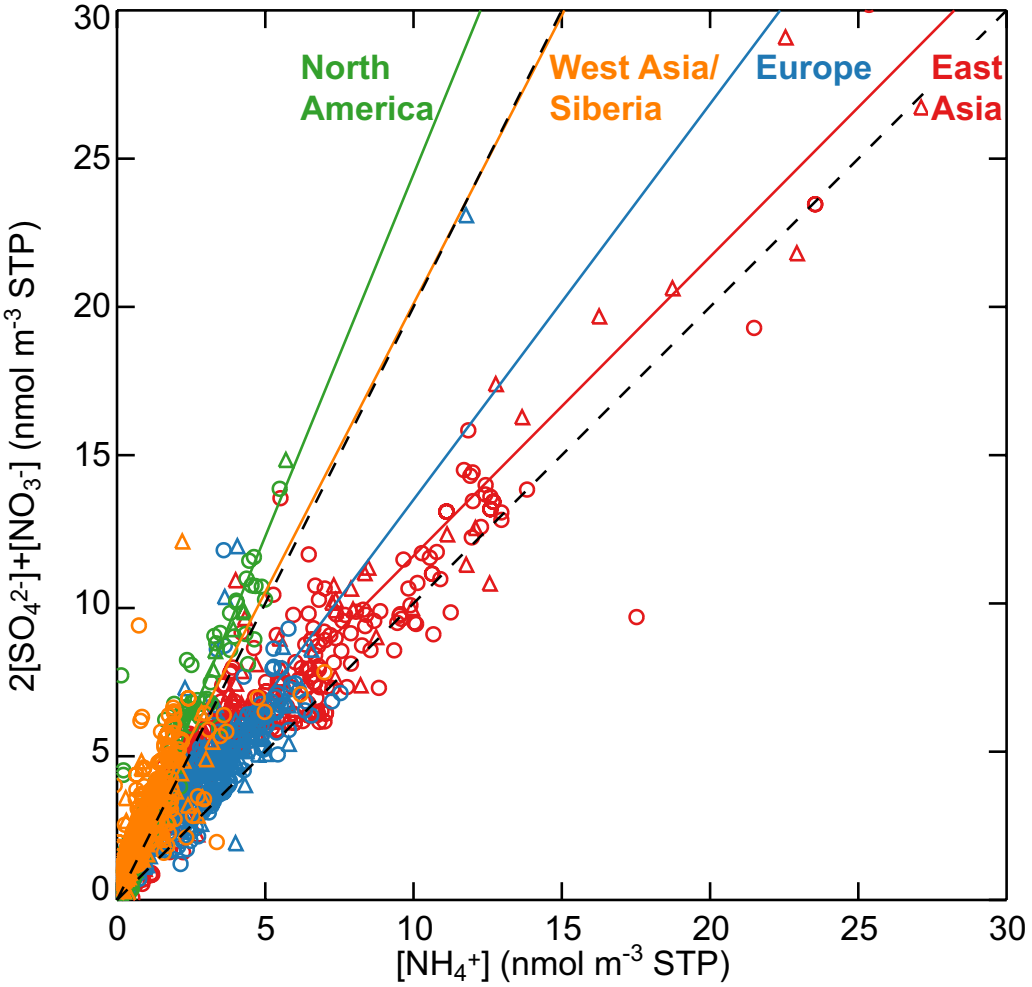

Figure 3.9: Scatterplot of the aerosol neutralization fraction for aerosol originating from the four major anthropogenic source regions in the GEOS-Chem simulation of the ARCTAS and ARCPAC aircraft data in April 2008. Colored lines show the reduced-major-axis linear regressions. Dashed lines indicate the $f = 0.5$ and $f = 1$ lines, as in Fig. 3.8.

and 2008, leading to a decrease in the ammonium-to-sulfate ratio of 6% a^{-1} (significance of 0.01) and implying an increasingly acidic aerosol (Quinn et al., 2009). In contrast, at Alert there was no significant trend in ammonium, sulfate, or the ammonium-to-sulfate ratio over this 10-year period, implying no change in aerosol neutralization there. Acidic West Asian emissions provide a major source of sulfate to Barrow but are less important at

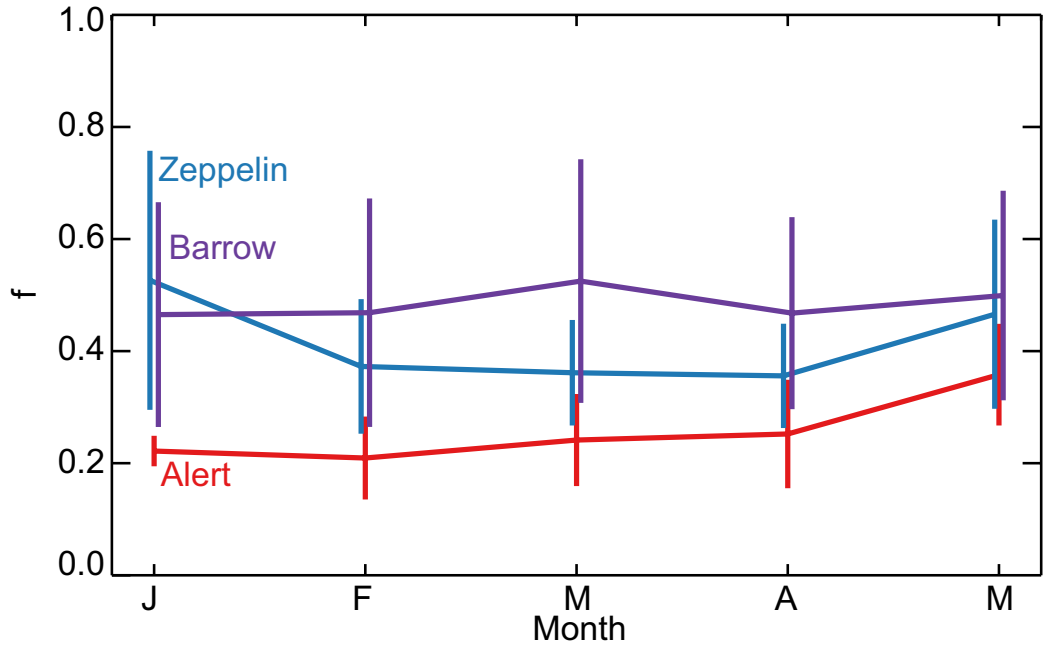

Figure 3.10: 2004-2008 monthly means and interannual standard deviations of aerosol neutralized fraction (f = $[NH_4^+]/(2[SO_4^{2-}]+[NO_3^-])$) observed at Zeppelin (blue), Barrow (purple), and Alert (red).

Alert, in part because deposition is higher en route to Alert due to the more direct, surface-level transport (Sharma et al., 2004; Sharma et al., 2006). In both Kazakhstan and Russia, coal production grew by 20-40% and petroleum by 50-80% between 2000 and 2007 (IEA Statistics, 2009; United Nations Statistics Division, http://unstats.un.org/unsd/industry/). This growth may mask decreases in SO_2 from Europe and North America, accounting for the slower decrease in sulfate relative to ammonium observed at Barrow.

3.6.3 Pan-Arctic perspective

Figure 3.11 shows the mean model distributions of aerosol neutralized fraction in surface air and the free troposphere (5 km) for winter (Jan-Feb) and spring (April). Patterns of aerosol acidity in April are consistent between the aircraft flight tracks and the High Arctic

in general, with more acidic aerosol at the surface than above. The most acidic aerosol is found in surface air over northern Eurasia where both West Asian sources and Norilsk have a major influence. Over Russia and Scandinavia, there is a strong meridional gradient in aerosol neutralization. This marks the edge of the polar front, which during April 2008 typically extended to at least 60°N and often further south over Eurasia (Fuelberg et al., 2010). Small areas of high acidity are also evident near local sulfate sources at Prudhoe Bay in Alaska and Norilsk in Russia. In the free troposphere, the aerosol is weakly acidic ($f \approx 0.6$) across the High Arctic. More neutralized air is found over eastern Siberia and the Bering Sea, where the contributions from biomass burning and East Asian emissions are largest.

We find that the free troposphere is much more acidic in winter ($f \approx 0.3$) than spring, and that the vertical gradient in aerosol acidity is reversed. Free tropospheric aerosol concentrations in winter are low, and high acidity arises from the contributions of volcanism and DMS (Fig. 3.7), with low Arctic emissions of the latter compensated by higher wind speeds and transport from further south. Modeled neutralization in High Arctic surface air in winter is promoted by high oceanic NH_3 emissions in the Arctic basin. This seasonal trend of increasing surface acidity from winter to spring is not seen in the observations (Fig. 3.10), again suggesting that these oceanic NH_3 emissions are too high in the model as previously discussed. The acidity maxima over the northern Atlantic and Pacific in winter reflect high surface wind speeds that drive NH_3 dry deposition over the oceans. Arctic sulfur emissions from Norilsk and Prudhoe Bay, which produced hotspots of aerosol acidity in

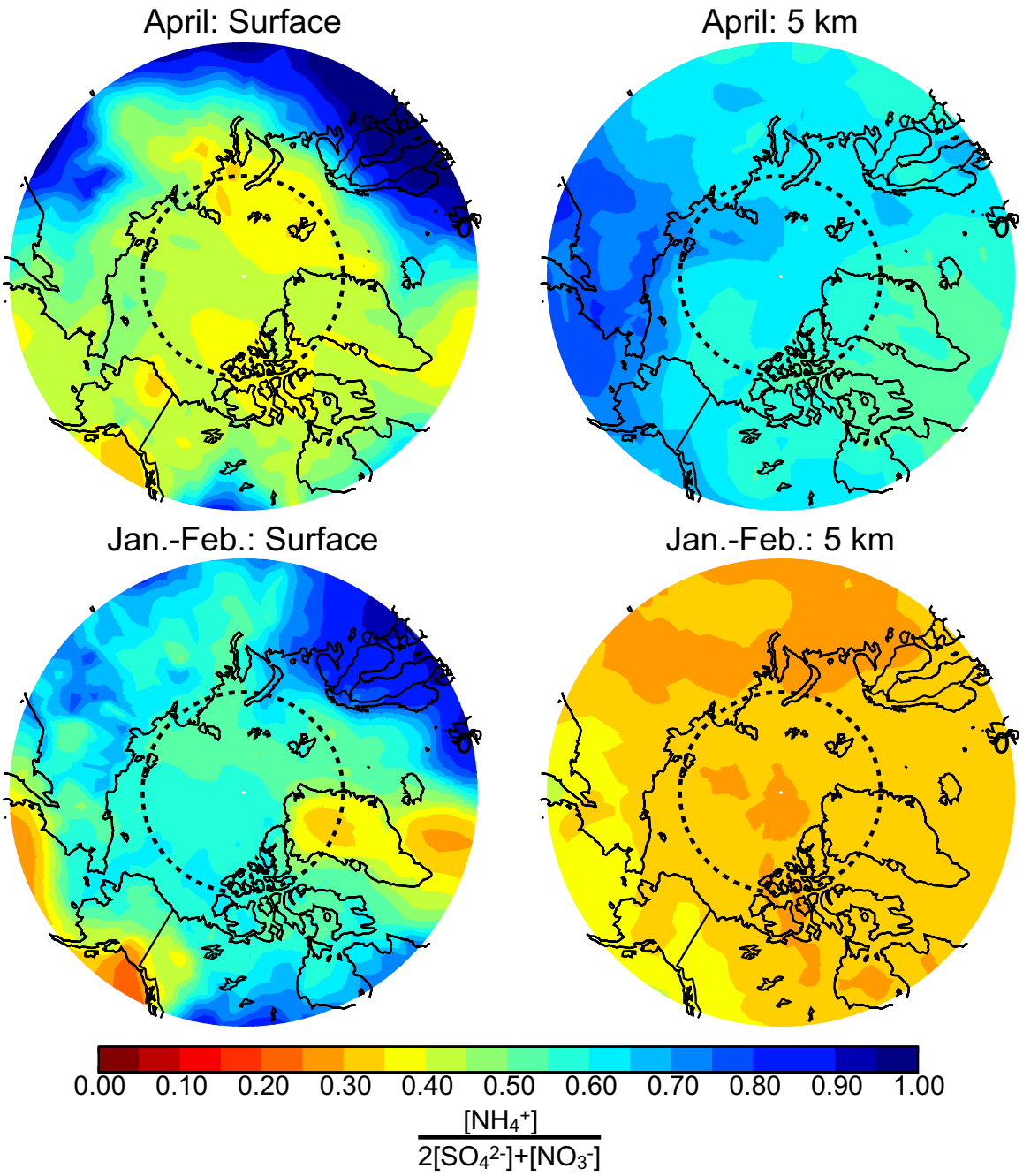

Figure 3.11: Maps of mean aerosol neutralized fraction ($f = [NH_4^+]/(2[SO_4^{2-}]+[NO_3^-])$) simulated by GEOS-Chem in surface air and at 5 km altitude for April and January-February 2008. The black dashed line marks the limit of the High Arctic at 75°N.

April, are less manifest in winter because of the slower SO_2 oxidation. The influence from West Asia, on the other hand, is evident in the widespread region of acidity over Eurasia that extends to lower latitudes within the polar front.

According to the Intergovernmental Panel on Climate Change (IPCC), global SO_2 emissions are expected to decrease over the coming decades while NH_3 emissions are expected to increase (RCP Database, http://www.iiasa.ac.at/web-apps/tnt/RcpDb/). Thus the Arctic aerosol should become increasingly neutralized. However, growth in West Asian energy production is projected for at least the next five years (Klotsvog et al., 2009) and could increase the acidity of the surface aerosol over the short-term horizon as observed by Quinn et al. (2009).

The extent of sulfate neutralization has implications for the properties of Arctic clouds in winter and spring. The formation and stability of mixed-phase Arctic clouds are highly sensitive to ice nuclei concentration (Harrington et al., 1999; Jiang et al., 2000; Harrington and Olsson, 2001). Arctic air masses with elevated sulfate concentrations have been shown to be depleted in ice nuclei relative to clean air in spring (Borys, 1989), which Girard et al. (2005) found to result in larger ice crystal sizes and enhanced ice precipitation followed by tropospheric dehydration. The dehydration reduces absorption of longwave radiation and cools the atmosphere (Blanchet and Girard, 1995; Curry, 1995), further increasing the dehydration rate (Girard et al., 2005). This relationship results in a positive feedback known as the dehydration-greenhouse feedback (DGF) that can cool the Arctic surface by as much as -3°C (Girard and Stefanof, 2007). Neutralization of sulfate by ammonium may decrease

the efficacy of this feedback cycle by providing an increased source of ice nuclei. At the temperatures and relative humidities characteristic of the Arctic free troposphere, ammonium sulfate particles are expected to be predominantly in the solid phase, even accounting for metastability hysteresis (J. Wang et al., 2008a). Ammonium sulfate can therefore serve as heterogenous ice nuclei under conditions unfavorable to homogeneous nucleation on sulfate particles (Abbatt et al., 2006; Wise et al., 2009; Baustian et al., 2010). An increased population of ammonium sulfate particles in the Arctic in the future may lead to increased ice nuclei formation, reduced dehydration, and enhanced Arctic warming.

3.7 Conclusions

We used observations from the ARCTAS and ARCPAC aircraft campaigns in April 2008 together with longer-term records from Arctic surface sites to better understand the sources of sulfate-ammonium aerosol in the Arctic in winter-spring and the implications for Arctic aerosol acidity. Aerosol concentrations in the Arctic are particularly high in winter-spring. Sulfate is a dominant component of this aerosol, and its neutralization by ammonium has important implications for climate forcing. Our analysis was based on simulations of observations with the GEOS-Chem chemical transport model, including sensitivity simulations to diagnose the contributions from different source regions and source types to aerosol concentrations and acidity.

Observed wet deposition fluxes of sulfate and ammonium in the U.S., Europe, and East Asia in April 2008 were used to test the emissions of SO_2 and NH_3 from these continental

source regions in GEOS-Chem. Results showed good agreement except for ammonium over the Midwest U.S., where spring agricultural emissions are apparently underestimated. Using the SO_2/NH_3 emission ratio and the SO_4^{2-}/NH_4^+ wet deposition flux ratio, we found that spring emissions are conducive to full neutralization by large NH_3 inputs from agricultural activity in both Europe ($E_{NH3}/2E_{SO2}$ = 1.3 mol mol^{-1}) and East Asia ($E_{NH3}/2E_{SO2}$ = 1.2 mol mol^{-1}), whereas emissions in the U.S. should lead to much more acidic aerosol ($E_{NH3}/2E_{SO2}$ = 0.3 mol mol^{-1}).

Sulfate concentrations in the aircraft observations were relatively uniform through the depth of the troposphere, and this is well simulated with the model. The model shows that a diversity of sources contribute to sulfate burdens in spring, with major contributions at all altitudes from East Asian and European anthropogenic sources, oxidation of DMS, and volcanic emission. North American anthropogenic emissions are also important below 2 km. Surface sites north of the Arctic front (Barrow, Alert, Zeppelin) show little variation of total sulfate from winter to spring, consistent with the model, but the model indicates an important seasonal shift in source attribution with non-Arctic West Asian sources (southwest Russia and Kazakhstan) dominating in winter. This strong West Asian influence dissipates in the spring with the northward contraction of the polar front, to be replaced by increasing sulfate contributions from East Asia and DMS emissions. We find that industrial sources of SO_2 in the Arctic (Norilsk, Kola Peninsula, Prudhoe Bay) make little contribution to the Arctic sulfate budget.

Our finding of non-Arctic West Asia (southwest Russia and Kazakhstan) as a major

source region for Arctic sulfate in winter, distinct from the well-known sources in northwest Russia and Siberia, does not seem to have been recognized before. Sharma et al. (2006) show back-trajectories for black carbon at Alert that also point to a significant source from that region. Oil fields and industrial centers in that region are a large and growing source of SO_2. These emissions are released at low enough latitudes to enable oxidation of SO_2 in winter but are still within the boundary of the Arctic front (which over Eurasia can extend as far south as 40°N in winter; Barrie and Hoff, 1984), facilitating rapid low-altitude transport to the Arctic. By contrast, oxidation of SO_2 emitted from Arctic industrial sources is limited in winter by darkness and cold clouds. West Asian emissions are highly uncertain and more work is needed to quantify them in view of their apparent importance as a source of Arctic sulfate.

Ammonium concentrations observed during ARCTAS and ARCPAC were higher in the free troposphere than in the boundary layer. The source influences in spring are less complex than for sulfate, with 80% of free tropospheric ammonium originating from a mix of biomass burning and East Asian and European anthropogenic emissions. Biomass burning and East Asian influences are stronger in the free troposphere due to lifting in warm conveyor belts over the Pacific. Surface sites show a general tendency for higher ammonium concentrations in spring than winter due to increased NH_3 emission associated with the onset of agricultural fires and fertilizer application. The model overestimates observed winter ammonium and therefore aerosol neutralization at the surface sites, likely because of poor representation of sea ice suppression of oceanic NH_3 emission in the GEIA

inventory of Bouwman et al. (1997). Work is needed to better quantify oceanic NH_3 emissions and their seasonal variation.

The aircraft data indicate predominantly acidic aerosol throughout the depth of the Arctic troposphere in spring, with higher acidity below 2 km (median neutralized fraction $f = [NH_4^+]/(2[SO_4^{2-}]+[NO_3^-]) = 0.5$) than above (median $f = 0.7$). Observed acidity at surface sites is even higher ($f = 0.4$). This gradient reflects the preferential transport of neutralized biomass burning and East Asian aerosol in the free troposphere. Simulation with GEOS-Chem indicates that the free troposphere is more acidic in winter than in spring, and natural emissions play a major role in driving this seasonality. DMS oxidation and volcanic emission provide a source of sulfate throughout the troposphere that is not matched by natural NH_3 emission. At the surface, observations show no seasonal variation in aerosol neutralization from winter to spring.

Source neutralization signatures computed from GEOS-Chem and consistent with observations indicate that East Asia and Europe provide neutralized aerosol to the Arctic, while West Asia is the dominant source of acidic aerosol. Our results help explain observed long-term trends in aerosol acidity at surface sites. Observations from Barrow show increasing acidity over the last decade due to more rapid decreases in ammonium than sulfate (Quinn et al., 2008), while there has been no change in aerosol acidity at Alert. Because Barrow is more heavily influenced by acidic West Asian sources than Alert, the impacts at Barrow of recent decreases in SO_2 emissions from North America and Europe may have been masked by concurrent increases in emissions from coal and petroleum pro-

duction in Russia and Kazakhstan. While further growth in this region is expected over the next few years (Klotsvog et al., 2009), longer-term projections suggest global decreases in SO_2 emissions over the next decades together with increases in NH_3 emissions (RCP Database, http://www.iiasa.ac.at/web-apps/tnt/RcpDb/). The resultant increase in the concentration of ammonium sulfate aerosols may lead to enhanced ice nuclei formation, initiating a dehydration-greenhouse feedback that could accelerate warming in the Arctic.

Bibliography

Abbatt, J. P. D., Benz, S., Czizco, D. J., Kanji, Z., Lohmann, U., and Möhler, O.: Solid Ammonium Sulfate Aerosols as Ice Nuclei: A Pathway for Cirrus Cloud Formation, Science, 313, 1770–1773, 2006.

Adams, P. J., Seinfeld, J. H., Koch, D., Mickley, L. J., and Jacob, D. J.: General circulation model assessment of direct radiative forcing by the sulfate-nitrate-ammonium-water inorganic aerosol system, Journal of Geophysical Research, 106, 1097–1111, 2001.

Alexander, B., Park, R. J., Jacob, D. J., and Gong, S.: Transition metal-catalyzed oxidation of atmospheric sulfur: Global implications for the sulfur budget, Journal of Geophysical Research, 114, 2009.

Andreae, M. O. and Merlet, P.: Emission of trace gases and aerosols from biomass burning, Global Biogeochemical Cycles, 15, 955–966, 2001.

Ayers, G. P., Gillett, R. W., Cainey, J. M., and Dick, A. L.: Chloride and bromide loss from sea-salt particles in Southern Ocean air, Journal of Atmospheric Chemistry, 33, 299–319, 1999.

Barrie, L. A.: Arctic air pollution: An overview of current knowledge, Atmospheric Environment, 20, 643–663, 1986.

Barrie, L. A. and Hoff, R. M.: The oxidation rate and residence time of sulphur dioxide in the Arctic atmosphere, Atmospheric Environment, 18, 2711–2722, 1984.

Barrie, L. A., Hoff, R. M., and Daggupaty, S. M.: The influence of mid-latitudinal pollution sources on haze in the Canadian Arctic, Atmospheric Environment, 15, 1407–1419, 1981.

Baughcum, S. L., Tritz, T. G., Henderson, S. C., and Pickett, D. C.: Scheduled Civil Aircraft Emission Inventories for 1992: Database Development and Analysis, NASA Contractor Report, 4700, 1996.

Baustian, K. J., Wise, M. E., and Tolbert, M. A.: Depositional ice nucleation on solid ammonium sulfate and glutaric acid particles, Atmospheric Chemistry and Physics, 10, 2307–2317, 2010.

Beusen, A. H. W., Bouwman, A. F., Heuberger, P. S. C., Van Drecht, G., and Van Der Hoek, K. W.: Bottom-up uncertainty estimates of global ammonia emissions from global agricultural production systems, Atmospheric Environment, 42, 6067–6077, 2008.

Blanchet, J.-P. and Girard, E.: Water vapor-temperature feedback in the formation of continental Arctic air: its implication for climate, Science of the Total Environment, 160/161, 793–802, 1995.

Borys, R. D.: Studies of ice nucleation by Arctic aerosol on AGASP-II, Journal of Atmospheric Chemistry, 9, 169–185, 1989.

Boucher, O. and Anderson, T. L.: General circulation model assessment of the sensitivity of direct climate forcing by anthropogenic sulfate aerosols to aerosol size and chemistry, Journal of Geophysical Research, 100, 26 117–26 134, 1995.

Bouwman, A. F., Lee, D. S., Asman, W. A. H., Dentener, F. J., Van Der Hoek, K. W., and Olivier, J. G. J.: A global high-resolution emission inventory for ammonia, Global Biogeochemical Cycles, 11, 561–587, 1997.

Boyd, R., Barnes, S.-J., De Caritat, P., Chekushin, V. A., Melezhik, V. A., Reimann, C., and Zientek, M. L.: Emissions from the copper–nickel industry on the Kola Peninsula and at Noril'sk, Russia, Atmos. Environ., 43, 1474–1480, 2009.

Brock, C. A., Cozic, A., Bahreini, R., Froyd, K. D., Middlebrook, A. M., McComiskey, A., Brioude, J., Cooper, O. R., Stohl, A., Aikin, K. C., de Gouw, J. A., Fahey, D. W., Ferrare, R. A., Gao, R.-S., Gore, W., Holloway, J. S., Hübler, G., Jefferson, A., Lack, D. A., Lance, S. M., Moore, R. H., Murphy, D. M., Nenes, A., Novelli, P. C., Nowak, J. B., Ogren, J. A., Peischl, J., Pierce, R. B., Pilewski, P., Quinn, P. K., Ryerson, T. B., Schmidt, K. S., Schwarz, J. P., Sodemann, H., Spackman, J. R., Stark, H., Thomson, D. S., Thornberyy, T., Veres, P., Watts, L. A., Warneke, C., and Wollny, A. G.: Characteristics, Sources, and Transport of Aerosols Measured in Spring 2008 During the Aerosol, Radiation, and Cloud Processes Affecting Arctic Climate (ARCPAC) Project, Atmospheric Chemistry and Physics, 11, 2423–2453, 2011.

Calhoun, J. A., Bates, T. S., and Charlson, R. J.: Sulfur isotope measurements of submicrometer sulfate aerosol particles over the Pacific Ocean, Geophysical Research Letters, 18, 1991.

Chin, M. and Jacob, D. J.: Anthropogenic and natural contributions to tropospheric sulfate: A global model analysis, Journal of Geophysical Research, 101, 18 691–18 699, 1996.

Chin, M., Rood, R., Lin, S., Müller, J., and Thompson, A.: Atmospheric sulfur cycle simulated in the global model GOCART: Model description and global properties, Journal of Geophysical Research, 105, 24 671, 2000.

Christensen, J. H.: The Danish Eulerian Hemispheric Model - a three-dimensional air pollution model used for the Arctic, Atmospheric Environment, 31, 4169–4191, 1997.

Clarisse, L., Clerbaux, C., Dentener, F., Hurtmans, D., and Coheur, P.-F.: Global ammonia distribution derived from infrared satellite observations, Nature Geoscience, 2, 479–483, 2009.

Curry, J. A.: Interactions among aerosols, clouds, and climate of the Arctic Ocean, Science of the Total Environment, 160/161, 777–791, 1995.

Dentener, F., Drevet, J., Lamarque, J. F., Bey, I., Eickhout, B., Fiore, A. M., Hauglustaine, D. A., Horowitz, L. W., Krol, M., Kulshrestha, U. C., Lawrence, M., Galy-Lacaux, C., Rast, S., Shindell, D., Stevenson, D., Van Noije, T., Atherton, C., Bell, N., Bergman, D., Butler, T., Cofala, J., Collins, B., Doherty, R., Ellingsen, K., Galloway, J., Gauss, M., Montanaro, V., Müller, J. F., Pitari, G., Rodriguez, J., Sanderson, M., Solmon, F., Strahan, S., Schultz, M., Sudo, K., Szopa, S., and Wild, O.: Nitrogen and sulfur deposition on regional and global scales: A multimodel evaluation, Global Biogeochem. Cy., 20, GB4003, 2006.

Dibb, J. E., Talbot, R. W., Scheuer, E. M., Seid, G., Avery, M. A., and Singh, H. B.: Aerosol chemical composition in Asian continental outflow during the TRACE-P campaign: Comparison with PEM-West B, Journal of Geophysical Research, 108, 8815, 2003.

Diehl, T.: A global inventory of volcanic SO2 emissions for hindcast scenarios, http://www-lscedods.cea.fr/aerocom/AEROCOM_HC/volc/ (Documents updated in subsequent years after 2009), 2009.

Dinar, E., Anttila, T., and Rudich, Y.: CCN activity and hygroscopic growth of organic aerosols following reactive uptake of ammonia, Environmental Science & Technology, 42, 793–799, 2008.

Drury, E., Jacob, D. J., Spurr, R. J. D., Wang, J., Shinozuka, Y., Anderson, B. E., Clarke, A. D., Dibb, J. E., McNaughton, C., and Weber, R.: Synthesis of satellite (MODIS), aircraft (ICARTT), and surface (IMPROVE, EPA-AQS, AERONET) aerosol observations over eastern North America to improve MODIS aerosol retrievals and constrain surface aerosol concentrations and sources, Journal of Geophysical Research, 115, D14 204, 2010.

Duan, B., Fairall, C. W., and Thomson, D. W.: Eddy correlation measurements of the dry deposition of particles in wintertime, Journal of Applied Meteorology, 27, 642–652, 1988.

Dunlea, E. J., DeCarlo, P. F., Aiken, A. C., Kimmel, J. R., Peltier, R. E., Weber, R. J., Tomlinson, J., Collins, D. R., Shinozuka, Y., McNaughton, C. S., Howell, S. G., Clarke, A. D., Emmons, L. K., Apel, E. C., Pfister, G. G., van Donkelaar, A., Martin, R. V., Millet, D. B., Heald, C. L., and Jimenez, J. L.: Evolution of Asian Aerosols during Transpacific Transport in INTEX-B, Atmospheric Chemistry and Physics, 9, 7257–7287, 2009.

Eastwood, M. L., Cremel, S., Wheeler, M., Murray, B. J., Girard, E., and Bertram, A. K.: Effects of sulfuric acid and ammonium sulfate coatings on the ice nucleation properties of kaolinite particles, Geophysical Research Letters, 36, L02 811, 2009.

EMEP/CCC: Acidifying and eutrophying compounds and particulate matter, Tech. rep., EMEP Co-operative Programme for Monitoring and Evaluation of the Long-Range Transmission of Air Pollutants in Europe, 2010.

Eyring, V., Köhler, H. W., Lauer, A., and Lemper, B.: Emissions from international shipping: 2. Impact of future technologies on scenarios until 2050, Journal of Geophysical Research, 110, D17 306, 2005a.

Eyring, V., Köhler, H. W., van Aardenne, J., and Lauer, A.: Emissions from international shipping: 1. The last 50 years, Journal of Geophysical Research, 110, D17 305, 2005b.

Fairlie, T. D., Jacob, D. J., Dibb, J. E., Alexander, B., Avery, M. A., van Donkelaar, A., and Zhang, L.: Impact of mineral dust on nitrate, sulfate, and ozone in transpacific Asian pollution plumes, Atmos. Chem. Phys., 10, 3999–4012, 2010.

Fan, S.-M. and Jacob, D. J.: Surface ozone depletion in Arctic spring sustained by bromine reactions on aerosols, Nature, 359, 522–524, 1992.

Fickert, S., Adams, J. W., and Crowley, J. N.: Activation of Br2 and BrCl via uptake of HOBr onto aqueous salt solutions, Journal of Geophysical Research, 104, 23 719–23 727, 1999.

Fisher, J. A., Jacob, D. J., Purdy, M. T., Kopacz, M., Le Sager, P., Carouge, C., Holmes, C. D., Yantosca, R. M., Batchelor, R. L., Strong, K., Diskin, G. S., Fuelberg, H. E., Holloway, J. S., Hyer, E. J., McMillan, W. W., Warner, J., Streets, D. G., Zhang, Q., Wang, Y., and Wu, S.: Source attribution and interannual variability of Arctic pollution in spring constrained by aircraft (ARCTAS, ARCPAC) and satellite (AIRS) observations of carbon monoxide, Atmospheric Chemistry and Physics, 10, 977–996, 2010.

Fountoukis, C. and Nenes, A.: ISORROPIA II: a computationally efficient thermodynamic equilibrium model for K+–Ca2+–Mg2+–NH+–Na+–SO2–NO–Cl–H2O aerosols, Atmospheric Chemistry and Physics, 7, 4639–4659, 2007.

Fuelberg, H. E., Harrigan, D. L., and Sessions, W.: A meteorological overview of the ARCTAS 2008 mission, Atmos. Chem. Phys., 10, 817–842, 2010.

Galloway, J. N., Townsend, A. R., Erisman, J. W., Bekunda, M., Cai, Z., Freney, J. R., Martinelli, L. A., Seitzinger, S. P., and Sutton, M. A.: Transformation of the Nitrogen Cycle: Recent Trends, Questions, and Potential Solutions, Science, 320, 889–892, 2008.

Garrett, T. J. and Zhao, C.: Increased Arctic cloud longwave emissivity associated with pollution from mid-latitudes, Nature, 440, 787–789, 2006.

Garrett, T. J., Zhao, C., and Novelli, P. C.: Assessing the relative contributions of transport efficiency and scavenging to seasonal variability in Arctic aerosol, Tellus, 62B, 190–196, 2010.

Girard, E. and Stefanof, A.: Assessment of the dehydration-greenhouse feedback over the Arctic during February 1990, International Journal of Climatology, 27, 1047–1058, 2007.

Girard, E., Blanchet, J.-P., and Dubois, Y.: Effects of arctic sulphuric acid aerosols on wintertime low-level atmospheric ice crystals, humidity and temperature at Alert, Nunavut, Atmospheric Research, 73, 131–148, 2005.

Gong, S. L., Zhao, T. L., Sharma, S., Toom-Sauntry, D., Lavoué, D., Zhang, X. B., Leaitch, W. R., and Barrie, L. A.: Identification of trends and interannual variability of sulfate and black carbon in the Canadian High Arctic: 1981-2007, Journal of Geophysical Research, 115, D07 305, 2010.

Grammelis, P., Koukouzas, N., Skodras, G., Kakaras, E., Tumanovsky, A., and Kotler, V.: Refurbishment priorities at the Russian coal-fired power sector for cleaner energy production—Case studies, Energy Policy, 34, 3124–3136, 2006.

Harrington, J. Y. and Olsson, P. Q.: On the potential influence of ice nuclei on surface-forced marine stratocumulus cloud dynamics, Journal of Geophysical Research, 106, 27 473–27 484, 2001.

Harrington, J. Y., Reisin, T., Cotton, W. R., and Kreidenweis, S. M.: Cloud resolving simulations of Arctic stratus Part II: Transition-season clouds, Atmospheric Research, 51, 45–75, 1999.

Heald, C. L., Jacob, D. J., Turquety, S., Hudman, R. C., Weber, R. J., Sullivan, A. P., Peltier, R. E., Atlas, E. L., de Gouw, J. A., Warneke, C., Holloway, J. S., Neuman, J. A., Flocke,

F. M., and Seinfeld, J. H.: Concentrations and sources of organic carbon aerosols in the free troposphere over North America, J. Geophys. Res., 111, D23S47, 2006.

Hegg, D. A., Warren, S. G., Grenfell, T. C., Doherty, S. J., and Clarke, A. D.: Sources of light-absorbing aerosol in arctic snow and their seasonal variation, Atmospheric Chemistry and Physics, 10, 10 923–10 938, 2010.

Herbert, G. A., Harris, J. M., and Bodhaine, B. A.: Atmospheric transport during the AGASP-II: The Alaskan flights (2-10 April 1986), Atmospheric Environment, 23, 2521–2535, 1989.

Hirdman, D., Burkhart, J. F., Sodemann, H., Eckhardt, S., Jefferson, A., Quinn, P. K., Sharma, S., Ström, J., and Stohl, A.: Long-term trends of black carbon and sulphate aerosol in the Arctic: changes in atmospheric transport and source region emissions, Atmospheric Chemistry and Physics, 10, 9351–9368, 2010a.

Hirdman, D., Sodemann, H., Eckhardt, S., Burkhart, J. F., Jefferson, A., Mefford, T., Quinn, P. K., Sharma, S., Ström, J., and Stohl, A.: Source identification of short-lived air pollutants in the Arctic using statistical analysis of measurement data and particle dispersion model output, Atmospheric Chemistry and Physics, 10, 669–693, 2010b.

Hirsch, R. M. and Gilroy, E. J.: Methods of fitting a straight line to data: examples in water resources, Journal of the American Water Resources Association, 20, 705–711, 1984.

Hole, L. R., Christensen, J. H., Ruoho-Airola, T., Tørseth, K., Ginzburg, V., and Glowacki, P.: Past and future trends in concentrations of sulphur and nitrogen compounds in the Arctic, Atmospheric Environment, 43, 928–939, 2009.

Holmes, C. D., Jacob, D. J., Corbitt, E. S., Mao, J., Yang, X., Talbot, R., and Slemr, F.: Global atmospheric model for mercury including oxidation by bromine atoms, Atmospheric Chemistry and Physics, 10, 12 037–12 057, 2010.

Huang, L., Gong, S. L., Jia, C. Q., and Lavoué, D.: Relative contributions of anthropogenic emissions to black carbon aerosol in the Arctic, Journal of Geophysical Research, 115, D19 208, 2010.

Hudman, R. C., Jacob, D. J., Turquety, S., Leibensperger, E. M., Murray, L. T., Wu, S., Gilliland, A. B., Avery, M., Bertram, T. H., and Brune, W.: Surface and lightning sources of nitrogen oxides over the United States: Magnitudes, chemical evolution, and outflow, Journal of Geophysical Research, 112, D12S05, 2007.

Hudman, R. C., Murray, L. T., Jacob, D. J., Millet, D. B., Turquety, S., Wu, S., Blake, D. R., Goldstein, A. H., Holloway, J., and Sachse, G. W.: Biogenic vs. anthropogenic sources of CO over the United States, Geophysical Research Letters, 35, L04 801, 2008.

Ibrahim, M., Barrie, L. A., and Fanaki, F.: An experimental and theoretical investigation of the dry deposition of particles to snow, pine trees, and artificial collectors, Atmospheric Environment, 17, 781–788, 1983.

IEA Statistics: Energy Statistics of Non-OECD Countries: 2009 Edition, Tech. rep., International Energy Agency, 2009.

Iversen, T. and Joranger, E.: Arctic air pollution and large scale atmospheric flows, Atmospheric Environment, 19, 2099–2108, 1985.

Jacob, D. J., Crawford, J. H., Maring, H., Clarke, A. D., Dibb, J. E., Emmons, L. K., Ferrare, R. A., Hostetler, C. A., Russell, P. B., Singh, H. B., Thompson, A. M., Shaw, G. E., McCauley, E., Pederson, J. R., and Fisher, J. A.: The Arctic Research of the Composition of the Troposphere from Aircraft and Satellites (ARCTAS) mission: design, execution, and first results, Atmospheric Chemistry and Physics, 10, 5191–5212, 2010.

Jacobson, M. Z.: Global direct radiative forcing due to multicomponent anthropogenic and natural aerosols, Journal of Geophysical Research, 106, 1551–1568, 2001a.

Jacobson, M. Z.: Strong radiative heating due to the mixing state of black carbon in atmospheric aerosols, Nature, 409, 695–697, 2001b.

Jiang, H., Cotton, W. R., Pinto, J. O., Curry, J. A., and Weissbluth, M. J.: Cloud Resolving Simulations of Mixed-Phase Arctic Stratus Observed during BASE: Sensitivity to Concentration of Ice Crystals and Large-Scale Heat and Moisture Advection, Journal of the Atmospheric Sciences, 57, 2105–2117, 2000.

Klonecki, A., Hess, P., Emmons, L., Smith, L., Orlando, J., and Blake, D.: Seasonal changes in the transport of pollutants into the Arctic troposphere-model study, Journal of Geophysical Research, 108, 8367, 2003.

Klotsvog, F. N., Sukhotin, A. B., and Chernova, L. S.: Forecast of Economic Growth in Russia, Belarus, Kazakhstan, and Ukraine within the Unified Economic Space, Studies on Russian Economic Development, 20, 366–372, 2009.

Koch, D. and Hansen, J.: Distant origins of Arctic black carbon: A Goddard Institute for Space Studies ModelE experiment, Journal of Geophysical Research, 110, D04 204, 2005.

Kondo, Y., Matsui, H., Moteki, N., Sahu, L., Takegawa, N., Kajino, M., Zhao, Y., Cubison, M. J., Jimenez, J. L., Vay, S., Diskin, G. S., Anderson, B., Wisthaler, A., Mikoviny, T., Fuelberg, H. E., Blake, D. R., Huey, G., Weinheimer, A. J., Knapp, D. J., and Brune, W. H.: Emissions of black carbon, organic, and inorganic aerosols from biomass burning in North America and Asia in 2008, Journal of Geophysical Research, 116, D08 204, 2011.

Koop, T., Luo, B., Tsias, A., and Peter, T.: Water activity as the determinant for homogeneous ice nucleation in aqueous solutions, Nature, 406, 611–614, 2000.

Liao, H., Henze, D. K., Seinfeld, J. H., Wu, S., and Mickley, L. J.: Biogenic secondary organic aerosol over the United States: Comparison of climatological simulations with observations, Journal of Geophysical Research, 112, D06 201, 2007.

Liu, H., Jacob, D. J., Bey, I., and Yantosca, R. M.: Constraints from 210 Pb and 7 Be on wet deposition and transport in a global three-dimensional chemical tracer model driven by assimilated meteorological fields, Journal of Geophysical Research, 106, 12 109–12 128, 2001.

Liu, H., Jacob, D. J., Bey, I., Yantosca, R. M., Duncan, B. N., and Sachse, G. W.: Transport pathways for Asian pollution outflow over the Pacific: Interannual and seasonal variations, Journal of Geophysical Research, 108, 8786, 2003.

Lowenthal, D. H. and Rahn, K. A.: Regional sources of pollution aerosol at Barrow, Alaska during winter 1979-80 as deduced from elemental tracers, Atmospheric Environment, 19, 2011–2024, 1985.

Lubin, D. and Vogelmann, A. M.: A climatologically significant aerosol longwave indirect effect in the Arctic, Nature, 439, 453–456, 2006.

Lubin, D. and Vogelmann, A. M.: Expected magnitude of the aerosol shortwave indirect effect in springtime Arctic liquid water clouds, Geophysical Research Letters, 34, L11 801, 2007.

Malm, W. C., Sisler, J. F., Huffman, D., Eldred, R. A., and Cahill, T. A.: Spatial and seasonal trends in particle concentration and optical extinction in the United States, Journal of Geophysical Research, 99, 1347–1370, 1994.

Mao, J., Jacob, D. J., Evans, M. J., Olson, J. R., Ren, X., Brune, W. H., St. Clair, J. M., Crounse, J. D., Spencer, K. M., Beaver, M. R., Wennberg, P. O., Cubison, M. J., Jimenez, J. L., Fried, A., Weibring, P., Walega, J. G., Hall, S. R., Weinheimer, A. J., Cohen, R. C., Chen, G., Crawford, J. H., McNaughton, C., Clarke, A. D., Jaeglé, L., Fisher, J. A., Yantosca, R. M., Le Sager, P., and Carouge, C.: Chemistry of hydrogen oxide radicals (HOx) in the Arctic troposphere in spring, Atmospheric Chemistry and Physics, 10, 5823–5838, 2010.

Martin, S. T., Hung, H. M., Park, R. J., Jacob, D. J., Spurr, R. J. D., Chance, K. V., and Chin, M.: Effects of the physical state of tropospheric ammonium-sulfate-nitrate particles on global aerosol direct radiative forcing, Atmospheric Chemistry and Physics, 4, 183–214, 2004.

McNaughton, C. S., Clarke, A. D., Kapustin, V., Shinozuka, Y., Howell, S. G., Anderson, B. E., Winstead, E., Dibb, J., Scheuer, E., Cohen, R. C., Wooldridge, P., Perring, A., Huey, L. G., Kim, S., Jimenez, J. L., Dunlea, E. J., DeCarlo, P. F., Wennberg, P. O., Crounse, J. D., Weinheimer, A., and Flocke, F.: Observations of heterogeneous reactions between Asian pollution and mineral dust over the Eastern North Pacific during INTEX-B, Atmospheric Chemistry and Physics, 9, 8283–8208, 2009.

Mensah, A. A., Buchholz, A., Mentel, T. F., Tillmann, R., and Kiendler-Scharr, A.: Aerosol mass spectrometric measurements of stable crystal hydrates of oxalates and inferred relative ionization efficiency of water, Journal of Aerosol Science, 42, 11–19, 2011.

Murakami, M., Kimura, T., Magono, C., and Kikuchi, K.: Observations of precipitation scavenging for water-soluble particles, Journal of the Meteorological Society of Japan, 61, 346–358, 1983.

National Atmospheric Deposition Program: Tech. rep., NADP Program Office, Illinois State Water Survey, 2010.

Nilsson, E. D. and Rannik, Ü.: Turbulent aerosol fluxes over the Arctic Ocean: 1. Dry deposition over sea and pack ice, Journal of Geophysical Research, 106, 32 125–32 137, 2001.

Olivier, J. G. J., Bloos, J. P. J., Berdowski, J. J. M., Visschedijk, A. J. H., and Bouwman, A. F.: A 1990 global emission inventory of anthropogenic sources of carbon monoxide on 1 ° x 1 ° developed in the framework of EDGAR/GEIA, Chemosphere: Global Change Science, 1, 1–17, 1999.

Park, R. J., Jacob, D. J., Field, B. D., Yantosca, R. M., and Chin, M.: Natural and transboundary pollution influences on sulfate-nitrate-ammonium aerosols in the United States: Implications for policy, Journal of Geophysical Research, 109, D15 204, 2004.

Parungo, F., Nagamoto, C., Herbert, G., Harris, J., Schnell, R., Sheridan, P., and Zhang, N.: Individual particle analyses of Arctic aerosol samples collected uring AGASP-III, Atmospheric Environment, 27A, 2825–2837, 1993.

Piot, M. and von Glasow, R.: The potential importance of frost flowers, recycling on snow, and open leads for ozone depletion events, Atmospheric Chemistry and Physics, 8, 2437–2467, 2008.

Prank, M., Sofiev, M., Denier van der Gon, H. A. C., Kaasik, M., Ruuskanen, T. M., and Kukkonen, J.: A refinement of the emission data for Kola Peninsula based on inverse dispersion modelling, Atmospheric Chemistry and Physics, 10, 10 849–10 865, 2010.

Pueschel, R. F. and Kinne, S. A.: Physical and radiative properties of Arctic atmospheric aerosols, The Science of the Total Environment, 160/161, 811–824, 1995.

Pye, H., Liao, H., Wu, S., Mickley, L., Jacob, D., Henze, D., and Seinfeld, J.: Effect of changes in climate and emissions on future sulfate-nitrate-ammonium aerosol levels in the United States, Journal of Geophysical Research, 114, D01 205, 2009.

Quinn, P. K., Miller, T. L., Bates, T. S., Ogren, J. A., Andrews, E., and Shaw, G. E.: A 3-year record of simultaneously measured aerosol chemical and optical properties at Barrow, Alaska, Journal of Geophysical Research, 107, 4130, 2002.

Quinn, P. K., Shaw, G., Andrews, E., Dutton, E. G., Ruoho-Airola, T., and Gong, S. L.: Arctic haze: current trends and knowledge gaps, Tellus B, 59, 99–114, 2007.

Quinn, P. K., Bates, T. S., Baum, E., Doubleday, N., Fiore, A. M., Flanner, M., Fridlind, A., Garrett, T. J., Koch, D., and Menon, S.: Short-lived pollutants in the Arctic: their climate impact and possible mitigation strategies, Atmospheric Chemistry and Physics, 8, 1723–1735, 2008.

Quinn, P. K., Bates, T. S., Schulz, K., and Shaw, G. E.: Decadal trends in aerosol chemical composition at Barrow, Alaska: 1976-2008, Atmospheric Chemistry and Physics, 9, 8883–8888, 2009.

Raatz, W. E. and Shaw, G. E.: Long-Range Tropospheric Transport of Pollution Aerosols into the Alaskan Arctic, Journal of Applied Meteorology, 23, 1052–1064, 1984.

Rahn, K. A.: Relative importances of North America and Eurasia as sources of arctic aerosol, Atmospheric Environment, 15, 1447–1455, 1981a.

Rahn, K. A.: The Mn/V ratio as a tracer of large-scale sources of pollution aerosol for the Arctic, Atmospheric Environment, 15, 1457–1464, 1981b.

Rahn, K. A., Lewis, N. F., Lowenthal, D. H., and Smith, D. L.: Noril'sk only a minor contributor to Arctic haze, Nature, 306, 459–461, 1983.

Rastigejev, Y., Park, R., Brenner, M. P., and Jacob, D. J.: Resolving intercontinental pollution plumes in global models of atmospheric transport, Journal of Geophysical Research, 115, D02 302, 2010.

Reid, J. S., Hyer, E. J., Prins, E. M., Westphal, D. L., Zhang, J., Wang, J., Christopher, S. A., Curtis, C. A., Schmidt, C. C., Eleuterio, D. P., Richardson, K. A., and Hoffman, J. P.: Global monitoring and forecasting of biomass-burning smoke: Description and lessons from the Fire Locating and Modeling of Burning Emissions (FLAMBE) program, IEEE Journal of Selected Topics in Applied Earth Observations and Remote Sensing, 2, 144–162, 2009.

Reis, S., Pinder, R. W., Zhang, M., Lijie, G., and Sutton, M. A.: Reactive nitrogen in atmospheric emission inventories, Atmospheric Chemistry and Physics, 9, 7647–7677, 2009.

Ritter, C., Notholt, J., Fischer, J., and Rathke, C.: Direct thermal radiative forcing of tropospheric aerosol in the Arctic measured by ground based infrared spectrometry, Geophysical Research Letters, 32, L23 816, 2005.

Scheuer, E., Talbot, R. W., Dibb, J. E., Seid, G. K., DeBell, L., and Lefer, B.: Seasonal distributions of fine aerosol sulfate in the North American Arctic basin during TOPSE, Journal of Geophysical Research, 108, 8370, 2003.

Seinfeld, J. H. and Pandis, S. N.: Atmospheric Chemistry and Physics: From Air Pollution to Climate Change, John Wiley, New York, 2nd edn., 2006.

Sharma, S., Lavoue, D., Cachier, H., Barrie, L. A., and Gong, S. L.: Long-term trends of the black carbon concentrations in the Canadian Arctic, J. Geophys. Res.-Atmos., 109, D15 203, 2004.

Sharma, S., Andrews, E., Barrie, L. A., Ogren, J. A., and Lavoué, D.: Variations and sources of the equivalent black carbon in the high Arctic revealed by long-term observations at Alert and Barrow: 1989–2003, J. Geophys. Res., 111, D14 208, 2006.

Shaw, G.: The Arctic haze phenomenon, Bulletin of the American Meteorological Society, 76, 2403–2413, 1995.

Sheridan, P. J. and Musselman, I. H.: Characterization of aircraft-collected particles present in the arctic aerosol: Alaskan Arctic, spring 1983, Atmospheric Environment, 19, 2159–2166, 1985.

Shindell, D. T. and Faluvegi, G.: Climate response to regional radiative forcing during the twentieth century, Nature Geoscience, 2, 294–300, 2009.

Shindell, D. T., Chin, M., Dentener, F., Doherty, R. M., Faluvegi, G., Fiore, A. M., Hess, P., Koch, D. M., MacKenzie, I. A., Sanderson, M. G., Schultz, M. G., Schulz, M., Stevenson, D. S., Teich, H., Textor, C., Wild, O., Bergmann, D. J., Bey, I., Bian, H., Cuvelier, C., Duncan, B. N., Folberth, G., Horowitz, L. W., Jonson, J., Kaminski, J. W., Marmer, E., Park, R., Pringle, K. J., Schroeder, S., Szopa, S., Takemura, T., Zeng, G., Keating, T. J., and Zuber, A.: A multi-model assessment of pollution transport to the Arctic, Atmospheric Chemistry and Physics, 8, 5353–5372, 2008.

Smith, S. J., van Aardenne, J., Klimont, Z., Andres, R., Volke, A., and Delgado Arias, S.: Anthropogenic sulfur dioxide emissions: 1850-2005, Atmospheric Chemistry and Physics, 11, 1101–1116, 2011.

Stephens, G. L., L'Ecuyer, T., Forbes, R., Gettlemen, A., Golaz, J.-C., Bodas-Salcedo, A., Suzuki, K., Gabriel, P., and Haynes, J.: Dreary state of precipitation in global models, Journal of Geophysical Research, 115, D24 211, 2010.

Stohl, A.: Characteristics of atmospheric transport into the Arctic troposphere, Journal of Geophysical Research, 111, D11 306, 2006.

Streets, D. G., Bond, T. C., Carmichael, G. R., Fernandes, S. D., Fu, Q., He, D., Klimont, Z., Nelson, S. M., Tsai, N. Y., and Wang, M. Q.: An inventory of gaseous and primary aerosol emissions in Asia in the year 2000, Journal of Geophysical Research, 108, 8809, 2003.

Tarrasón, L. and Iversen, T.: Modelling intercontinental transport of atmospheric sulphur in the northern hemisphere, Tellus, 50B, 331–352, 1998.

Toom-Sauntry, D. and Barrie, L.: Chemical composition of snowfall in the high Arctic: 1990-1994, Atmospheric Environment, 36, 2683–2893, 2002.

Trenberth, K. E., Jones, P., Ambenje, R., Bojariu, R., Easterling, D., Klein Tank, A., Parker, F., Rahimzadeh, J. A., Renwick, M., Soden, B., and Zhai, P.: Observations: Surface and Atmospheric Climate Change, in: Climate Change 2007: The Physical Science Basis. Contribution of Working Group I to the Fourth Assessment Report of the Intergovernmental Panel on Climate Change, edited by Solomon, S., Qin, D., Manning, M., Chen, Z., Marquis, M., Averyt, K. B., Tignor, M., and Miller, H. L., Cambridge University Press, Cambridge, United Kingdom and New York, NY, USA, 2007.

Vestreng, V. and Klein, H.: Emission data reported to UNECE/EMEP: quality assurance and trend analysis and presentation of WebDab, MSC-W Status Report EMEP/MSC-W Note 1/02, Norwegian Meteorological Institute, 2002.

Wang, J., Hoffmann, A. A., Park, R. J., Jacob, D. J., and Martin, S. T.: Global distribution of solid and aqueous sulfate aerosols: Effect of the hysteresis of particle phase transitions, Journal of Geophysical Research, 113, D11 206, 2008a.

Wang, J., Jacob, D. J., and Martin, S. T.: Sensitivity of sulfate direct climate forcing to the hysteresis of particle phase transitions, J. Geophys. Res., 113, 2008b.

Wang, Q., Jacob, D. J., Fisher, J. A., Mao, J., Leibensperger, E. M., Carouge, C. C., Le Sager, P., Kondo, Y., Jimenez, J. L., Cubison, M. J., and Doherty, S. J.: Sources of carbonaceous aerosols and deposited black carbon in the Arctic in winter-spring: implications for radiative forcing, Atmospheric Chemistry and Physics Discussions, 11, 19 395–19 442, 2011.

Wang, Y., Jacob, D. J., and Logan, J. A.: Global simulation of tropospheric O3-NOx-hydrocarbon chemistry: 1. Model formulation, Journal of Geophysical Research, 103, 10 713–10 725, 1998.

Warneke, C., Bahreini, R., Brioude, J., Brock, C. A., de Gouw, J. A., Fahey, D. W., Froyd, K. D., Holloway, J. S., Middlebrook, A., Miller, L., Montzka, S., Murphy, D. M., Peischl,

J., Ryerson, T. B., Schwarz, J. P., Spackman, J. R., and Veres, P.: Biomass burning in Siberia and Kazakhstan as the main source for Arctic Haze over the Alaskan Arctic in April 2008, Geophysical Research Letters, 36, L02 813, 2009.

Warneke, C., Froyd, K. D., Brioude, J., Bahreini, R., Brock, C. A., Cozic, A., de Gouw, J. A., Fahey, D. W., Ferrare, R. A., Holloway, J. S., Middlebrook, A. M., Miller, L., Montzka, S., Schwarz, J. P., Sodemann, H., Spackman, J. R., and Stohl, A.: An important contribution to springtime Arctic aerosol from biomass burning in Russia, Geophysical Research Letters, 37, L01 801, 2010.

Wesely, M. L.: Parameterization of surface resistances to gaseous dry deposition in regional-scale numerical models, Atmospheric Environment, 23, 1293–1304, 1989.

Wise, M. E., Baustian, K. J., and Tolbert, M. A.: Laboratory studies of ice formation pathways from ammonium sulfate particles, Atmospheric Chemistry and Physics, 9, 1639–1646, 2009.

Yamagata, S., Kobayashi, D., Ohta, S., Murao, N., Shiobara, M., Wada, M., Yabuki, M., Konishi, H., and Yamanouchi, T.: Properties of aerosols and their wet deposition in the arctic spring during ASTAR2004 at Ny-Alesund, Svalbard, Atmospheric Chemistry and Physics, 9, 261–270, 2009.

Zhang, Q., Jimenez, J. L., Worsnop, D. R., and Canagaratna, M.: A case study of urban particle acidity and its influence on secondary organic aerosol, Environmental Science & Technology, 41, 3213–3219, 2007a.

Zhang, Q., Streets, D. G., He, K., Wang, Y., Richter, A., Burrows, J. P., Uno, I., Jang, C. J., Chen, D., and Yao, Z.: NOx emission trends for China, 1995-2004: The view from the ground and the view from space, Journal of Geophysical Research, 112, D22 306, 2007b.

Zhang, Q., Streets, D. G., Carmichael, G. R., He, K. B., Huo, H., Kannari, A., Klimont, Z., Park, I. S., Reddy, S., Fu, J. S., Chen, D., Duan, L., Lei, Y., Wang, L. T., and Yao, Z. L.: Asian emissions in 2006 for the NASA INTEX-B mission, Atmospheric Chemistry and Physics, 9, 5131–5153, 2009.

Chapter 4

Large mercury evasion from the Arctic Ocean in summer: a source from circumpolar rivers?

Abstract

Elevated mercury in Arctic ecosystems is a major environmental and human health concern. Observations of elemental mercury (Hg^0) concentrations in Arctic surface air show a large seasonal amplitude with a spring minimum and summer maximum. The spring minimum is known to be driven by bromine chemistry over polar sea ice causing rapid oxidation of Hg^0 to Hg^{II} followed by deposition, but the summer maximum is not understood. Here we use the GEOS-Chem atmosphere-ocean model of mercury to explore its origin. We argue that it cannot be explained by re-emission of Hg^{II} deposited to snowpacks, atmospheric transport from mid-latitudes, or ocean kinetics. We propose instead that Russian Arctic rivers may provide a large mercury source to the Arctic Ocean in spring-summer, driving Hg^0 evasion and from there the atmospheric summer maximum. We find that when large riverine fluxes are considered, the Arctic Ocean acts as a net source of to the atmosphere, with rivers representing the dominant source of mercury to the Arctic environment.

4.1 Introduction

Mercury is a potent neurotoxin that bioaccumulates and biomagnifies in aquatic ecosystems (Mergler et al., 2007; Munthe et al., 2007). Anthropogenic emissions from coal combustion, waste incineration, and mining have enhanced atmospheric transport and deposition to remote ecosystems (Mason and Sheu, 2002; Selin et al., 2008; Smith-Downey et al., 2010; Fitzgerald et al., 2005; Schuster et al., 2002). Environmental mercury accumulation is a particular concern in the Arctic where indigenous populations rely heavily on diets of fish and marine mammals (Butler Walker et al., 2006; Dewailly et al., 2001; Van Oostdam et al., 1999). Deposition of atmospheric mercury has been implicated as a major source of mercury to the Arctic Ocean (Ariya et al., 2004; Lindberg et al., 2002; Lu et al., 2001; Skov et al., 2004), but estimates of the contribution from the atmosphere vary by more than an order of magnitude (Ariya et al., 2004; Dastoor et al., 2008; Outridge et al., 2008; Skov et al., 2004). Here we interpret the observed seasonal variation of atmospheric mercury in the Arctic using a global biogeochemical model (GEOS-Chem). We argue that a large non-atmospheric summertime source of mercury to the Arctic Ocean is necessary to explain the observations and suggest that circumpolar rivers might provide such a source. This would have important implications for the factors controlling mercury in the Arctic environment and the effects of climate change.

Mercury is emitted from anthropogenic and natural sources primarily as elemental mercury (Hg^0). The Hg^0 atmospheric lifetime of 6-12 months allows efficient transport from

sources at mid-latitudes (Durnford et al., 2010; Hirdman et al., 2009). Eventual oxidation to highly soluble Hg^{II} drives deposition in remote regions. Hg^0 has been measured continuously at sites across the Arctic since the mid-1990s (Berg et al., 2008; Cole and Steffen, 2010; Steffen et al., 2005). As seen in Fig. 4.1, Hg^0 concentrations in Arctic surface air display a strong seasonality with a minimum in spring and a maximum in summer. This contrasts with northern mid-latitudes where observations of both Hg^0 and total gaseous mercury (TGM $\equiv$ Hg^0 + Hg^{II}) typically show a weak minimum in late summer due to the photochemical sink (Kellerhals et al., 2003; Selin et al., 2007). The spring decrease in the Arctic reflects Atmospheric Mercury Depletion Events (AMDEs) driven by atmospheric oxidation by bromine atoms (Br), as manifested in concurrent observation of depleted mercury and elevated bromine monoxide (BrO; Bottenheim and Chan, 2006; Lindberg et al., 2002; Lu et al., 2001). AMDEs are initiated by the photochemical release of bromine from sea salt deposited to sea ice (see e.g., Steffen et al., 2008, and references therein). This drives rapid oxidation of Hg^0 to Hg^{II} (Ariya et al., 2004; Brooks et al., 2006; Calvert and Lindberg, 2003; Skov et al., 2004) and subsequent deposition of Hg^{II} to snow and ice surfaces.

The summer maximum of Hg^0 in the Arctic is less understood. This summer peak was initially attributed to re-emission of the mercury deposited to snow and ice during the previous spring (Steffen et al., 2005). Recent work has called this assumption into question, invoking instead an oceanic source (Cole and Steffen, 2010; Hirdman et al., 2009). Summertime cruise data in the Arctic Ocean show elevated concentrations of both atmospheric

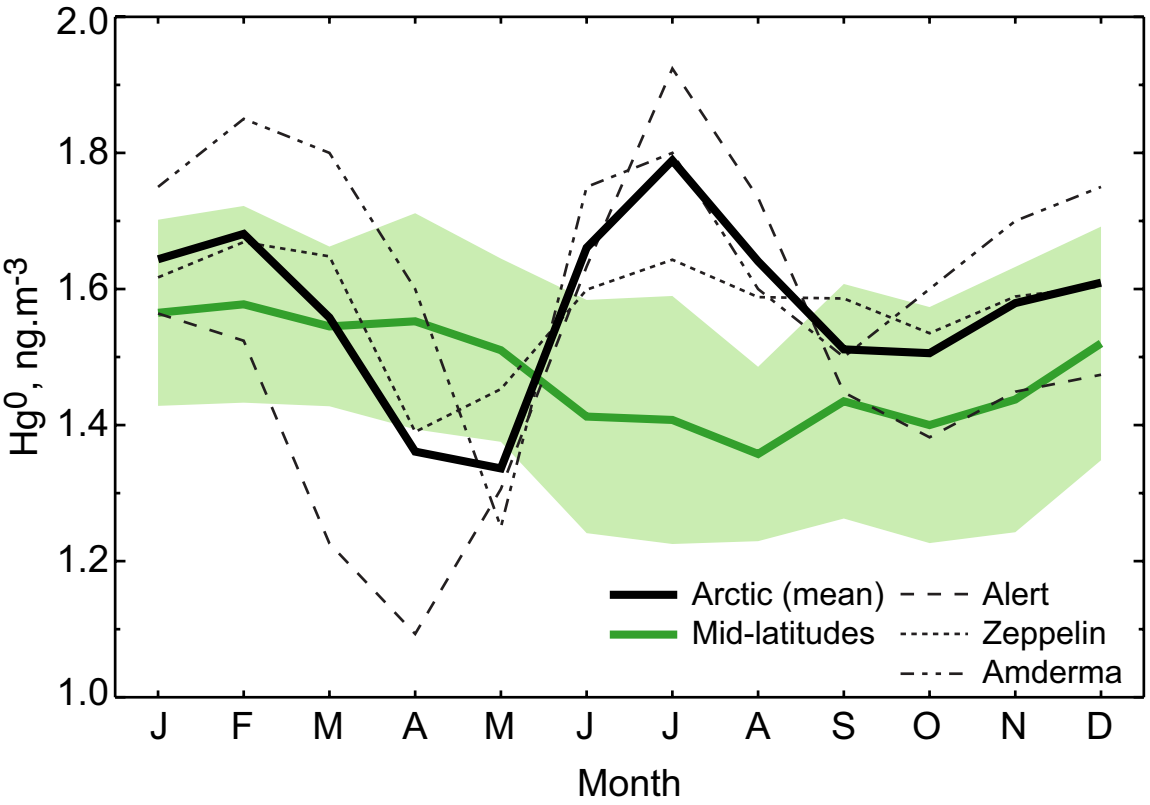

Figure 4.1: Mean observed seasonal variation of elemental mercury (Hg^0) in surface air in the Arctic (thick black line) and at northern mid-latitudes (thick green line). Values in the Arctic are an average over three sites: Alert, Canada (83°N, 62°W; 2005-2009; Steffen et al., 2005); Zeppelin, Norway (79°N, 12°E; 2000-2009; Berg et al., 2008); and Amderma, Russia (70°N, 62°E; 2001-2003; Steffen et al., 2005). Data for the individual sites are shown as thin lines. Values at northern mid-latitudes are an average over four contiguous US sites: Cheeka Peek, Washington (48°N, 125°W; 2001-2002; Weiss-Penzias et al., 2003); Pac Monadnock, New Hampshire (43°N, 72°W; 2007; Sigler et al., 2009); Athens, Ohio (39°N, 82°W; 2004-2005; Yatavelli et al., 2006); and Pensacola, Florida (31°N, 87°W; 2005-2008; Holmes et al., 2010). The light green shading indicates the standard deviation among mid-latitude sites. Concentrations are in ng m^{-3} for standard temperature and pressure (STP) conditions.

mercury in the boundary layer above partial sea ice (Aspmo et al., 2006; Sommar et al., 2010) and dissolved gaseous mercury in the ocean below sea ice (Andersson et al., 2008). These studies suggest the atmospheric summer maximum is driven by large fluxes of Hg^0 to the atmosphere from supersaturated ocean surface waters (Andersson et al., 2008; Mason

and Sullivan, 1999). However, the mechanisms supplying the oceanic pool of Hg^0 subject to evasion have not been explained.

Sea ice cover and large freshwater inputs to the Arctic Ocean differentiate this system from other major ocean basins and are important for mercury dynamics (Stein and Macdonald, 2004). Freshwater inputs from Arctic rivers account for 10% of global oceanic freshwater inputs (Lammers et al., 2001) and thus are an important source of dissolved and particulate phase mercury inputs to the Arctic Ocean. Sea-ice cover and seasonal dynamics greatly affect light availability and algal growth, important drivers of air-sea exchange of Hg^0. In addition, seasonal patterns in mercury inputs are driven by sea-ice formation and melting. We therefore hypothesize that oceanic dynamics exert an important influence on the seasonality of atmospheric concentrations observed in the Arctic. To further explore these phenomena, we apply the GEOS-Chem coupled atmosphere-ocean mercury model to the Arctic and use the model to interpret the atmospheric data and explore the origin of the observed atmospheric summer peak.

4.2 GEOS-Chem model description

We use the GEOS-Chem v9-01-01 mercury simulation (http://geos-chem.org). The simulation is driven by MERRA assimilated meteorological data from the Global Modeling and Assimilation Office (GMAO) Goddard Earth Observing System (GEOS), produced at 0.5°x0.667° horizontal resolution but downgraded here to 4°x5° for input to GEOS-Chem. The MERRA data have 3-hour temporal resolution for atmospheric variables and 1-hour

resolution for surface variables (including boundary layer height, surface temperature, and sea ice coverage). The GEOS-Chem atmospheric mercury simulation is described in detail by Holmes et al. (2010). We use Br as the global oxidant, with background BrO concentrations based on the p-TOMCAT model and Br concentrations derived from photochemical steady-state with BrO. Gas-particle partitioning of reactive mercury and mercury deposition schemes are from Amos et al. (in prep.). Dynamic coupling to the ocean mixed layer is described by Soerensen et al. (2010). The ocean mixed layer model includes atmospheric input (deposition) of Hg^{II}/Hg^{P}, exchange of Hg^{0} with the atmosphere, and photochemical, biological, and dark redox Hg^{0}/Hg^{II} chemistry. Mercury exchanges with subsurface waters below the ocean mixed layer depth (MLD) through settling of mercury sorbed to biological material and through seasonal entrainment/detrainment, but the model does not include lateral transport.

Here we define the Arctic as 70-90°N. Mercury concentrations in subsurface Arctic waters are 1.6 pM, specified based on observations (Kirk et al., 2008). MLD in the central Arctic (80-90°N in the Norwegian/Greenland/Barents Seas; 70-90°N elsewhere) is based on five years of profile data from Toole et al. (2010). Elsewhere, including in the Norwegian, Greenland, and Barents Seas, an interpolated MLD climatology is used (de Boyer Montégut et al., 2004). Seasonal variation is small in the central Arctic (Toole et al., 2010) but large in the region of North Atlantic Deep Water formation (de Boyer Montégut et al., 2004), driving detrainment in spring-summer and entrainment in fall-winter in our broadly defined Arctic region.

Relative to previous versions of GEOS-Chem, our simulation includes an improved representation of polar sea ice and its implications for bromine chemistry and air-sea exchange. Sea ice fractional coverage is from the MERRA assimilated meteorological data archive and is based on the climatology of Reynolds et al. (2002). We assume that each 4°x5° grid square in GEOS-Chem has sufficient sea ice coverage for bromine emission if at least 50% of native resolution grid squares have more than 10% sea ice. Br/BrO radical formation and cycling is photochemically driven (Simpson et al., 2007), and we require here incident shortwave radiation at the surface to be greater than 100 W m^{-2} as observations show little BrO below this threshold (Pöhler et al., 2010). Based on the ship and aircraft observations by Pöhler et al. (2010) and Prados-Roman et al. (2011) in the Arctic in March-April, we specify BrO concentrations in the Arctic boundary layer as a function of 2-m air temperature T: [BrO] = 20 pptv for $T \leq 248$ K, 10 pptv for $248 < T \leq 253$ K, and 5 pptv for $253 < T \leq 268$ K, and background for $T > 268$ K. Finally, we restrict enhanced BrO formation to polar spring, which we define based on BrO column data from the GOME2 satellite (http://bro.aeronomie.be/level3_monthly.php) as February-June in the northern hemisphere and August-December in the southern hemisphere.

Our simulation also includes an improved treatment of Hg^{II} deposited to snow. Photoreduction of deposited Hg^{II} followed by Hg^0 re-emission is known to take place (e.g., Dommergue et al., 2007; Lalonde et al., 2002; Poulain et al., 2004). However, laboratory and field experiments suggest that not all deposited Hg^{II} is easily reduced. Halide ions in the snowpack can stabilize oxidized mercury, especially for sea ice (Durnford and Dastoor,

2011; Lalonde et al., 2003; St. Louis et al., 2007), and mercury deposited in particulate form is not readily reduced (Durnford and Dastoor, 2011; Witherow and Lyons, 2008). Observational estimates of the reducible component of Hg^{II} range from less than 10% (Dommergue et al., 2003; Faïn et al., 2008) to more than 90% (Poulain et al., 2004). Here, we assume that 60% of deposited Hg^{II} is reducible as in Holmes et al. (2010) but test the sensitivity to this assumption. Hg^{II} photo-reduction for the reducible component is assumed to be a first-order process with rate constant $k_S = 2.5 \times 10^{-9} R$ s^{-1}, where R is the incident solar radiation at the surface in W m^{-2}. The coefficient was chosen to optimize the simulation of Hg^0 in spring. For R = 100 W m^{-2} it implies $k_S = 1 \times 10^{-3}$ h^{-1}, in the mid-range of the large spread of observed estimates ranging from 7×10^{-6} to 0.6 h^{-1} (Durnford and Dastoor, 2011). At snowmelt, the entire accumulated non-reducible pool as well as the remaining reducible pool are eluted with the meltwater (Dommergue et al., 2003, 2010) and transferred to the underlying ocean or land.

4.3 Interpreting the seasonal variation of mercury in the Arctic

Figure 4.1 shows the observed climatological seasonal cycle of Hg^0 at three long-term Arctic monitoring sites: Alert, Amderma, and Zeppelin. Absolute concentrations vary across sites but all show similar seasonal variation, with an Hg^0 minimum in April-May and a maximum in July. GEOS-Chem cannot reproduce the differences between sites due to lack of data to constrain the spatial variability of Arctic mixed layer depths and below-ice

primary productivity. We focus therefore on simulating the mean seasonal behavior across the three sites (thick black lines in Figs. 4.1 and 4.2).

Figure 4.2 compares the multi-year mean observed seasonal variation (black) with that simulated by the standard GEOS-Chem model for 2008 (red). GEOS-Chem accurately reproduces the spring decrease, which is driven by AMDE chemistry. Model simulation of the spring depletion is sensitive to the assumed dependences of BrO on temperature and of snow-pack re-emission on solar radiation. Using only a temperature-based threshold for re-emission, as in Holmes et al. (2010), resulted in spring depletion that was too weak and too early.

In summer, the standard simulation shows a weak peak in June driven by re-emission from snow and ice. It fails to capture the July timing of the peak or the sustained elevated Hg^0 concentrations from July through September that characterize the observed summer peak. This summer underestimate cannot be explained in terms of atmospheric sources. As seen in Fig. 4.1, observed mercury concentrations in summer are much higher in the Arctic than at mid-latitudes. As a result, we expect the Arctic to be a net exporter rather than an importer of atmospheric mercury in summer. This is consistent with a Lagrangian sensitivity analysis showing observed high concentrations at Zeppelin to be associated with transport from mid-latitudes in winter and spring but not in summer (Hirdman et al., 2009). Atmospheric redox chemistry is also unable to explain the model underestimate as Hg^{II} accounts for less than 2% of total gas-phase mercury in the Arctic in summer both in the model and in the observations (Cobbett et al., 2007; Sommar et al., 2010; Steen et al.,

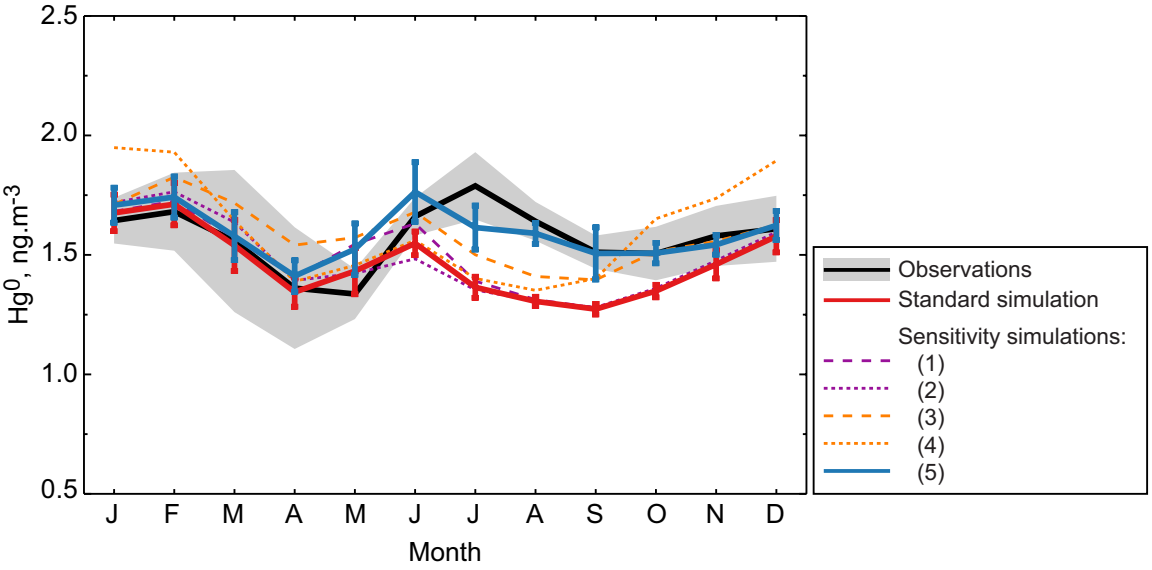

Figure 4.2: Observed mean seasonal cycle of Hg^0 concentrations in Arctic surface air. Observations (black) are averages across the three Arctic sites of Fig. 4.1. Model results are sampled at those sites in 2008. The standard simulation (red) uses the GEOS-Chem model as described in Section 4.2. Other lines show the results of sensitivity simulations: (1) reducible percentage of mercury in snow increased from 60% to 90% (purple dashed); (2) in-snow reduction rate constant increased by a factor of 100 (purple dotted); (3) rate of photo-reduction increased by a factor of five and rate of photo-oxidation decreased by a factor of five in the Arctic Ocean (orange dashed); (4) oceanic biotic reduction rate constant increased to its maximum value constrained by observations (orange dotted); and (5) 160 Mg a^{-1} of riverine Hg^{II} added to the surface ocean with peak inputs in May-June (blue). The standard deviation among sites is indicated by the gray shading for the observations and by the vertical bars for the standard simulation and the sensitivity simulation with riverine inputs.

2011).

We next investigate whether the summer peak could be driven by re-emission of mercury deposited to the Arctic cryosphere in spring, a tempting hypothesis since the magnitude of the peak roughly matches the magnitude of the spring depletion. To understand the potential role of cryospheric emission, we test the influence of our assumptions about snowpack cycling on the model's ability to reproduce the observed seasonal cycle. We perform sensitivity simulations with (1) the reducible percentage of mercury in snow increased

from 60% to 90% and (2) the net reduction rate in snow (k_S) increased by a factor of 100.

Results from these sensitivity simulations, shown in Fig. 4.2 (purple), indicate that our assumptions about in-snow reduction and re-emission have a negligible impact on the simulation of either the timing or the magnitude of the summer peak. This result reflects the seasonality of the balance between snowpack deposition, re-emission, and meltwater removal. In early spring (March-April), re-emission and meltwater formation are minimal due to limited radiation and cold temperatures, resulting in net deposition to snowpacks. By late spring (May-June), available radiation and temperature have both increased dramatically, leading to both re-emission and snowmelt combining to deplete mercury from the snowpack. Changes to modeled in-snow reduction change the balance between re-emission and meltwater removal but cannot sustain an increase from June to July due to depletion of the snowpack mercury. When the snowpack reduction rate is increased (sensitivity simulation 2), re-emission happens almost immediately after deposition and the snowpack becomes depleted earlier. This means that atmospheric concentrations in June are lower than in the standard simulation. When the snowpack reduction rate is decreased, the snow mercury reservoir is removed with the meltwater before re-emission can occur. Even if all deposited mercury were reducible in snow, it would have to be re-emitted to the atmosphere by June to prevent removal with the meltwater, too early to explain the summer peak.

The model shows that half of the mercury released by meltwater is transferred to land and the other half to the ocean. This suggests that even if all mercury transferred to land

during snowmelt was re-emitted over the summer, it would not be enough to replenish the atmospheric mercury lost in spring. A substantial fraction of the mercury transferred to land will enter longer-lived soil pools (Smith-Downey et al., 2010), while empirical studies show that less than half is rapidly re-emitted from soils (Hintelmann et al., 2002). The remainder may be transferred to the ocean through river outflow, a fate we discuss in more detail below.

Mercury delivered to the ocean with meltwater may also eventually be re-emitted to the atmosphere along with mercury deposited directly to the open ocean. The evasion flux is controlled by the available Hg^0 in the ocean mixed layer, which is determined by the total pool of mercury in the surface ocean and Hg^0/Hg^{II} redox kinetics. Observations show strongly supersaturated dissolved gaseous mercury (DGM $\equiv$ Hg^0 plus a negligible contribution from dimethyl mercury in surface waters) in the Arctic Ocean in summer (Andersson et al., 2008), similar to other major ocean basins (Gårdfeldt et al., 2003; Mason and Sullivan, 1999). Globally, photo-reduction dominates oceanic DGM production in most environments (Rolfhus and Fitzgerald, 2004; Soerensen et al., 2010) and may be particularly important in the Arctic in summer due to enhanced light penetration (Soerensen et al., 2010). The balance between photo-oxidation and photo-reduction limits DGM production, and in our standard simulation is insufficient to drive elevated DGM in the Arctic Ocean in summer. We perform a third sensitivity simulation to test whether increasing net photo-reduction to an extreme upper limit could produce sufficient DGM in the Arctic. In this test, the rate of Arctic photo-reduction is increased and the rate of photo-oxidation decreased,

both by a factor of five. While this represents unlikely conditions (Qureshi et al., 2010), testing the sensitivity of the model to such a dramatic increase in Hg^{II} reduction allows us to determine whether photo-reduction alone is sufficient to explain the observed summer enhancements in DGM and atmospheric Hg^0.

We also examine the sensitivity to biotic reduction. In coastal Arctic environments, biologically-mediated reduction by mercury-resistant microbes has been shown to be a dominant source of DGM (Poulain et al., 2007). Because this reduction pathway is independent of light availability, it can operate in winter and below sea ice where photo-reduction is minimized and has therefore been suggested as a major driver of DGM formation across the Arctic (Aspmo et al., 2006; Poulain et al., 2007). We test this hypothesis using a fourth sensitivity study with enhanced biotic reduction in the Arctic. For this, the biotic reduction rate constant (k_{bio}) is increased in the Arctic from its standard global value in our model of $k_{bio} = 4.5 \times 10^{-7}$NPP (where NPP is the net primary productivity in units of gC m^{-2} d^{-1} and k_{bio} is in units of s^{-1}; Soerensen et al., 2010), to its maximum observed value of $k_{bio} = 2.8 \times 10^{-5}$ s^{-1} (Amyot et al., 1997), about 100 times larger than the modeled global mean. As for photo-reduction, use of such an extreme value provides an upper limit on the possible importance of biotic reduction for determining oceanic DGM and atmospheric Hg^0.

Figure 4.2 shows the results of these sensitivity simulations (orange) compared to the standard simulation (red). The overestimate in winter in the case of maximized biotic reduction is expected given that in this sensitivity test k_{bio} is not tied to NPP, which would

be at a minimum in winter. In both cases, the model underestimate of the summer peak persists despite the increased ocean reduction. This result indicates that the total pool of oceanic mercury is too small in summer in the standard model, despite increased inputs to the surface ocean from AMDEs in spring and meltwater in summer. Figure 4.3a shows that removal from the surface ocean to the subsurface waters also peaks during spring and summer as stratification drives shoaling of the mixed layer (de Boyer Montégut et al., 2004; Toole et al., 2010) and increased biological activity enhances losses through settling of particulate mercury sorbed to organic carbon (Sunderland and Mason, 2007). These losses from the surface ocean result in a July-September minimum in oceanic mercury in our simulation that is inconsistent with observations of elevated summer DGM concentrations (Andersson et al., 2008).

We conclude that the Arctic Ocean in the model is missing a large seasonal source of mercury necessary to enable sustained evasion in summer. As we have seen, this source cannot be explained by meltwater delivery or atmospheric deposition. Nor is it likely to be transport from the North Atlantic. Because Atlantic water in the Arctic is found at intermediate depths below the base of the polar mixed layer (Carmack, 1990; Stein and Macdonald, 2004), high mercury concentrations from the North Atlantic would be expected primarily in subsurface waters. In our model, subsurface mercury concentrations are defined based on observations and therefore already include any North Atlantic influence. Additional limited North Atlantic inflow does occur at the surface (Carmack, 1990). However, this surface inflow is characterized by minimal seasonal variation with a weak minimum in

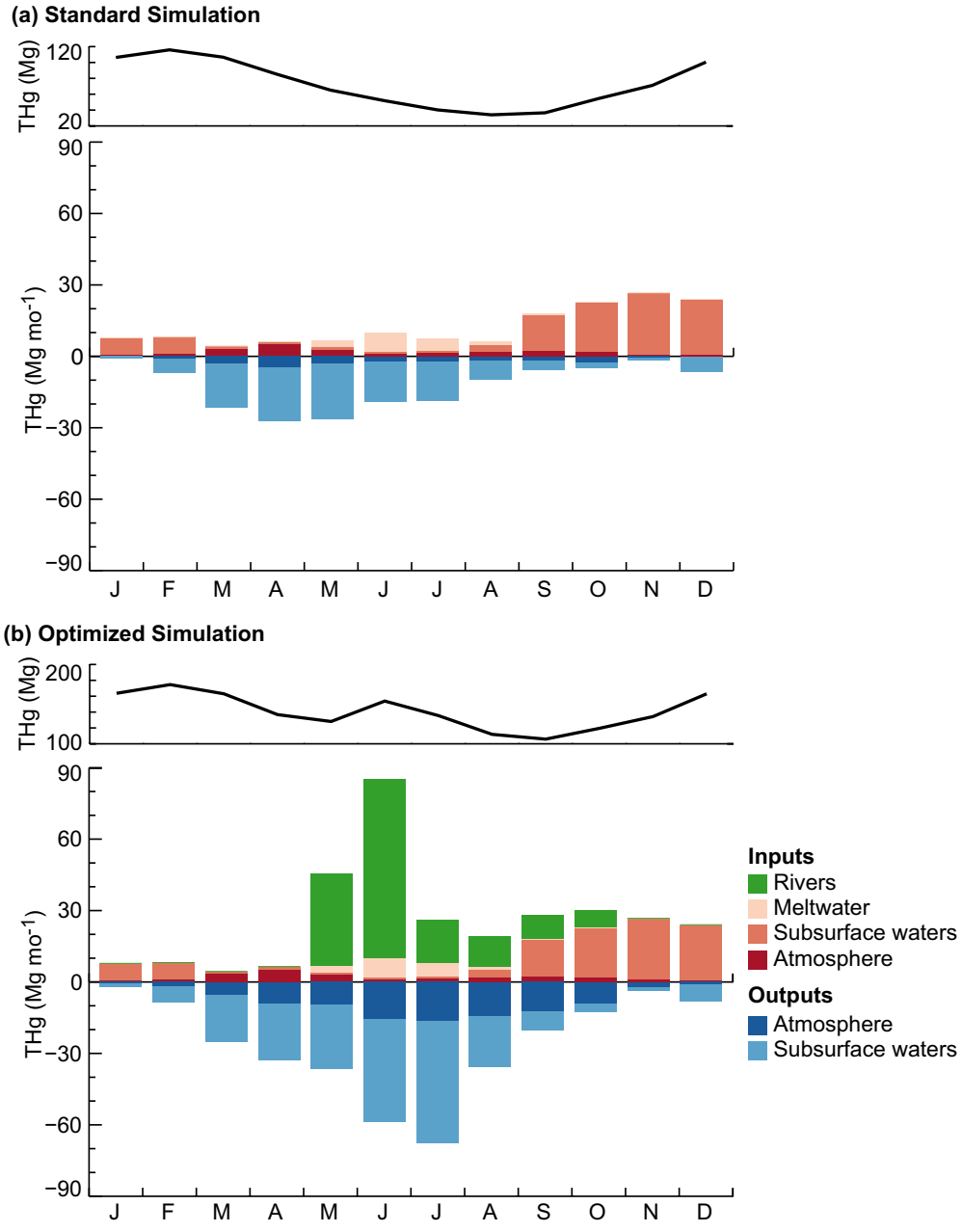

Figure 4.3: Modeled seasonal variation of total mercury (THg $\equiv Hg^0 + Hg^{II} + Hg^P$) mass and fluxes into and out of the Arctic Ocean (70-90°N) in (a) the standard simulation and (b) the optimized simulation including riverine inputs. The thick black lines show the seasonal variation of THg mass in the surface ocean. Inputs (red and green bars) include the sources from rivers, meltwater, subsurface waters via entrainment, and the atmosphere via Hg^{II}/Hg^P deposition. Outputs include removal to the atmosphere through net Hg^0 evasion and to the subsurface ocean through detrainment and settling particles.

summer (Hansen and Østerhus, 2000; Ingvaldsen et al., 2004; Orvik et al., 2001; Østerhus et al., 2001) and therefore cannot provide the spring-summer mercury source needed to sustain high summer DGM concentrations in the Arctic Ocean.

We propose that the missing source may come from large rivers discharging mercury into the Arctic Ocean. Rivers have been found to be regionally important sources of mercury to other basins, including the Mediterranean Sea and the northern mid-latitude Atlantic mixed layer (Sunderland and Mason, 2007). Three of the ten largest river systems in the world are located in the Eurasian Arctic, passing through large drainage basins into the relatively small and shallow Arctic Ocean (Peterson et al., 2002). They provide a major source of organic carbon to the Arctic Ocean (Dittmar and Kattner, 2003; Gordeev et al., 1996) and may also be an important source of mercury: boreal soils and peatlands in Arctic and sub-Arctic catchment basins are known to be highly enriched in stored mercury. Total terrestrial mercury stocks have been estimated to be as high as 15,000-44,000 tons in boreal forests (Friedli et al., 2007) and are expected to be even larger in peatlands (Grigal, 2003). In Arctic Russia, gold, silver, and mercury mines (USGS, 2011) may also provide a large local source of mercury emissions, potentially leading to enhanced Hg^{II} deposition in nearby river outflow basins.

Previous estimates of the annual riverine mercury flux to the Arctic Ocean range from 5-39 Mg a^{-1} but are based on extremely limited data (Coquery et al., 1995; Outridge et al., 2008). In each of the three largest Arctic rivers, all in Russia (Yenisei, Lena, and Ob), mercury has been measured only once, all in the early 1990s and all in September (Coquery

et al., 1995). The Mackenzie River in North America is only somewhat better characterized, with samples from spring-summer 2003-2005 (Graydon et al., 2009; Leitch et al., 2007). In all cases, the limited sampling leads to very large uncertainties in the estimated mercury fluxes. The episodic nature of river transport means instantaneous concentration measurements are generally not representative of mean concentrations, even for periods of a week or less (Walling and Webb, 1985). Extrapolation of these instantaneous concentrations to annual timescales therefore leads to large errors, with the resultant flux estimates generally significantly underestimated (Quémerais et al., 1999; Walling and Webb, 1985).

In addition to short-term variations in river fluxes, there are very large seasonal variations, especially in the Arctic. As shown in Fig. 4.4, the seasonal cycle of Arctic freshwater discharge from rivers is strongly peaked in early summer following ice break-up. Riverine mercury concentrations show similar seasonality: sampling from the Mackenzie River indicates that concentrations during peak flow are up to 7 times larger than those measured later in the year (Leitch et al., 2007). As a result, mercury fluxes (the product of mercury concentration and river discharge) could be an order of magnitude larger in early summer than during the rest of the year. This suggests that previous estimates of the annual mercury flux from Russian rivers based solely on measurements from September (Coquery et al., 1995; Outridge et al., 2008) are likely grossly underestimated.

To test the importance of a riverine source, we conducted a sensitivity simulation that included an additional source of Hg^{II} to the Arctic Ocean. We find that the observed summer atmospheric and oceanic mercury concentrations are consistent with a total annual

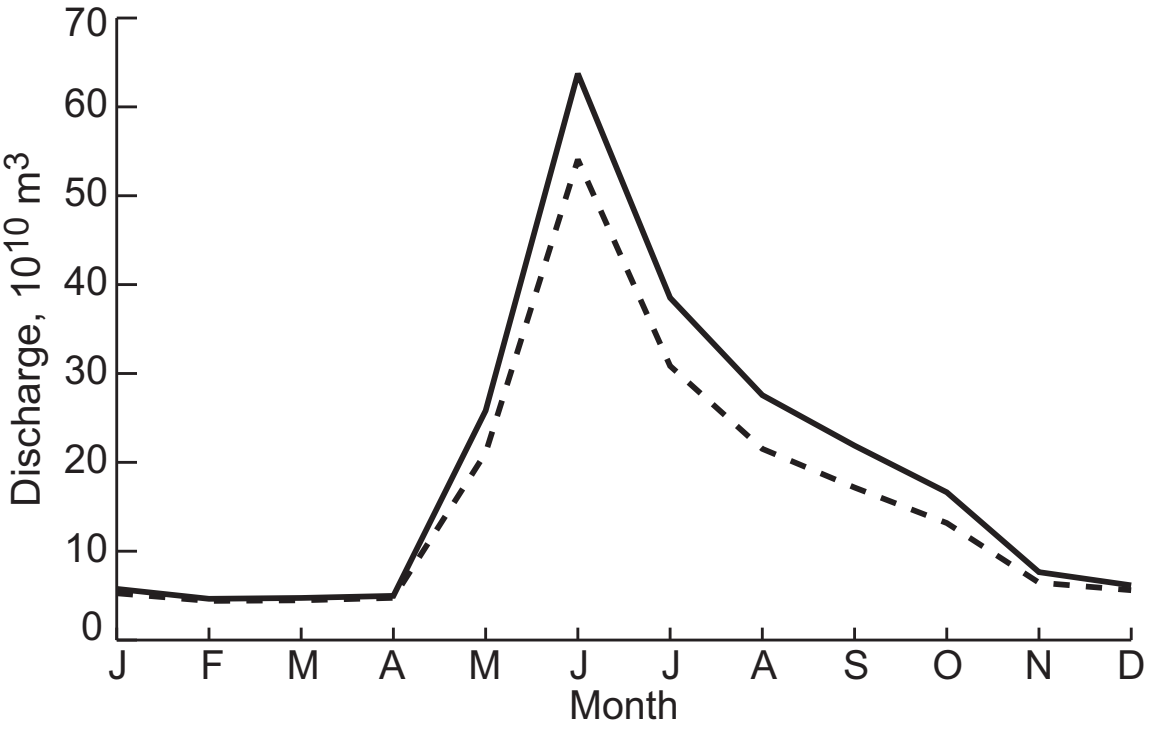

Figure 4.4: Mean seasonal variation in the monthly water discharge into the Arctic Ocean of the eight largest circumpolar rivers (solid line): Yenisei (Russia), Lena (Russia), Ob (Russia), Mackenzie (Canada), Yukon (Canada/Alaska), Pechora (Russia), Dvina (Russia), Kolyma(Russia). The dashed line shows the contribution from Russian rivers. Discharge data are from the University of New Hampshire Global Runoff Data Centre (UNH-GRDC) Composite Runoff Fields V1.0 (http://www.grdc.sr.unh.edu/index.html), compiled based on long-term monitoring at river gauging stations (Fekete et al., 2000).

riverine flux of 160 Mg a^{-1}. This is distributed monthly as shown in Fig. 4.3b by assuming open water conditions from May-October with riverine mercury concentrations three times higher in spring (May-June) than later in summer and with water discharge seasonality as in Fig. 4.4. While considerably larger than previous annual estimates (Coquery et al., 1995; Outridge et al., 2008), we consider our estimate of 160 Mg a^{-1} within the very large uncertainty described above.

Figure 4.2 (blue) shows that the simulation including a large seasonal flux of river-

ine Hg^{II} to the Arctic Ocean successfully reproduces the observed summer peak in atmospheric mercury. We therefore suggest a major role for Russian rivers in explaining the atmospheric summer maximum. This hypothesis is consistent with the statistical Lagrangian model analyses by Hirdman et al. (2009) for Zeppelin showing that the highest atmospheric concentrations were associated with an Arctic Ocean source. Closer examination of their source attribution maps shows hotspots along the Russian coast in the outflow basins of the Ob, Yenisei, and Kolyma rivers. In situ observations also indicate elevated concentrations of both oceanic and atmospheric mercury in the Mackenzie River discharge area (Andersson et al., 2008; Sommar et al., 2010).

4.4 Budget of mercury for the Arctic Ocean

Figure 4.5 shows a proposed annual budget of mercury in the Arctic ocean-atmosphere system (70-90°N), constructed using the GEOS-Chem simulation including a source of 160 Mg a^{-1} from Arctic rivers. Non-riverine inputs to the surface ocean are primarily from atmospheric deposition, either directly to the open ocean (25 Mg a^{-1}) or via meltwater runoff following deposition to snow and sea ice (20 Mg a^{-1}). On an annual basis, entrainment and detrainment fluxes for the oceanic mixed layer are roughly balanced, and net transport to the subsurface ocean is mainly by particle settling. There are however large seasonal net fluxes driven by entrainment/detrainment as seen in Fig. 4.3.

Our modeled mean total mercury (THg $\equiv$ Hg^0 + Hg^{II} + Hg^P) in the Arctic Ocean is [THg] = 3.4 pM, within the range of observations from surface waters of the Canadian

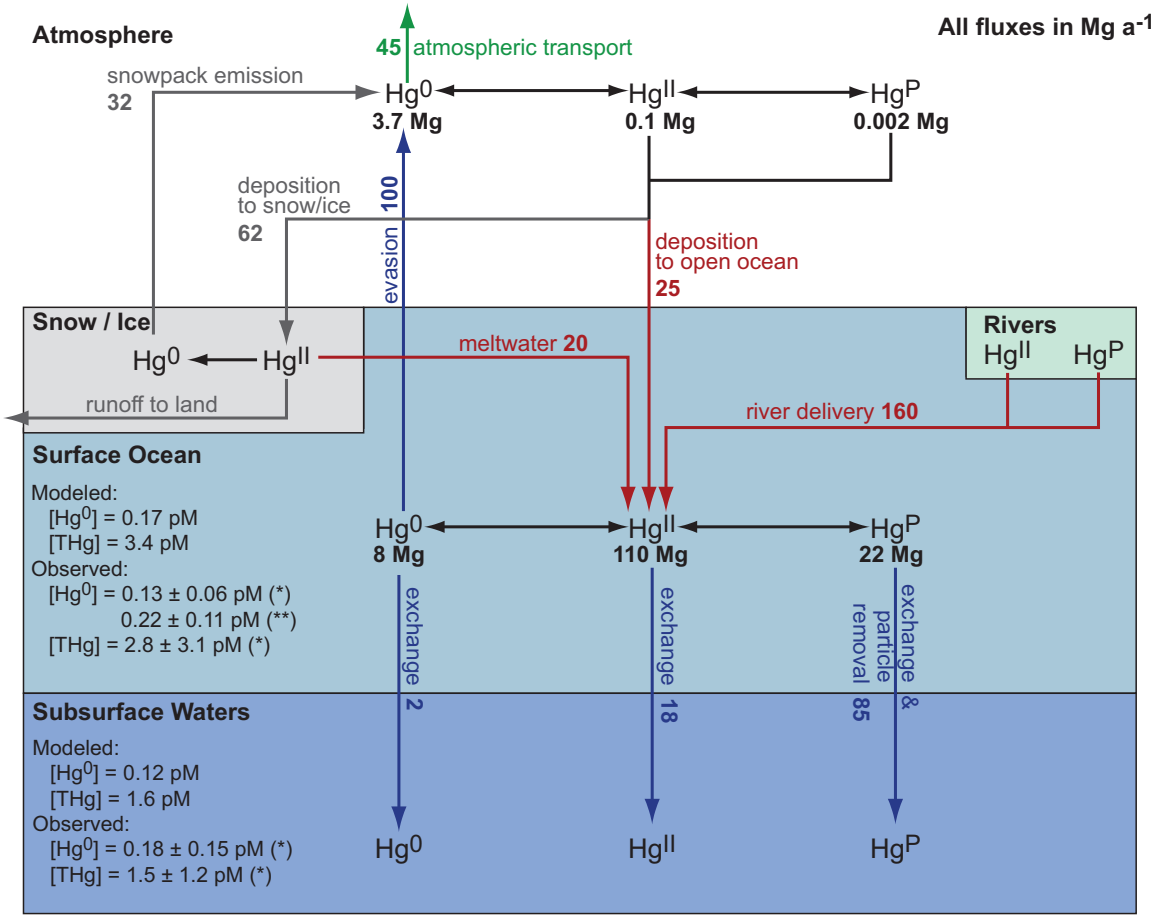

Figure 4.5: Annual budget of mercury for the Arctic (70-90°N) as simulated by GEOS-Chem. Red arrows show net inputs to the surface ocean, blue arrows show net removal from the surface ocean, gray arrows show fluxes between the atmosphere and the cryosphere, black arrows show partitioning between species, and the green arrow shows atmospheric transport to mid-latitudes. Observed concentrations are from Kirk et al. (2008) (*), including only observations north of 70°N, and from Andersson et al. (2008) (**).

Arctic with [THg] = 2.9 ± 2.8 pM (Kirk et al., 2008). Mean simulated [Hg^0] = 0.17 pM compares well to observations from the Arctic Ocean with mean [DGM] = 0.22 ± 0.11 pM (Andersson et al., 2008) but is somewhat larger than expected from measurements in surface waters of the Canadian Arctic Archipelago with [Hg^0] = 0.13 ± 0.06 pM (Kirk et al., 2008).

An outcome of our hypothesized large riverine input is that the Arctic Ocean provides a net source of mercury to the atmosphere. Without this input, net evasion of Hg^0 from the ocean is approximately balanced by atmospheric deposition. When we include the riverine source, net evasion from the ocean (100 Mg a^{-1}) is more than twice the combined fluxes from atmospheric deposition (25 Mg a^{-1}) and meltwater delivery (20 Mg a^{-1}). This implies that on an annual basis, the ocean is a net source of atmospheric mercury, not a net sink as has been suggested previously (Ariya et al., 2004).

The current cycling of mercury between the atmosphere, ocean, and cryosphere represented in Fig. 4.5 will likely be altered by rapid climate change presently taking place in the Arctic. In spring, warmer temperatures and earlier break-up of sea ice may explain recent shifts in AMDE occurrence to earlier in spring as well as reductions in their frequency (Cole and Steffen, 2010), suggesting reduced atmospheric deposition in the future. However, warming may simultaneously increase the areal coverage of salty first-year sea ice and associated bromine production, driving an increase in AMDE deposition (Macdonald et al., 2005). In summer, projected reductions in seasonal sea ice cover (Perovich and Richter-Menge, 2009) will increase the ocean surface area and therefore the oceanic mercury pool available for evasion to the atmosphere. Changes in ocean redox kinetics are also likely given projected changes in ocean microbial community structure and algal productivity (Lovejoy et al., 2006; Michelutti et al., 2007; Smol et al., 2005) as well as increased light penetration.

The magnitude of the riverine mercury source to the Arctic Ocean will be impacted by

climate through changes in watershed dynamics. Mercury stored in boreal soils is becoming increasingly mobilized due to thawing permafrost (Rydberg et al., 2010) and increased incidence of boreal wildfires (Turetsky et al., 2006). Simultaneously, river discharge rates are increasing, and further intensification is probable (Peterson et al., 2002; Rawlins et al., 2010). Combined, these changes in Arctic watersheds are expected to drive future large enhancements in mercury fluxes to the ocean. Our work shows that circumpolar rivers may already be the dominant source of mercury to the Arctic Ocean. There is therefore an urgent need to better understand the current drivers of riverine mercury inputs as well as the impacts of climate change on Arctic watershed dynamics.

Bibliography

Amos, H. A., Jacob, D. J., Holmes, C. D., Yantosca, R. M., Corbitt, E. S., Graydon, J. A., St. Louis, V. L., Edgerton, E., Gustin, M., Talbot, R. W., Steffen, A., Galarneau, E., and Sunderland, E. M.: Hg(II) gas-particle partitioning and its effect on global mercury deposition, in prep.

Amyot, M., Gill, G., and Morel, F.: Production and loss of dissolved gaseous mercury in coastal seawater, Environmental Science & Technology, 31, 3606–3611, 1997.

Andersson, M., Sommar, J., Gårdfeldt, K., and Lindqvist, O.: Enhanced concentrations of dissolved gaseous mercury in the surface waters of the Arctic Ocean, Marine Chemistry, 110, 190–194, 2008.

Ariya, P. A., Dastoor, A. P., Amyot, M., Schroeder, W. H., Barrie, L., Anlauf, K., Raofie, F., Ryzhkov, A., Davignon, D., and Lalonde, J.: The Arctic: a sink for mercury, Tellus B, 56, 397–403, 2004.

Aspmo, K., Temme, C., Berg, T., Ferrari, C., Gauchard, P., Fain, X., and Wibetoe, G.: Mercury in the atmosphere, snow and melt water ponds in the North Atlantic Ocean during Arctic summer, Environmental Science & Technology, 40, 4083–4089, 2006.

Berg, T., Aspmo, K., and Steinnes, E.: Transport of Hg from Atmospheric mercury depletion events to the mainland of Norway and its possible influence on Hg deposition, Geophysical Research Letters, 35, L09 802, 2008.

Bottenheim, J. and Chan, E.: A trajectory study into the origin of spring time Arctic boundary layer ozone depletion, Journal of Geophysical Research, 111, D19 301, 2006.

Brooks, S., Saiz-Lopez, A., Skov, H., Lindberg, S., Plane, J., and Goodsite, M.: The mass balance of mercury in the springtime arctic environment, Geophysical Research Letters, 33, L13 812, 2006.

Butler Walker, J., Houseman, J., Seddon, L., McMullen, E., Tofflemire, K., Mills, C., Corriveau, A., Weber, J., LeBlanc, A., Walker, M., et al.: Maternal and umbilical cord blood levels of mercury, lead, cadmium, and essential trace elements in Arctic Canada, Environmental Research, 100, 295–318, 2006.

Calvert, J. and Lindberg, S.: A modeling study of the mechanism of the halogen-ozone-mercury homogeneous reactions in the troposphere during the polar spring, Atmospheric Environment, 37, 4467–4481, 2003.

Carmack, E.: Large-scale physical oceanography of polar oceans, in: Polar Oceanography Part A: Physical Science, edited by Smith, Jr., W. O., Academic Press, 1990.

Cobbett, F., Steffen, A., Lawson, G., and Van Heyst, B.: GEM fluxes and atmospheric mercury concentrations (GEM, RGM and HgP) in the Canadian Arctic at Alert, Nunavut, Canada (February-June 2005), Atmospheric Environment, 41, 6527–6543, 2007.

Cole, A. S. and Steffen, A.: Trends in long-term gaseous mercury observations in the Arctic and effects of temperature and other atmospheric conditions, Atmospheric Chemistry and Physics, 10, 4661–4672, 2010.

Coquery, M., Cossa, D., and Martin, J.: The distribution of dissolved and particulate mercury in three Siberian estuaries and adjacent Arctic coastal waters, Water, Air, & Soil Pollution, 80, 653–664, 1995.

Dastoor, A. P., Davignon, D., Theys, N., Van Roozendael, M., Steffen, A., and Ariya, P. A.: Modeling Dynamic Exchange of Gaseous Elemental Mercury at Polar Sunrise, Environmental Science & Technology, 42, 5183–5188, 2008.

de Boyer Montégut, C., Madec, G., Fischer, A., Lazar, A., and Iudicone, D.: Mixed layer depth over the global ocean: An examination of profile data and a profile-based climatology, Journal of Geophysical Research, 109, C12 003, 2004.

Dewailly, E., Ayotte, P., Bruneau, S., Lebel, G., Levallois, P., and Weber, J.: Exposure of the Inuit population of Nunavik (Arctic Quebec) to lead and mercury, Archives of Environmental Health: An International Journal, 56, 350–357, 2001.

Dittmar, T. and Kattner, G.: The biogeochemistry of the river and shelf ecosystem of the Arctic Ocean: A review, Marine Chemistry, 83, 103–120, 2003.

Dommergue, A., Ferrari, C., Gauchard, P., Boutron, C., Poissant, L., Pilote, M., Jitaru, P., and Adams, F.: The fate of mercury species in a sub-arctic snowpack during snowmelt, Geophysical Research Letters, 30, 1621, 2003.

Dommergue, A., Bahlmann, E., Ebinghaus, R., Ferrari, C., and Boutron, C.: Laboratory simulation of Hg0 emissions from a snowpack, Analytical and Bioanalytical Chemistry, 388, 319–327, 2007.

Dommergue, A., Sprovieri, F., Pirrone, N., Ebinghaus, R., Brooks, S., Courteaud, J., and Ferrari, C. P.: Overview of mercury measurements in the Antarctic troposphere, Atmospheric Chemistry and Physics, 10, 3309–3319, 2010.

Durnford, D. and Dastoor, A.: The behavior of mercury in the cryosphere: A review of what we know from observations, Journal of Geophysical Research, 116, D06 305, 2011.

Durnford, D. A., Dastoor, A., Figueras-Nieto, D., and Ryjkov, A.: Long range transport of mercury to the Arctic and across Canada, Atmospheric Chemistry and Physics, 10, 6063–6086, 2010.

Faïn, X., Ferrari, C. P., Dommergue, A., Albert, M., Battle, M., Arnaud, L., Barnola, J.-M., Cairns, W., Barbante, C., and Boutron, C.: Mercury in the snow and firn at Summit Station, Central Greenland, and implications for the study of past atmospheric mercury levels, Atmospheric Chemistry and Physics, 8, 3441–3457, 2008.

Fekete, B. M., Vörösmarty, C. J., and Grabs, W.: Global, composite runoff fields based on observed river discharge and simulated water balances, Tech. rep., University of New Hampshire and Global Runoff Data Centre, 2000.

Fitzgerald, W., Engstrom, D., Lamborg, C., Tseng, C., Balcom, P., and Hammerschmidt, C.: Modern and historic atmospheric mercury fluxes in northern Alaska: global sources and Arctic depletion, Environmental Science & Technology, 39, 557–568, 2005.

Friedli, H., Radke, L., Payne, N., McRae, D., Lynham, T., and Blake, T.: Mercury in vegetation and organic soil at an upland boreal forest site in Prince Albert National Park, Saskatchewan, Canada, Journal of Geophysical Research, 112, 2007.

Gårdfeldt, K., Sommar, J., Ferrara, R., Ceccarini, C., Lanzilllotta, E., Munthe, J., Wängberg, I., Lindqvist, O., Pirrone, N., Sprovieri, F., Pesenti, E., and Strömberg, D.: Evasion of mercury from coastal and open waters of the Atlantic Ocean and the Mediterranean Sea, Atmospheric Environment, 37, S73–S84, 2003.

Gordeev, V., Martin, J., Sidorov, I., and Sidorova, M.: A reassessment of the Eurasian river input of water, sediment, major elements, and nutrients to the Arctic Ocean, American Journal of Science, 296, 664–691, 1996.

Graydon, J., Emmerton, C., Lesack, L., and Kelly, E.: Mercury in the Mackenzie River delta and estuary: Concentrations and fluxes during open-water conditions, Science of the Total Environment, 407, 2980–2988, 2009.

Grigal, D.: Mercury sequestration in forests and peatlands: a review, Journal of Environmental Quality, 32, 393–405, 2003.

Hansen, B. and Østerhus, S.: North Atlantic-nordic seas exchanges, Progress in Oceanography, 45, 109–208, 2000.

Hintelmann, H., Harris, R., Heyes, A., Hurley, J., Kelly, C., Krabbenhoft, D., Steve Lindberg, O., Rudd, J., Scott, K., and Louis, V.: Reactivity and mobility of new and old mercury deposition in a boreal forest ecosystem during the first year of the METAALICUS study, Environmental Science & Technology, 36, 5034–5040, 2002.

Hirdman, D., Aspmo, K., Burkhart, J. F., Eckhardt, S., Sodemann, H., and Stohl, A.: Transport of mercury in the Arctic atmosphere: Evidence for a spring- time net sink and summer-time source, Geophysical Research Letters, 36, L12 814, 2009.

Holmes, C. D., Jacob, D. J., Corbitt, E. S., Mao, J., Yang, X., Talbot, R., and Slemr, F.: Global atmospheric model for mercury including oxidation by bromine atoms, Atmospheric Chemistry and Physics, 10, 12 037–12 057, 2010.

Ingvaldsen, R., Asplin, L., and Loeng, H.: The seasonal cycle in the Atlantic transport to the Barents Sea during the years 1997-2001, Continental Shelf Research, 24, 1015–1032, 2004.

Kellerhals, M., Beauchamp, S., Belzer, W., Blanchard, P., Froude, F., Harvey, B., McDonald, K., Pilote, M., Poissant, L., Puckett, K., et al.: Temporal and spatial variability of total gaseous mercury in Canada: results from the Canadian Atmospheric Mercury Measurement Network (CAMNet), Atmospheric Environment, 37, 1003–1011, 2003.

Kirk, J., St. Louis, V., Hintelmann, H., Lehnherr, I., Else, B., and Poissant, L.: Methylated mercury species in marine waters of the Canadian high and sub Arctic, Environmental Science & Technology, 42, 8367–8373, 2008.

Lalonde, J., Poulain, A., and Amyot, M.: The role of mercury redox reactions in snow on snow-to-air mercury transfer, Environmental Science & Technology, 36, 174–178, 2002.

Lalonde, J., Amyot, M., Doyon, M., and Auclair, J.: Photo-induced Hg (II) reduction in snow from the remote and temperate Experimental Lakes Area (Ontario, Canada), Journal of Geophysical Research, 108, 4200, 2003.

Lammers, R., Shiklomanov, A., Vörösmarty, C., Fekete, B., and Peterson, B.: Assessment of contemporary Arctic river runoff based on observational discharge records, Journal of Geophysical Research, 106, 3321–3334, 2001.

Leitch, D., Carrie, J., Lean, D., Macdonald, R., Stern, G., and Wang, F.: The delivery of mercury to the Beaufort Sea of the Arctic Ocean by the Mackenzie River, Science of the Total Environment, 373, 178–195, 2007.

Lindberg, S., Brooks, S., Lin, C., Scott, K., Landis, M., Stevens, R., Goodsite, M., and Richter, A.: Dynamic oxidation of gaseous mercury in the Arctic troposphere at polar sunrise, Environmental Science & Technology, 36, 1245–1256, 2002.

Lovejoy, C., Massana, R., and Pedros-Alio, C.: Diversity and distribution of marine microbial eukaryotes in the Arctic Ocean and adjacent seas, Applied and Environmental Microbiology, 72, 3085, 2006.

Lu, J., Schroeder, W., Barrie, L., Steffen, A., Welch, H., Martin, K., Lockhart, L., Hunt, R., Boila, G., and Richter, A.: Magnification of atmospheric mercury deposition to polar regions in springtime: the link to tropospheric ozone depletion chemistry, Geophysical Research Letters, 28, 3219–3222, 2001.

Macdonald, R., Harner, T., and Fyfe, J.: Recent climate change in the Arctic and its impact on contaminant pathways and interpretation of temporal trend data, Science of the Total Environment, 342, 5–86, 2005.

Mason, R. and Sheu, G.: Role of the ocean in the global mercury cycle, Global Biogeochemical Cycles, 16, 1093, 2002.

Mason, R. and Sullivan, K.: The distribution and speciation of mercury in the South and equatorial Atlantic, Deep-Sea Research Part II, 46, 937–956, 1999.

Mergler, D., Anderson, H., Chan, L., Mahaffey, K., Murray, M., Sakamoto, M., and Stern, A.: Methylmercury exposure and health effects in humans: a worldwide concern, AMBIO: A Journal of the Human Environment, 36, 3–11, 2007.

Michelutti, N., Wolfe, A., Briner, J., and Miller, G.: Climatically controlled chemical and biological development in Arctic lakes, Journal of Geophysical Research, 112, G03 002, 2007.

Munthe, J., Bodaly, R., Branfireun, B., Driscoll, C., Gilmour, C., Harris, R., Horvat, M., Lucotte, M., and Malm, O.: Recovery of mercury-contaminated fisheries, AMBIO: A Journal of the Human Environment, 36, 33–44, 2007.

Orvik, K., Skagseth, Ø., and Mork, M.: Atlantic inflow to the Nordic Seas: current structure and volume fluxes from moored current meters, VM-ADCP and SeaSoar-CTD observations, 1995-1999, Deep Sea Research Part I: Oceanographic Research Papers, 48, 937–957, 2001.

Østerhus, S., Turrell, W., Hansen, B., Lundberg, P., and Buch, E.: Observed transport estimates between the North Atlantic and the Arctic Mediterranean in the Iceland–Scotland region, Polar Research, 20, 169–175, 2001.

Outridge, P., Macdonald, R., Wang, F., Stern, G., and Dastoor, A.: A mass balance inventory of mercury in the Arctic Ocean, Environmental Chemistry, 5, 89–111, 2008.

Perovich, D. K. and Richter-Menge, J. A.: Loss of Sea Ice in the Arctic, Annual Reviews of Marine Science, 1, 417–441, 2009.

Peterson, B., Holmes, R., McClelland, J., Vörösmarty, C., Lammers, R., Shiklomanov, A., Shiklomanov, I., and Rahmstorf, S.: Increasing river discharge to the Arctic Ocean, Science, 298, 2171, 2002.

Pöhler, D., Vogel, L., Frieß, U., and Platt, U.: Observation of halogen species in the Amundsen Gulf, Arctic, by active long-path differential optical absorption spectroscopy, Proceedings of the National Academy of Sciences, 107, 6582–6587, 2010.

Poulain, A., Lalonde, J., Amyot, M., Shead, J., Raofie, F., and Ariya, P.: Redox transformations of mercury in an Arctic snowpack at springtime, Atmospheric Environment, 38, 6763–6774, 2004.

Poulain, A., Ni Chadhain, S., Ariya, P., Amyot, M., Garcia, E., Campbell, P., Zylstra, G., and Barkay, T.: Potential for mercury reduction by microbes in the high arctic, Applied and Environmental Microbiology, 73, 2230, 2007.

Prados-Roman, C., Butz, A., Deutschmann, T., Dorf, M., Kritten, L., Minikin, A., Platt, U., Schlager, H., Sihler, H., Theys, N., Van Roozendael, M., Wagner, T., and Pfeilsticker, K.: Airborne DOAS limb measurements of tropospheric trace gas profiles: case studies on the profile retrieval of O4 and BrO, Atmospheric Measurement Techniques, 4, 1241–1260, 2011.

Quémerais, B., Cossa, D., Rondeau, B., Pham, T. T., Gagnon, P., and Fortin, B.: Sources and Fluxes of Mercury in the St. Lawrence River, Environmental Science & Technology, 33, 840–849, 1999.

Qureshi, A., O'Driscoll, N., MacLeod, M., Neuhold, Y., and Hungerbühler, K.: Photoreactions of mercury in surface ocean water: gross reaction kinetics and possible pathways, Environmental Science & Technology, 44, 644–649, 2010.

Rawlins, M., Steele, M., Holland, M., Adam, J., Cherry, J., Francis, J., Groisman, P., Hinzman, L., Huntington, T., Kane, D., Kimball, J. S., Kwok, R., Lammers, R., Lee, C. M., Lettenmaier, D. P., McDonald, K. C., Podest, E., Pundsack, J. J., Rudels, B., Serreze, M. C., Shiklomanov, A., Skagseth, Ø., Troy, T. J., Vörösmarty, C. J., Wensnahan, M., Wood, E. F., Woodgate, R., Yang, D., Zhang, K., and Tingjun, Z.: Analysis of the arctic

system for freshwater cycle intensification: Observations and expectations, Journal of Climate, 2010.

Reynolds, R. W., Rayner, N. A., Smith, T. M., Stokes, D. C., and Wang, W.: An Improved In Situ and Satellite SST Analysis for Climate, Journal of Climate, 15, 1609–1625, 2002.

Rolfhus, K. and Fitzgerald, W.: Mechanisms and temporal variability of dissolved gaseous mercury production in coastal seawater, Marine Chemistry, 90, 125–136, 2004.

Rydberg, J., Klaminder, J., Rosén, P., and Bindler, R.: Climate driven release of carbon and mercury from permafrost mires increases mercury loading to sub-arctic lakes, Science of the Total Environment, 2010.

Schuster, P., Krabbenhoft, D., Naftz, D., Cecil, L., Olson, M., Dewild, J., Susong, D., Green, J., and Abbott, M.: Atmospheric mercury deposition during the last 270 years: a glacial ice core record of natural and anthropogenic sources, Environmental Science & Technology, 36, 2303–2310, 2002.

Selin, N., Jacob, D., Park, R., Yantosca, R., Strode, S., Jaeglé, L., and Jaffe, D.: Chemical cycling and deposition of atmospheric mercury: Global constraints from observations, Journal of Geophysical Research, 112, D02 308, 2007.

Selin, N., Jacob, D., Yantosca, R., Strode, S., Jaeglé, L., and Sunderland, E.: Global 3-D land-ocean-atmosphere model for mercury: Present-day versus preindustrial cycles and anthropogenic enrichment factors for deposition, Global Biogeochemical Cycles, 22, 13, 2008.

Simpson, W. R., von Glasow, R., Riedel, K., Anderson, P., Ariya, P., Bottenheim, J., Burrows, J., Carpenter, L., Frieß, U., and Goodsite, M. E.: Halogens and their role in polar boundary-layer ozone depletion, Atmospheric Chemistry and Physics, 7, 4375–4418, 2007.

Skov, H., Christensen, J., Goodsite, M., Heidam, N., Jensen, B., Wåhlin, P., and Geernaert, G.: Fate of elemental mercury in the Arctic during atmospheric mercury depletion episodes and the load of atmospheric mercury to the Arctic, Environmental Science & Technology, 38, 2373–2382, 2004.

Smith-Downey, N., Sunderland, E., and Jacob, D.: Anthropogenic impacts on global storage and emissions of mercury from terrestrial soils: Insights from a new global model, Journal of Geophysical Research, 115, 2010.

Smol, J., Wolfe, A., Birks, H., Douglas, M., Jones, V., Korhola, A., Pienitz, R., Rühland, K., Sorvari, S., Antoniades, D., Brooks, S. J., Fallu, M.-A., Hughes, M., Keatley, B. E., Laing, T. E., Michelutti, N., Nazarova, L., Nyman, M., Paterson, A. M., Perren, B., Quinlan, R., Rautio, M., Saulnier-Talbot, E., Siitonen, S., Solvieva, N., and Weckström, J.:

Climate-driven regime shifts in the biological communities of arctic lakes, Proceedings of the National Academy of Sciences, 102, 4397, 2005.

Soerensen, A., Sunderland, E., Holmes, C., Jacob, D., Yantosca, R., Skov, H., Christensen, J., Strode, S., and Mason, R.: An improved global model for air-sea exchange of mercury: high concentrations over the North Atlantic, Environmental Science & Technology, 2010.

Sommar, J., Andersson, M. E., and Jacobi, H.-W.: Circumpolar measurements of speciated mercury, ozone and carbon monoxide in the boundary layer of the Arctic Ocean, Atmospheric Chemistry and Physics, 10, 5031–5045, 2010.

St. Louis, V. L., Hintelmann, H., Graydon, J. A., Kirk, J. L., Barker, J., Dimock, B., Sharp, M. J., and Lehnherr, I.: Methylated Mercury Species in Canadian High Arctic Marine Surface Waters and Snowpacks, Environmental Science & Technology, 41, 6433–6441, 2007.

Steen, A., Berg, T., Dastoor, A., Durnford, D., Engelsen, O., Hole, L., and Pfaffhuber, K.: Natural and anthropogenic atmospheric mercury in the European Arctic: a fractionation study, Atmospheric Chemistry and Physics, 11, 6273–6284, 2011.

Steffen, A., Schroeder, W., Macdonald, R., Poissant, L., and Konoplev, A.: Mercury in the Arctic atmosphere: An analysis of eight years of measurements of GEM at Alert (Canada) and a comparison with observations at Amderma (Russia) and Kuujjuarapik (Canada), Science of the Total Environment, 342, 185–198, 2005.

Steffen, A., Douglas, T., Amyot, M., Ariya, P., Aspmo, K., Berg, T., Bottenheim, J., Brooks, S., Cobbett, F., Dastoor, A., Dommergue, A., Ebinghaus, R., Ferrari, C., Gårdfeldt, K., Goodsite, M. E., Lean, D., Poulain, A. J., Scherz, C., Skov, H., Sommar, J., and Temme, C.: A synthesis of atmospheric mercury depletion event chemistry in the atmosphere and snow, Atmospheric Chemistry and Physics, 8, 1445–1482, 2008.

Stein, R. and Macdonald, R.: The Organic Carbon Cycle in the Arctic Ocean, Springer-Verlag, Berlin, 2004.

Sunderland, E. and Mason, R.: Human impacts on open ocean mercury concentrations, Global Biogeochemical Cycles, 21, 2007.

Toole, J., Timmermans, M., Perovich, D., Krishfield, R., Proshutinsky, A., and Richter-Menge, J.: Influences of the ocean surface mixed layer and thermohaline stratification on Arctic Sea ice in the central Canada Basin, Journal of Geophysical Research, 115, C10 018, 2010.

Turetsky, M., Harden, J., Friedli, H., Flannigan, M., Payne, N., Crock, J., and Radke, L.: Wildfires threaten mercury stocks in northern soils, Geophysical Research Letters, 33, 16 403, 2006.

USGS: Minerals Information, URL http://minerals.usgs.gov/minerals/pubs/country/maps/94349.gif, 2011.

Van Oostdam, J., Gilman, A., Dewailly, E., Usher, P., Wheatley, B., Kuhnlein, H., Neve, S., Walker, J., Tracy, B., Feeley, M., et al.: Human health implications of environmental contaminants in Arctic Canada: a review, The Science of the Total Environment, 230, 1–82, 1999.

Walling, D. and Webb, B.: Estimating the discharge of contaminants to coastal waters by rivers: some cautionary comments, Marine Pollution Bulletin, 16, 488–492, 1985.

Witherow, R. and Lyons, W.: Mercury deposition in a polar desert ecosystem, Environmental Science & Technology, 42, 4710–4716, 2008.